TKK Dissertations 234
Espoo 2010

ENERGY-BASED MAGNETO-MECHANICAL MODEL FOR ELECTRICAL STEEL SHEETS

Doctoral Dissertation

Katarzyna Anna Fonteyn

Aalto University
School of Science and Technology
Faculty of Electronics, Communications and Automation
Department of Electrical Engineering

TKK Dissertations 234
Espoo 2010

ENERGY-BASED MAGNETO-MECHANICAL MODEL FOR ELECTRICAL STEEL SHEETS

Doctoral Dissertation

Katarzyna Anna Fonteyn

Doctoral dissertation for the degree of Doctor of Science in Technology to be presented with due permission of the Faculty of Electronics, Communications and Automation for public examination and debate in Auditorium S4 at the Aalto University School of Science and Technology (Espoo, Finland) on the 20th of August 2010 at 12 noon.

Aalto University
School of Science and Technology
Faculty of Electronics, Communications and Automation
Department of Electrical Engineering

Aalto-yliopisto
Teknillinen korkeakoulu
Elektroniikan, tietoliikenteen ja automaation tiedekunta
Sähkötekniikan laitos

Distribution:
Aalto University
School of Science and Technology
Faculty of Electronics, Communications and Automation
Department of Electrical Engineering
P.O. Box 13000 (Otakaari 5)
FI - 00076 Aalto
FINLAND
URL: http://sahkotekniikka.tkk.fi/en/
Tel. +358-9-470 22394
Fax +358-9-470 22991
E-mail: katarzyna.fonteyn@tkk.fi

ISBN 978-952-60-3287-0
ISBN 978-952-60-3288-7 (PDF)
ISSN 1795-2239
ISSN 1795-4584 (PDF)
URL: http://lib.tkk.fi/Diss/2010/isbn9789526032887/

TKK-DISS-2791

Picaset Oy
Helsinki 2010

Aalto University
School of Science
and Technology

ABSTRACT OF DOCTORAL DISSERTATION	AALTO UNIVERSITY SCHOOL OF SCIENCE AND TECHNOLOGY P.O. BOX 11000, FI-00076 AALTO http://www.aalto.fi

Author: Katarzyna Anna Fonteyn

Name of the dissertation:
Energy-Based Magneto-Mechanical Model for Electrical Steel Sheets

Manuscript submitted: 26.03.2010	Manuscript revised: 10.06.2010

Date of the defence: 20.08.2010

☒ Monograph	☐ Article dissertation (summary + original articles)

Faculty: Faculty of Electronics, Communications and Automation
Department: Department of Electrical Engineering
Field of research: Electromechanics
Opponent(s): Prof. dr. ir. Lieven Vandevelde
Supervisor: Prof. Antero Arkkio
Instructor: D.Sc. (Tech.) Anouar Belahcen

Abstract:
Within this dissertation an energy-based model for magneto-mechanical coupling in electrical steels has been developed, studied and implemented in finite element software. The method introduces a novel way of explicitly solving magnetic and mechanical fields. Starting from the knowledge of the dependence of magnetostriction on stress and magnetic field, and of the dependence of the magnetic field on the stress, a Helmholtz free energy is presented. The material constitutive equations are explicitly written. The parameters of the model are identified experimentally from a modified Epstein frame. This setup allows stressing a pack of electrical steel sheets and measuring the magnetostriction and B-H curves under pre-stresses. The resulting strains are acquired with a piezo-electric force transducer. The measurements are compared with data obtained from a vertical yoke system at no pre-stress with strain gauges and discussed.

The method is then applied to study magneto-mechanical coupling in radial-flux rotating electrical machines. A test device is studied; it consists of a stack of round electrical steel sheets assembled with windings wound to obtain a magnetic flux density as in real electrical machines. This one enables the coupled method to be verified when there is no air gap. The last device is a sample machine wound in the same way as an asynchronous machine used for studying losses. Its advantage is that there is no outer frame that would prevent the placement of accelerometers for measuring the acceleration of the iron yoke when excited. The validity of the model for real electrical machines is verified by the good agreement between those measurements show good agreement with the computed results

The method appeared to be suitable and robust for the computation of displacements in rotating electrical machines. The tangential and radial displacements on the teeth of stators are obtained from the method. The influences of magnetic forces on the structures are studied and quantified.

Keywords: Magneto-mechanical coupling, magnetostriction, stress, single sheet testers, Epstein frame, finite element modelling, electrical steel sheets, rotating electrical machines.

ISBN (printed) 978-952-60-3287-0	ISSN (printed) 1795-2239
ISBN (pdf) 978-952-60-3288-7	ISSN (pdf) 1795-4584
Language: English	Number of pages: 134

Publisher: Department of Electrical Engineering, Aalto University

Print distribution: Department of Electrical Engineering, P.O. Box 13000 FI-02015 Aalto, Finland

☒ The dissertation can be read at http://lib.tkk.fi/Diss/2010/isbn9789526032887/

Acknowledgments

"Life is not easy for any of us. But what of that? We must have perseverance and above all confidence in ourselves. We must believe that we are gifted for something and that this thing must be attained."

Quote attributed to Marie Sklodowska-Curie,
Nobel Prize in Physics (1903) and in Chemistry (1910)

This work has been completed in the Department of Electrical Engineering at Aalto University. I am indebted to Prof. Antero Arkkio, D.Sc. Anouar Belahcen and D.Sc. Reijo Kouhia for the supervision and guidance offered during my research. I am grateful to D.Sc. Stefania Fortino who contributed, in the early stage of this research to the theoretical definition of the problem. Besides my advisors, I acknowledge the past and present managerial, administrative and technical staff of the Department of Electrical Engineering and in general at Aalto University who provided me with quick and efficient assistance for experimental apparatuses, for organizing my research stays abroad and for supporting me in various matters since the very beginning. I send my special thanks to D.Sc. Jarmo Perho, Eero Pyharanta and M.Sc. Ari Haavisto among others, for their contribution to the design and construction of the test devices. Finally, thanks to Emeritus Prof. Tapani Jokinen who has always been a constant source of encouragement for creative and innovative thinking during my post-graduate studies. I would like to emphasize that the trust and freedom I enjoyed, allowing me to develop my talents in various fields besides my research has a valuable significance and impact on my life.

I gratefully acknowledge the financial support of the major players within this project: TEKES (KOMASI) project under grant 210543, the Graduate School of Electrical and Communications Engineering, Academy of Finland (DYCOLO) project under grant 125819 and the research group of Electromechanics at the Aalto University. Being additionally rewarded for one's achievements is essential for increasing motivation. For this reason, I particularly acknowledge the generous yearly extra support from Fortum Foundation. Furthermore, the scholarships of Emil Aalto, Walter Ahlstrom and the Association of Electrical Engineers in Finland foundations are extremely appreciated. Without the funding provided by all these bodies, my thesis and ambition to study and work abroad could not have been realized.

Knowledge has no real value if not shared. Special thanks go to my peers, past and present colleagues at Aalto University, students from around the world for a multitude of random work-related conversations and extra-curricular activities. Their experiences, questions and shared discussions contributed to build my knowledge and

motivation through my research. I also thank the researchers and professors I met during conferences, courses and research stays for having exchanged their views, listened, read and commented on my work. I am indebted to the research team at the Laboratory of Electrical Engineering in Paris (LGEP), where I worked from October 2007 to January 2008; particularly to Dr. Laurent Daniel, Prof. Alain Bossavit, Prof. Adel Razek and Prof. Frederic Bouillaut who shared interest and knowledge on material modeling. My regards go to Prof. Amalyia Ivany who discussed experimental setups during my stay in Hungary in October 2005. Prof. Joe Zhu and Prof. Peter Watterson made my stay in UTS, Sydney possible in 2010 and I wish to thank them for their fruitful discussions and feedback. Finally, I am indebted to the pre-examiners of this thesis, Prof. Herbert De Gersem and Prof. Göran Engdhal, for their time to review this work and their precious technical feedback.

I would like to give distinctive acknowledgements to Prof. Philippe Lataire, from the Vrije Universiteit in Brussels who awakened my real interest in the field of electrical engineering. I am thankful to Christine Manet, teaching assistant at the Université Libre de Bruxelles who was confident in my capabilities and provided me with the right supervision and motivation in my first and second years of studies.

Every single life- and work- related experience during my post-graduate studies I was granted is a precious gift. They mould me, building my skills, responsibility, strengths and self-awareness. I made amazing acquaintances in Finland. Thanks to all for the get-together's and great parties and for letting me into your lives. My deepest thanks go to every single person whose road has crossed mine, leading my journey to its next destination. Although I could not cite you directly here, I value your presence in my life from the bottom of my heart. Finally, special thanks go to a dear friend, Gaelle Cohen, who has the unique talent to bring joy to our conversations. I could not have imagined those years without her spontaneity, flexibility and openness to adventure.

I turn to the love of my dearest and closest ones whom I carry within me every day of my life. For that, I am deeply grateful to my mother, Janina Zuchora who takes so much care of me and thank her for her friendship, respect and understanding for my choices and support throughout my studies, and life. She is a model of strength and perseverance. Next, my gratitude flows to my grandmother, Agata Zuchora, who is my source of inspiration and trust. She lives within my heart, fills it with courage, hope and kindness. Both of them taught me to follow my dreams, never give up and taught me to think out of the box. Finally, I would like to thank Paavo Rasilo for standing by my side, for his patience, strength, moral support, sharing of knowledge and unconditional trust through this work and in life.

Sydney, June the 10th 2010.

Katarzyna Anna Fonteyn

Contents

List of Symbols

		SI based units
α_i	Material dependent parameter *i*	*dimensionless*
$\mathbf{A}$	Magnetic vector potential	$m \cdot kg \cdot s^{-2} \cdot A^{-1}$
$\mathbf{a}^k$	Column vector of nodal values of **A**	$m \cdot kg \cdot s^{-2} \cdot A^{-1}$
a^*, u^*, v^*	Initial values for the boundary conditions	*varying*
$\mathbf{B}$	Magnetic flux density	$kg \cdot s^{-2} \cdot A^{-1}$
$\mathbf{b}$	Body force	$m \cdot kg \cdot s^{-2}$
β	Parameter for the recurrence scheme	*dimensionless*
$\mathbf{C}_r$	Matrix that couple the circuit equations	*not predefined*
$\mathbf{C}$	Elasticity tensor	$m^{-1} \cdot kg \cdot s^{-2}$
C	Viscous damping coefficient matrix	$m^{-1} \cdot kg \cdot s^{-1}$
C_{ijkl}	Entries of the elasticity tensor	$m^{-1} \cdot kg \cdot s^{-2}$
c_1, c_2	Coefficients	*dimensionless*
$\mathbf{D}$	Electric displacement	$A \cdot s \cdot m^{-2}$
δ_{ij}	Kronecker delta	*dimensionless*
Δl	Length variation	m
Δl_{ms}	Equivalent magnetostrictive elongation	m
$\Delta \mathbf{x}$	Iterative change of quantity **x**	*not predefined*
$\mathbf{E}$	Electric field	$kg \cdot m \cdot s^{-3} \cdot A^{-1}$
E	Modulus of elasticity	$m^{-1} \cdot kg \cdot s^{-2}$
$\boldsymbol{\varepsilon}$	Total strain tensor	*dimensionless*
ε_{ij}	Entries of the strain tensor	*dimensionless*
$\bar{\boldsymbol{\varepsilon}}$	Concatenated form of **ε**, vector	*dimensionless*
ε_0	Permittivity of free space	$m^{-3} \cdot kg^{-1} \cdot s^4 \cdot A^2$
ϕ	Scalar potential	$m^2 \cdot kg \cdot s^{-1} \cdot A^{-1}$
$\boldsymbol{\Phi}$	Matrix for the magneto-mechanical coupling	*not predefined*
$\mathbf{f}_{mag}$	Electromagnetic body force	$m \cdot kg \cdot s^{-2}$
$\mathbf{f}_{mec}$	Mechanical body force	$m \cdot kg \cdot s^{-2}$
$\mathbf{f}_{inert}$	Inertial force	$m \cdot kg \cdot s^{-2}$
f	Frequency	s^{-1}
$\mathbf{G}_s$	Matrix that couple the circuit equations	*not predefined*

G	Shear modulus	$m^{-1} \cdot kg \cdot s^{-2}$
g	Specific Gibbs energy	$m^2 \cdot s^{-2}$
γ	Electrical conductivity	$m^{-3} \cdot kg^{-1} \cdot s^3 \cdot A^2$
$\tilde{\gamma}$	Parameter for the recurrence scheme	*dimensionless*
g_i	Functions	*dimensionless*
$\mathbf{H}$	Magnetic flux	$A \cdot m^{-1}$
$\mathbf{H}_0$	Vector of initial values of $\mathbf{H}$	$A \cdot m^{-1}$
$\hbar$	Specific enthalpy	$m^2 \cdot s^{-2}$
$\mathbf{i}_s^k$	Column vector of stator currents	A
$\mathbf{I}$	Identity tensor	*dimensionless*
I_i	Invariant *i*	*dimensionless*
$\mathbf{J}$	Electric current density	$A \cdot m^{-2}$
$\mathbf{J}_f$	Free current density	$A \cdot m^{-2}$
K	Bulk modulus	$m^{-1} \cdot kg \cdot s^{-2}$
k	when used as a superscript, time step	*dimensionless*
l	Final length	m
l_0	Initial length	m
λ	First lamé parameter	*dimensionless*
$\lambda_{e,c}$	Total elongation/ contraction	*dimensionless*
$\lambda_{x,y}$	Deformation in *x*-or *y*-direction	*dimensionless*
$\mathbf{M}$	Magnetisation	$A \cdot m^{-1}$
$\boldsymbol{\mu}$	Magnetic permeability tensor	$m \cdot kg \cdot s^{-2} \cdot A^{-2}$
μ_0	Permeability of free space	$m \cdot kg \cdot s^{-2} \cdot A^{-2}$
$\mathcal{M}$	Mass matrix	kg
N_i	Basis functions	*dimensionless*
υ	Poisson's ratio	*dimensionless*
p	Pressure	$m^{-1} \cdot kg \cdot s^{-2}$
$\mathbf{q}$, $\mathbf{p}$	Vector quantities	*not predefined*
$\mathbf{q}^k$	Column vector	*not predefined*
Q, P	Parameters	*dimensionless*
ρ	Mass density	$m^{-3} \cdot kg$
σ_{ij}	Entries of the stress tensor	$m^{-1} \cdot kg \cdot s^{-2}$
$\boldsymbol{\sigma}$	Stress tensor	$m^{-1} \cdot kg \cdot s^{-2}$
$\mathcal{S}$	Entropy	$m^2 \cdot kg \cdot s^{-2} \cdot K^{-1}$
S	Surface	m^2
s	Specific entropy	$m^2 \cdot s^{-2} \cdot K^{-1} s$
T	Temperature	K

t	Time	s
$\boldsymbol{\tau}_0$	Tensor of initial values of $\boldsymbol{\tau}$	$m^{-1}\cdot kg\cdot s^{-2}$
$\boldsymbol{\tau}_m$	Electromagnetic stress tensor in iron	$m^{-1}\cdot kg\cdot s^{-2}$
τ_m^{air}	Electromagnetic stress tensor in air	$m^{-1}\cdot kg\cdot s^{-2}$
θ	Angle	$m\cdot m^{-1}$
$\mathbf{u}$	Displacement vector	m
$\mathbf{u}^k$	Column vector of displacements	m
u	Specific internal energy	$m^2\cdot s^{-2}$
$\mathcal{U}$	Internal energy	$m^2\cdot kg\cdot s^{-2}$
$\mathbf{v}_r^k$	Column vector of bar potential differences	$m^2\cdot kg\cdot s^{-2}\cdot A^{-2}$
v	Volume per unit mass	$m^3\cdot kg^{-1}$
$\mathbf{v}$	Velocity	m^2
V	Volume	m^3
$\mathbf{W}$	Matrix for connection of the stator winding	*dimensionless*
$\mathbf{w}$	Vector of weight functions	*dimensionless*
$\mathcal{X}$, $\mathcal{X}_{mag}$, $\mathcal{X}_{mec}$	Matrixes	*not predefined*
$\boldsymbol{\chi}$	Magnetic susceptibility	*dimensionless*
ψ	Helmholtz free energy	$m^2\cdot s^{-2}$
$\mathcal{Y}$	Matrix	*not predefined*

Remark: the units for the vectors and tensors are given for their coefficients.

Operators

$\mathcal{L}$, $\mathcal{L}'$	Linear operators
$\mathbf{X}^T$	Transpose of $\mathbf{X}$
$\boldsymbol{\nabla}\cdot$	Divergence operator
$\boldsymbol{\nabla}\times$	Rotational operator
$\boldsymbol{\nabla}$	Gradient operator
tr($\mathbf{X}$)	Trace of $\mathbf{X}$
:	Tensor product between two tensors
$\otimes$	Product of two vector fields resulting into a tensor

Notes on font types and subscripts

- Vectors, vector fields, tensors and matrixes are all typed in bold, e.g. $\mathbf{B}$, $\boldsymbol{\varepsilon}$, etc…

- Scalar functions, varying parameters are all typed in italic, e.g. ψ, λ, etc…
- Constants are all typed in normal font, e.g. μ_0.
- Subscripts *x* and *y* used within a vector quantity refer respectively to the *x* and *y* component of that quantity in a Cartesian coordinate system.
- Subscripts r and θ used within a vector quantity refer respectively to the radial and tangential component of that quantity in a polar coordinate system.
- Subscripts r and s within a matrix quantity refer respectively to the rotor and the stator.

Trademarks and abbreviations

COMSOL Multiphysics® is a registered trademark of COMSOL, Inc.

MATLAB® is a registered trademark of MathWorks™, Inc.

LabVIEW ® is a registered trademark of National Instruments, Inc.

MAXWELL® is a registered trademark of Ansoft Corportation™.

FCSMEK is a program for analysing synchronous and asynchronous radial-flux machines developed at the Department of Electrical Engineering, Aalto University School of Science and Technology.

1-D, 2-D and 3-D stand for one-, two- and three-dimensional.

Chapter 1

Introduction

This chapter outlines the field of study and presents the purpose and scientific contributions of the energy-based magneto-mechanical model for electrical steel sheets. As an introduction to the subject, general definitions are established.

1.1 General considerations

In the industrial design of rotating electrical machines and transformers, noise and vibrations are difficult to deal with. Electrical machines consist mainly of a stationary stator and a rotor rotating around its axis. They convert electrical energy into magnetic energy, which itself is transformed into mechanical energy or vice-versa. When the challenges in the design of these machines are being formulated, three main factors come into consideration: loss and noise reduction and reliability. The first point lies beyond the direct scope of this research. The latter two are indirectly covered within this work. That is, reliability is considered trivial when designing codes to assess the accuracy of an electrical machine. Noise is a consequence not only of vibrations but also of magnetostrictive effects in electrical steel sheets. It has been ascertained for example that noise in transformers, built of grain-oriented electrical steel sheets is related to magnetostriction.

Nowadays, the numerical analysis of the behaviour of complex time-dependent systems within a short simulation time is achievable as a result of improvements in the speed of computers.

Magnetostriction and its related effects have attracted the attention of scientists for more than 150 years. Existing in most known magnetic materials, this phenomenon is observed at a grain level and depends on the studied material. Since such research has high interdisciplinary characteristics, it has been on the borderline between thermodynamics, mechanics, measuring techniques, and magnetism. Each work has

been unique and brought further insights into magneto-mechanical coupling methods, measurements, and constitutive equations.

Moreover, magnetostriction has been extensively treated as a force acting inside the iron core. In electrical machines, forces of magnetic origin include electromagnetic forces inside the iron core and at the iron-air boundary. They act, for example, in the air gap between the rotor and the stator.

Addressing the shortages in previous studies, this thesis provides a model for coupling the magnetic and mechanical constitutive equations with the aim of studying the behaviour of the 2-D cross-sectional geometries of electrical machines. The model is developed within the frame of the research and integrated into finite element software. Its validity is examined with results from experimental machines. Furthermore, the robustness of the method resides in its ability to simulate rotating electrical machines, with the knowledge of seven parameters characterising the magneto-mechanical behaviour of the electrical sheets they are composed of. Measurements to identify these parameters are performed.

1.2 Aim

The purpose of this study is to model magneto-mechanical coupling in ferromagnetic materials. This thesis examines the influence of strains attributed to magnetic fields and stresses on the mechanical and magnetic behaviour of electrical steel sheets. Within this framework, four major questions, which will be answered in the final Chapter 6, are considered.

(1) Can an energy-based magneto-mechanical model be fully implemented and operational for the computation of electrical machines?

(2) How can we account for the effects of magnetostriction and magnetic stress tensors in iron, as well as the electromagnetic stress tensor in air? Can these effects be separated? What is the contribution of each of these?

(3) How can we compare measurement techniques and verify the validity of the study with appropriate devices?

(4) Is it possible to produce a solid computational-based and measurement-based tool for the further investigation of magneto-mechanical problems in electrical machines?

1.3 Scientific contributions

The scientific contributions are divided into seven distinctive parts.

(1) An energy-based magneto-mechanical model is derived. The coupling takes place through magneto-mechanical constitutive equations. The model was established in collaboration with the Department of Structural Engineering and Building Technology at Aalto University.

(2) A finite element procedure to couple non-linear mechanical to non-linear magnetic problems for the application of rotating machinery is developed.

(3) The influence of the effect of electromagnetic stress and magnetostriction within the iron is studied and extended to the computation within the air gap of electrical machines in order to evaluate their importance.

(4) A measurement system for predicting dynamic hysteresis loops within a magnetic material is designed and built and magnetostrictive curves are measured with strain gauges under rotating magnetic field at zero external stress. The results are compared with measurements on a modified Epstein frame.

(5) A dynamic recurrence scheme is implemented, which studies the displacements caused by the different components of the total stress in electrical machines.

(6) Simulated results are verified on a test device that accounts for stresses of magnetic origin only; no air gap is present. The measurements of displacements on the outer surface caused by internal forces in iron are compared with computed results.

(7) Verifications for the inclusion of the effect of electromagnetic stress in the air gap are performed on a test electrical machine. The displacements on the outer surface of the stator of this experimental asynchronous machine are measured. The existing additive contribution of the electromagnetic stresses in the air gap is thus considered.

1.4 Terminology

This section summarises the main concepts and defines the general terms that will be used through the work.

The focus is on modelling the effect of *magnetostriction* and *electromagnetic stress* in *ferromagnetic* materials. Accordingly, the definition of an energy function based on a *thermo-dynamical potential* is fundamental. The constitutive equations are coupled magneto-mechanically in Chapter 3. The material is considered not to be linear from the magnetic and mechanical points of view and the *Cauchy stress tensor* or *elasticity tensor* is rewritten because of its dependence on the magnetic field. An extensive discussion regarding the coupling methods for magneto-mechanical problems is given later in this work.

1.4.1 Ferromagnetism

Ferromagnetism is a property of materials such as iron that enables interaction with magnets to take place. Ferromagnetic materials have a crystal structure. Hence, they are subdivided into grains with a uniform crystal structure but with possible different magnetic orientations.

At equilibrium, the magnetic dipoles are not necessarily aligned and form different areas within each grain. These areas are called the magnetic domains. The region where the magnetisation flips is the domain wall or the Bloch wall, after the name of the researcher, Bloch (1932), who first observed that a ferromagnetic crystal consists magnetically of elementary regions. In Figure 1.1, the walls separating the grains are shown with dotted lines. Landau (1935) pointed out that the elementary regions should be considered as elementary layers.

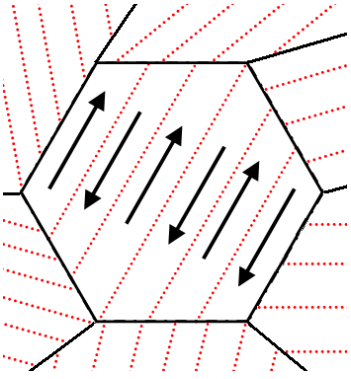

Figure 1.1: Structure of a grain with different orientations of the magnetic domains.

These alignments occur only below the Curie temperature, which for pure iron is 1043 K. The domain theory was developed in an extensive paper by Kittel (1949) that also introduces experiments, common at that time to underline his arguments.

1.4.2 Magnetostriction

In 1842, Joule discovered that ferromagnetic materials have the property of changing their shapes when subjected to a magnetic field (Joule, 1847). When an external magnetic field is applied to a piece of iron, the walls between the domains tend to move. The domains with a magnetic orientation in the same direction as the one of the magnetic field tend to grow at the expense of the others, as in Figure 1.2 (b). At saturation, 90^o domains disappear and there is a rotation of the self-magnetisation. These microscopic movements tend to change the shape of the material, thus introducing internal strains.

When some materials are magnetised, an increase or decrease in their length may be observed. The first type of materials thus has a positive magnetostriction, and the second type a negative magnetostriction. This increase in length is depicted in Figure 1.2 (b). There, l_0 is the initial length of the specimen, l is the final length, and Δl is called the elongation. It should be noted that materials such as Terfenol-D have the property of being giant magnetostrictive materials. This means that they are severely deformed under an external magnetic field.

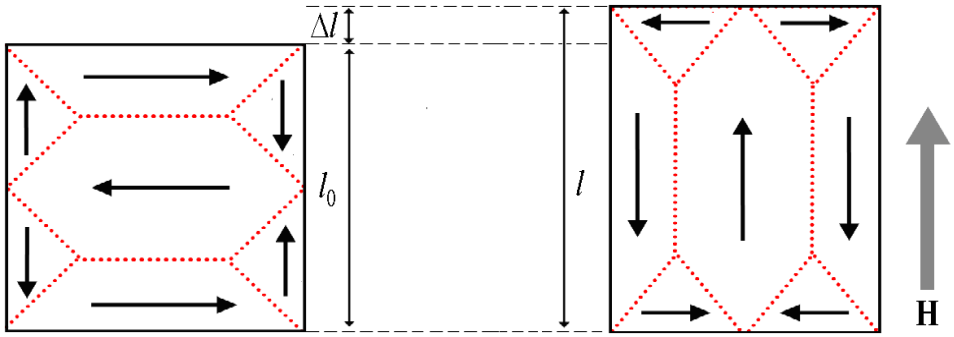

(a) Orientation of the magnetic dipoles in a piece of iron.

(b) Reorientation of the magnetic dipoles under external magnetic field, **H**.

Figure 1.2: Process of magnetisation in a ferromagnetic material.

1.4.3 Effects related to magnetostriction

Here, the effects related to magnetostriction are enumerated.

The inverse effect of the Joule magnetostriction is the Villari effect. Ferromagnetic materials have crystal symmetries. Therefore, theoretically an external stress will never by itself magnetise such a material in the absence of an external magnetic field (Lee 1955). However, anti-ferromagnetic materials being non-symmetric have the property of piezo-magnetism. When submitted to mechanical stress and not magnetised beforehand, this particular type of material produces a non-zero piezo-electric moment. Examples of anti-ferromagnetic materials are, for instance, Fe-Mn alloys.

In 1862, Wiedemann noticed that a torsion effect happens in a cylindrical shaft as a result of a helicoidal magnetic flux density when it was magnetised along the axis. This effect is commonly known as the Wiedemann effect. Its inverse is the Matteucci effect. These effects are widely discussed in the literature; see for example the book by du Trémolet de Lacheisserie (1993).

1.4.4 Magnetic forces

According to The IEEE Standard Dictionary of Electrical and Electronics Terms, a force is defined as "*any physical cause that is capable of modifying the motion of a body*" (Radatz, 1996). As it runs, a rotating electrical machine will be subjected to forces with various origins such as mechanical and magnetic ones.

Magnetic forces are classified in three groups. The first group gathers the predominant forces acting on the boundary regions from the air side onto the iron and which are commonly known as the reluctance forces or Maxwell forces. The second group contains the forces that find their source in the microscopic magnetic properties of the ferromagnetic material. Chapter 3 will focus primarily widely on these ones. The third group gathers the forces, called the Lorentz forces that act on currents in the magnetic field. This latter group will be omitted in this thesis.

1.4.5 Elasticity tensor

Tensors are understood throughout this work as a mathematical framework for formulating physical problems, such as the problem of elasticity. Tensors, Q x P, are mathematical objects in Q dimensions with P indices.

In the case of linear elasticity, $\boldsymbol{\sigma}$ being the Cauchy stress tensor, $\boldsymbol{\varepsilon}$ the strain tensor, and $\mathbf{C}$ the elasticity tensor, Hooke's law (e.g. in Zienkiewicz, 1967) is defined, generally as

$$\boldsymbol{\sigma} = \mathbf{C} : \boldsymbol{\varepsilon} \tag{1}$$

$$\sigma_{ij} = C_{ijkl}\varepsilon_{kl}\,. \tag{2}$$

Under the hypothesis of isotropy, the elasticity tensor becomes:

$$C_{ijkl} = K\delta_{ij}\delta_{kl} - G\left(\delta_{ik}\delta_{jl} + \delta_{il}\delta_{jk} - \frac{2}{3}\delta_{ij}\delta_{kl}\right). \quad (3)$$

In this definition, δ_{ij} is the Kronecker delta, K is the elastic bulk modulus, and G is the shear modulus. K gives a measure of the size of the external force that will be needed to modify the volume of the sample by a certain percentage. G gives a measure of the response of the material to external shearing strains.

1.4.6 Thermodynamic potentials

For deriving phenomenological non-linear constitutive laws of magnetostrictive materials, the need to derive an energy function is fundamental. For this reason, the major thermodynamic equalities are presented here in summary. Books such as Van Wylen (1981) describe the basic theory of thermodynamics and its applications in detail.

For a transformation that is reversible and quasi-static, the first and second laws of thermodynamics together stipulate that

$$d\mathcal{U} = Td\mathcal{S} - pdV\,. \quad (4)$$

In other words, the infinitesimal energy added by heating the system, here $Td\mathcal{S}$, equals the sum of the infinitesimal work pdV and the internal energy $d\mathcal{U}$.

Two types of energy are introduced under specific conditions. The first one is the Helmholtz free energy, which measures the process-initiated work that is obtained from a closed isothermal and isochoric system and is defined as

$$\psi = u - Ts\,, \quad (5)$$

where u is the internal energy per unit mass and, s is the entropy per unit mass. The second one is the Gibbs free energy, which measures the process initiated work that is obtained from a closed isobaric and isothermal system and which is defined as

$$g = h - Ts \quad (6)$$

where the enthalpy per unit mass is:

$$h = u + pv\,. \quad (7)$$

Specific conceptual terminology that has not been defined here will be presented as the thesis develops. In fact, the purpose of this section was to be precise and concise and to give the main tools for reading the work.

1.5 Outline

The thesis is divided into six chapters.

Chapter 1 puts the topic of the study by presenting general information regarding the main issues. The motive for this work is described, as are the scientific contributions of the research.

Chapter 2 details the background of the essential research in interdisciplinary topics that are needed to cover this research topic. The chapter reviews previous work, analysing, among others, different approaches to modelling magneto-mechanical coupling and ways to measure magnetostriction.

Chapter 3 concentrates on the local magneto-mechanically coupled model, the approach used for its derivation, the method used for finite element implementation and general results from basic geometries to intricate 2-D rotating electrical machines.

Chapter 4 focuses on the measurement of the magneto-mechanical properties of electrical steel sheets. Experimental setups designed and built within the scope of the research are described and their major results are presented and analysed. The chapter concentrates on extracting the required data from the measurements in order to obtain the parameters needed for the model presented in Chapter 3.

Chapter 5 aims at justifying the research presented in Chapters 3 and 4 by describing a novel test device and its design, building, and results, as a verification method for the theory and hypothesis used in the previous chapters. In addition, measurements conducted on a test induction machine are analysed. All the measurements are compared with numerical calculations.

Chapter 6 summarises the achievements of the research. The work presented throughout the thesis is assessed and concluded. The discussion includes the insights gained in the literature review in Chapter 2 and questions that arose in the thesis and are left open for further study. Additional attention is paid to three topics, which are the supplementary developments in measuring systems and in finite element modelling, and the further investigation of theoretical models for coupled problems.

Chapter 2

Overview of previous relevant research

The study of coupled problems has evolved not only into an essential aspect of modelling the behaviour of electro-sensitive components but also into understanding complex effects arising in electrical machines. Coupled problems include the treatment of two or more interconnected phenomena in two manners: simultaneously or by post-processing. This will be discussed in more detail later in this literature review. The major coupled problems solve thermal, mechanical, fluid dynamics and/or magnetic field equations. This literature review is primarily concerned with the coupling of magnetic and mechanical fields.

Section 2.1 presents specific problematic matters related to the stresses occurring or existing in electrical steel sheets. The noise arising from magnetostriction and intrinsic electromagnetic forces and the vibrations are briefly surveyed. Section 2.2 examines the established major theories on how to model the coupled magneto- and electro-mechanical phenomena. In parallel, the next section explores the methods associated with these models on computing non-linear coupled problems through an appropriate finite element procedure.

Physical models commonly require extensive measurements to extract the needed parameters characterising the studied material. Therefore, Section 2.3 introduces the problem of 1-D and 2-D magnetic measurements before casting a glance at “coupled” experimental setups. These setups aim at evaluating the effect of strain and/or stress on magnetic fields and vice versa.

2.1 Importance of the study of the magneto-mechanical properties of electrical steel sheets

This section provides the reason for this dissertation. The phenomenon of magnetostriction is clarified based on the definition in Chapter 1. Factors influencing

the properties of electrical steels guaranteeing the good functioning of rotating electrical machines are presented. A central concern in those machines and transformers is the study of vibrations and noise, which are reviewed.

The first studies on magnetostriction date back to the middle of the 19th century. Joule (1847) investigated the influence of magnetic fields on the dimensions of steel bars. An examination of the excellent reviews presented in Kittel (1949) and Lee (1955) offers an exhaustive introduction and detailed definitions. Specifically, magnetostriction is a property of ferrites and alloys and has been analysed extensively, for instance by Bozorth (1951) and Kikuchi (1968).

Focusing on some of the first attempts to characterise the phenomenon, Bozorth (1945) applied cyclic stresses to samples of iron-nickel alloys and stated that the change in induction can be attributed to the stress dependence on saturation magnetostriction; saturation magnetisation and the crystal anisotropy constant. Brown (1949) derived theoretical magnetisation-stress curves based on equivalent fields acting in the same way as small stresses on domain walls. Later, in the ’70s, studies suggested taking into account a possible discontinuous change in domain structure under stress (Craik et al., 1970 and Briss et al., 1971).

Stress and temperature are the main factors affecting the magnetic properties of ferromagnetic materials. The degradation of the steel is obvious in a region affected by punching, welding, pressing and cutting. Local plastic strains and residual stresses modify the magnetic properties and increase the losses.

Takezawa et al. (2006) studied the domain structure of Fe-Si electrical steel sheets for motor applications before and after the punching process. Their experimental results indicated that the shear stress accounted for by the punching process reduces the in-plane permeability to a distance equal to the thickness of the sheet.

Ossart et al. (2000) measured the magnetic properties of an annealed and non-annealed quarter of a stator and observed a clear difference in the average induction for a given feeding current. Their measurements were in accordance with the finite element analysis where a refined mesh on the critical regions was used.

Meanwhile, Schoppa et al. (2000a) investigated the influence of different grades of non-oriented electrical steels on the manufacturing of electrical machines. High Si-alloyed grades are more sensitive to the processing steps. The study concluded that the cutting process is the most critical and increases the losses by up to 35% in some cases (Schoppa et al., 2000b). Later on, experiments were conducted on a toroïdal core in Schoppa et al. (2003). Losses resulting from the different assembling processes were sequentially evaluated and this time the welding process increased the

losses by 20% to 27% and the cutting only by 17% as the toroïd had fewer deteriorated areas as a result of this last process.

Moses et al. (1989) determined the loss repartition on an annealed (stator 1) and non-annealed (stator 2) stator core geometry through measurements using thermal probes. The set of data obtained by applying a compressive stress to the outer surface of stator 1 experiences an increase in the losses with increasing stress. The same observations were made with stator 2; however, the losses are about 2.5 times higher at 0 MPa in this case.

These studies were conducted with the aim of understanding not only losses but also vibrations in electrical machines. Vibrations have various sources; they may be aerodynamic, electronic, mechanical, and magnetic (Vijayrghavan et al., 1998). A large amount of research work has been conducted in the field of vibrations originating from mechanical and magnetic problems, which have been studied and discussed intensively. Among others, Verma et al. (1987a, b) offer extensive theoretical and experimental approaches.

As it is directly related to the vibrations, it is essential to consider noise when designing electrical machines. Reyne (1987) stated that "*a numerical tool allowing the quantitative determination of noise and vibration levels of a machine is lacking*". Accordingly, Reyne (1987), Låftman (1995), Delaere (2002) and Belahcen (2004) studied the topic and concluded that noise originates from the deformation resulting from magnetisation in static machines and in the cores of rotating electrical machines.

The aim in this dissertation is to review only the vibrations that have their origin in the properties of the material, such as the effect of magnetostriction and electromagnetic forces within the iron. Knowledge of coupling problems is thus a central field of study based on the wide range of literature that discusses the topic. The matter of this work focuses on developing a magneto-mechanical model to understand the influence of stress in electrical steels, with a thorough discussion of the relevant topics being discussed. Thermal problems and loss-related matters are left aside, as are external stresses on the structure.

2.2 Coupled magneto-mechanical problems

Here, a discussion of the different ways to solve magnetic and mechanical field problems is presented. Because of their complexity and dependence on the structure that is being analysed, numerical methods are usually preferred to analytical ones. A review of finite element methods, especially those for rotating electrical machines is

provided. Finally, for the purpose of this dissertation, models for describing magneto- or electro-elastic materials are challenged.

2.2.1 Magneto-mechanical coupling methods

Different methods for coupling the mechanical and magnetic problems in electrical machines have been defined and used in previous research. A quick review of the understanding of different authors on the subject is investigated; and the terminology used depends on the researchers.

The coupling methods can be divided into *phenomenological* and *computational* couplings. First, phenomenological coupling is *local* or *global*. Local coupling means a coupling that physically describes the material by means of constitutive equations interacting with each other. Global coupling in the case of a magneto-mechanical problem is understood as the calculation of the new variables in the deformed geometry (Vandevelde et al., 2001 and Belahcen, 2004). Second, computational coupling, which is achieved by iterative schemes, can be *explicit* or *implicit* depending on the intricacy of the problem and the way the system of equations is formulated. The terms direct and indirect coupling are often used in this latter case and are understood differently by the authors.

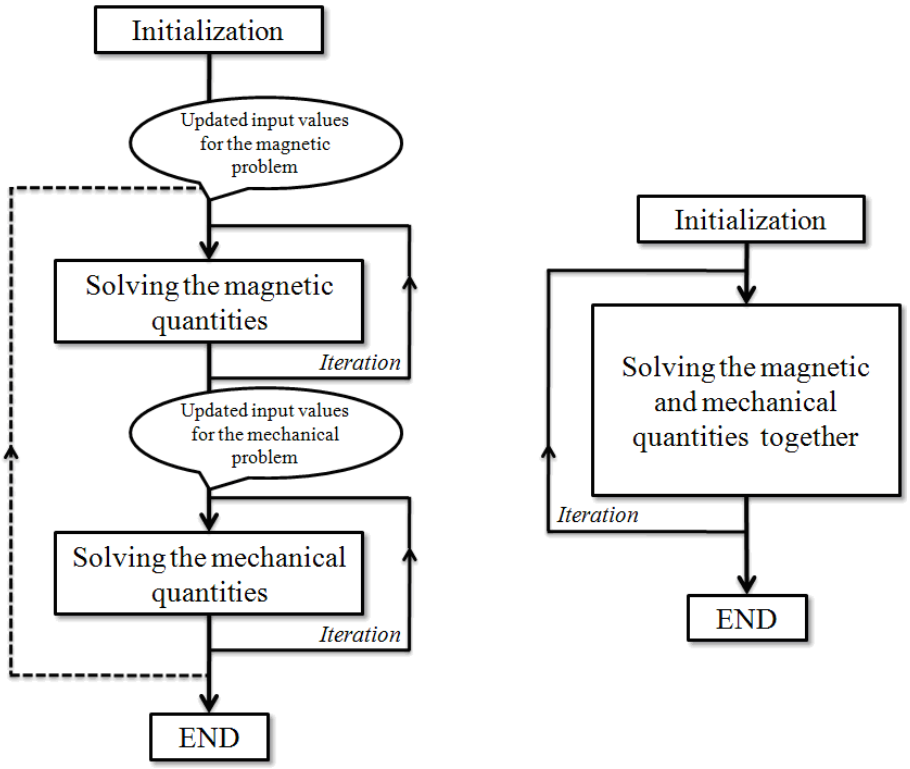

Figure 2.1: Schematic views of two different types of coupling methods.

The left-hand flowchart in Figure 2.1 presents a so-called *indirect* strong coupling according, for example, to Gros et al. (1998). This coupling is *strong* because the new magnetic input quantities are evaluated from the previous output mechanical quantities, through, for instance a set of curves setting the dependence. The iteration for solving mechanical quantities is generally not necessary when a linear problem is considered. In the case of an indirectly *weakly* coupled problem, the computation of the magnetic quantities and mechanical quantities is performed separately, often with different software such as in Låftmann (1995), Reyne et al. (1988) or Javadi et al. (1995). The right-hand flowchart in Figure (2.1) describes a *direct* coupling to solve the magnetic and mechanical equations simultaneously through suitable dependencies, such as the expression of the magnetostriction as a set of forces.

Belahcen (2004) proposed a hybrid method based, according to the author on a directly strong coupling method. The constitutive equations were coupled within the solver and forces were derived to account for the phenomenon of magnetostriction. The effect of the magnetostriction on the magnetic field was taken into account through the dependence of the reluctivity on the stress tensor (Fonteyn et al., 2006).

All methods are numerically acceptable. However, post-processing the mechanical quantities to calculate the new magnetic quantities does not describe the problem accurately. In fact, the magnetic and mechanical fields are inter-correlated and the solution of each is complementary.

2.2.2 Finite element method for rotating electrical machines

In the case of rotating electrical machines the use of 2-D or 3-D finite element tools is crucial, whether for the design process or purely research interest, as it gives an approximate overview of the operation of the machine. Those devices are genuinely complex and require the simultaneous computation of the thermal, mechanical and magnetic fields to create an accurate picture of the mechanisms. However, these coupling methods in 3-D or even in 2-D require a long period of computational time and a large amount of memory. In order to establish a historical background to the finite element method for rotating electrical machines, an introductory overview is given next.

In the finite element method, the partial differential equations of the magnetic field are formulated using the variational principle. The study region is divided into elements where the minimisation of the functional gives the required solution. The iron has nonlinear properties requiring an iterative solution process that is achieved through the fixed point method or the Newton-Raphson method as an example (Zienkiewicz, 1967). Chari (1980) applied the variational method to electrical

machinery and devices, feeding the coils directly with current. Some years later, Shen et al. (1985) and Strangas (1985) suggested a coupled method for simultaneously solving the circuit equations and the field equations and applied it to induction machines. They were followed by Arkkio (1987, 1988), Preston et al. (1988) and Vassent et al. (1990), who proposed in addition time-stepping schemes such as the Crank-Nicolson method with a changing mesh for representing the rotation of the rotor. Starting from the ’90s, coupled field analysis became an important topic of research. Finite element schemes were developed to solve magnetic, thermal or mechanical problems simultaneously or in a post-processing way (Zienkiewicz, 1967).

Within this work, a FORTRAN-based software that couples the magnetic field and circuit equations for analysing synchronous and asynchronous radial-flux machines is modified to include the mechanical effects on the magnetic field and vice versa.

The next section focuses on a coupled field problem that was addressed by numerous researchers, cited later in the text, in the last century: magneto-mechanical coupling. The complexity of the behaviour of iron subjected to an external magnetic field, and the numerous mechanical processes affecting the building and functioning of electrical machines, led research teams to focus on magneto-mechanical coupling methods.

2.2.3 Finite element methods for magneto-mechanical problems

The advances in coupling the magnetic and mechanical field problems are presented next. Here again, a large amount of work has been published regarding finite element models for magneto-elastic or mechanical coupled problems. The purpose is to summarise the major lines of research that are of interest for this thesis.

When dealing with forces inside an electrical machine, the literature is confusing, and different approaches exist. One may consider magnetostriction as a force acting on a piece of iron and define it as part of the magnetic forces.

Mainly, there are five distinctive formulations for calculating the force distribution in magnetic media: three methods of equivalent sources (equivalent currents, equivalent magnetic charges, and equivalent surface charges and currents), the method of the derivative of the energy or the virtual work method, and, finally, the electromagnetic stress tensor method. These are considered and compared by Sadowski et al. (1992) and Ren et al. (1994). These studies emphasised the differences in the force density evaluation resulting from the different methods. For the global force calculation, all methods give similar results when the mesh is fine

enough. For the local force calculation, Ren et al. (1994) conclude that the principle of virtual work is the most accurate one.

Reyne et al. (1987) presented a survey on the computation of magnetic forces and on the different ways to solve magneto-mechanical coupled models with finite elements. It was concluded that energy methods are beneficial for the modelling and challenges were set regarding the experimental setups for the determination of the parameters in the models that were developed. Later, in Reyne et al. (1988a, b), the authors suggested a simplified model implemented in finite element software, based on the principle of virtual work. Although limited to the linearity of the magnetic and mechanical properties, the study is supported by measurements on an Epstein frame. The calculations of the magnetic forces on the stator and rotor of a DC machine are plotted roughly but these attempts are nevertheless incomplete as a quantitative evaluation of the deformation is lacking.

Delince et al. (1991) took the Joule magnetostriction into account in the post-processing of the computation of the magnetic field. This effect was included into a force vector. Benbouzid et al. (1995) developed a computational method based on the "typical" dependence of **B** on **H** and on the mechanical stress and which expresses the magnetic field and mechanical strain using the "*Surface Spline Method*". Both sets of findings are incomplete as there were no measurements to corroborate the methods and model presented.

Meanwhile, Låftman (1995) concluded that the effect of magnetostriction in the iron cores of electrical machines has a relevant influence on the noise emitted. The method consisted of solving the field equations, and subsequently the elastic equations, with two distinctive pieces of software. A novel setup made of a pile of disks, where a hole was extracted and with slots to insert the windings into, was developed to validate the finite element analysis. However, the results of this device are questionable as the author failed to consider a leakage flux circulating in the air that introduces forces, due to the electromagnetic stress tensor in air on the inner boundary of the machine.

Following the definition of the authors, Body et al. (1997) suggested strongly coupled finite element method formulations to solve nonlinear magneto-mechanical problems for giant magnetostrictive materials. The first method was called the indirect strong coupling. The authors derived an analytical exponential formula to express **H** as a function of the stress tensor, $\boldsymbol{\sigma}$ and **B** and $\boldsymbol{\sigma}$ as a function of **H** and the strain tensor, $\boldsymbol{\varepsilon}$. In the second method, the direct strong coupling, the unidirectional magnetostrictive coefficient λ_x as a function of H_x is directly used. Hence the terms coupling the mechanical and magnetic quantities are directly introduced into the stiffness matrix. In fact, this approach solves the magnetic and mechanical quantities

explicitly, which is attractive for the purpose of this dissertation. However, at the time of the work, the authors had no material parameters from experimental work and the approach is not clearly justified physically. Gros et al. (1998) applied the latter method for modelling rods.

Besbes et al. (1996) define weakly coupled modelling as first solving the magnetic field equations, then extracting the magnetic forces that serve as an input for solving the mechanical equations. The permeability as a function of the stress is used to update the value of the magnetic field. A strong coupling method, where the computation of magnetic forces and mechanical stiffness matrix is needed, has been presented and applied to a 2-D magnetic field and elastic stress problem. This latter method, introduced in the papers of Ren et al. (1995) and Besbes et al. (1996), has the major advantage of converging more quickly.

In the same way as Body et al. (1997) did for giant magnetostriction materials, Mohammed et al. (1999) used a simple magnetostriction curve for a non-oriented Fe-Si sample. The same type of exponential formula was derived. The data were taken directly from the manufacturer. The numerical methods consisted of processing stress-dependent permeability curves and including them into the system of equations within the iteration process. This method was applied to permanent magnet motors (Mohammed et al., 2001). Later, a 1-D measurement setup was developed that enables magnetisation curves under several stress levels to be used as an input in the model described above (Mohammed et al., 2003). Here, no clear physical justification of the model is given, but measurements are used to support the work.

De Medeiros et al. (1998) compared different methods of calculating the global force on permanent magnets. The study claims that for 3-D finite element problems, methods based on volume integration, such as the virtual work method and the electromagnetic stress tensor, are the most precise ones. The electromagnetic stress tensor integrated over a surface is, however, faster.

Delaere et al. (2001a) computed magnetostrictive forces in a stator core with a similar approach but, additionally, investigated the influence of coupling terms. One coupling term is the variation in the elastic energy with respect to the variation in the magnetic vector potential. The significance of this term, related to magnetostriction is developed in Delaere et al. (2001b). Another term is related to magnetic forces. However, these terms tend to vanish as the authors express the contribution of magnetostriction and magnetic forces as extra terms added to the external forces. The authors model the strain caused by the magnetostriction as a set of forces, which gives an easy way to model this complicated effect but is inaccurate. Indeed, even if the relative elongation is modelled correctly, the magnetostrictive stress is null for a piece of iron with fixed boundaries, which does not describe the actual behaviour.

The same observation was made for free boundaries, where the total magnetostrictive stress is then different from the real case. The method described was applied to different types of electrical machines and transformers to get the displacements of the structure caused by each modelled force (Delaere, 2002). Similar observations as in previous research studies (Låftman, 1995 and Mohammed et al., 2002) were discussed, such as the positive effect of the magnetostriction on the noise of the electrical machines.

Vandevelde et al. (2001) challenged the usual way of treating magnetic forces and magnetostriction as two distinct phenomena. They introduced a free energy density, which was divided into a magneto-static energy, a magnetostrictive energy and an elastic energy (Vandevelde et al., 2002). In Vandevelde et al. (2008), the authors discussed the inclusion of a magnetic couple density originating, according to them, from anisotropy or magnetic hysteresis, for example. They also added a term that provides the magneto-elastic interaction to account for the magnetostrictive deformation resulting from a magnetic field on a body with mechanically fixed boundaries.

This latter approach gives a transition to the next subsection where energy-based models are discussed.

2.2.4 Energy-based models of magneto-elastic materials

Works by Toupin (1956) and later, Maugin (1988) were a great inspiration for further investigations in the field of magneto-mechanical coupling. The difficulty in this area of research resides mainly in getting a deep knowledge in interdisciplinary fields such as mechanics, thermodynamics, and magneto-dynamics to construct physically consistent, mathematically prevalent and numerically efficient models.

Previous researches focused on modelling the nonlinear constitutive equations for giant magnetostrictive materials. Different models were developed such as the standard square (SS) constitutive model, hyperbolic tangent (HT) constitutive model, and density of domain switching (DDS) constitutive model. The SS model, introduced by Carman (1995), involves writing the Gibbs energy function in a series form. The chosen independent variables are $\boldsymbol{\varepsilon}$ and $\mathbf{B}$. The dependence of the strain on the magnetic flux density for different pre-stresses is modelled correctly for low to moderate magnetic fields, where the strain is small or moderate too. However, for higher magnetic fields, the model does not approximate at all the saturation effect observed through experimental results. To overcome this limitation, the HT model was developed by Duenas et al. (1996). It expresses the Gibbs energy using the hyperbolic tangent function. Although the saturation effect could be represented, the

error between the modelled and experimental curves is large enough for this model not to be taken into consideration. The DDS model, suggesting that magnetic domain switching underlies magnetostrictive deformations, was published by Wan et al. (2003). The piezo-electric coefficient, i.e. the partial derivative of the strain tensor with respect to the magnetic field strength when the stress tensor is kept constant, is expressed by means of an exponential function that depends on the magnetic flux density and external stress. This function is the density function related to the domain switching density. The DDS model, similarly to the HT model does not approximate the phenomenon correctly.

Fang et al. (2004) derived a nonlinear constitutive model for the deformation of ferromagnetic materials. The independent variables chosen in this case are the stress tensor and the magnetic flux density and the Helmholtz free energy is expressed by use of the remanent stress and remanent magnetisation. The model fits the theoretical results and the experimental data for the magnetostrictive curve poorly.

The so-called "D-H model" was advanced by Liu et al. (2005); here, the internal energy density function is expressed as a function of $\mathbf{M}$, $\boldsymbol{\varepsilon}$, and the entropy, S . Here, the total strain was expressed as the sum of the elastic strain produced by a pre-stress and a component depending on both $\mathbf{M}$ and $\boldsymbol{\sigma}$. The model appeared to present accurate results for a Terfenol-D rod up to a certain magnetisation level. In Zheng et al. (2006), the same model was extended to the case of magneto-thermo-mechanical problems, so that the Gibbs energy density function is dependent on $\mathbf{M}$, $\boldsymbol{\sigma}$, and the temperature, T. The dependence of $\mathbf{M}$ on T was extracted from the theory of ferromagnetic materials.

A clearer perspective on the modelling of magneto-sensitive elastic solids (i.e. elastomers, and later piezo-electric materials) is provided by Dorfmann et al. (2003) and Dorfmann et al. (2004). They defined a Helmholtz free energy that accounts for the dependence of the magnetic field on the stress tensor and vice versa by introducing the dependence of parameters within the constitutive equations on an appropriately chosen set of invariants (Spencer, 1971), to represent the required behaviours. They adopted the formulation of the magneto-static Maxwell stress tensor following Tiersten (1964) and later Collet et al. (1974) and decomposed the total stress tensor into its symmetric and asymmetric parts. The symmetric part is known in classical mechanics as the Cauchy stress tensor, but is rewritten to take into account the coupling and the asymmetric part, also called the electromagnetic stress tensor. This asymmetry is discussed in Espinosa (2003). The equations were presented in the Lagrangian space, as well as in the Eulerian space, as the material deformations studied are not always negligible, especially in the case of piezo

materials. The stability of a half-space under constant deformation and an electric field is discussed in Dorfmann et al. (2008).

Recently, Zhou et al. (2009) presented a fulfilling non-linear coupled constitutive model. The theoretical model is developed with a similar approach as in Liu et al. (2004). The parameters needed are the maximum magnetostrictive strain, the saturation magnetisation, which is supposed to be equal to the saturation domain wall motion magnetisation, and the maximum susceptibility. The model was verified with measurements from Kururaz et al. (1973). The model, however, does not predict the experimental results accurately.

It should be noted that all these theories do not model the butterfly hysteresis behaviour of magnetostrictive materials. To overcome this shortage, Dapino et al. (1999) and later Linnemann et al. (2009), among others, developed simplified models. The first group of researchers introduced the effect of stress into the formulation of Jiles-Atherton to model the phenomenon of hysteresis in magnetostrictive transducers. The second authors defined a free energy function and a switching criterion, decomposed the stresses into a reversible and irreversible part and applied the model to ferromagnetic materials, including their hysteretic behaviour.

Within this dissertation, the energy-based approaches are privileged above the magnetic force methods for the reasons cited in Section 2.2.3. From this review it can be concludes that little research has been conducted on coupling the magnetic and mechanic constitutive equations for soft magnetic materials. Restricted studies attempted to justify these models. In particular, the implementation of such models turned out to be tediously lengthy. Nevertheless, they are the most rigorous and physically admissible approaches. Moreover, even less has been done on coupling magnetic fields and magnetostrictive strain through constitutive equations under different pre-stresses. Two major challenges arise from this review. The first is the need for measurements of magnetostrictive strain under pre-stresses, in the case of the study. The second is the definition of a suitable free energy to deduce the constitutive equations.

2.3 Measurement of magnetic and mechanical properties of electrical steel sheets

This section depicts the different measurement apparatuses used to determine the properties of magneto-elastic materials. First, methods for quantifying the hysteresis

curves and the first magnetisation curves of ferromagnetic materials are reviewed. Then the setups extended to the application of mechanical stress onto the samples are surveyed. Each time, the sensors used or developed for acquiring the desired quantities are evaluated.

2.3.1 Measurement of magnetic properties for modelling

Considerable research has been focused on the measurement of the magnetic properties of electrical steel sheets, not only from a computational but also from a measuring point of view. Indeed, almost all existing models require parameter identification on 1-D or 2-D measurement setups, such as single sheet testers; good examples combining 2-D measurements and computations can be found in Bergqvist et al. (1996) and Bergqvist (1994).

In electrical rotating machines, losses are divided into four main study areas: losses in iron, copper losses, field winding losses, and losses resulting from the mechanical friction. In the last three cases, there exist some well-established calculation methods. Energy is dissipated when a material is magnetised. The total amount of energy lost during the process depends on many internal and external factors, such as the microstructure of the material, the supply frequency, the direction of the magnetisation, and the geometry of the sheets. In statistical loss theory, the total losses in the iron are separated into three components: the hysteresis loss component, the classical loss component, and the excess loss component (Bertotti, 1998). All components are frequency- and magnetic flux density-dependent. Loss models such as the Jiles-Atherton model offer a phenomenological definition of hysteresis within electrical steel sheets. Other models, such as the Preisach model, try to approximate the phenomenon mathematically. Lately, tendencies to join both the mathematical approach and physical approach have been proved to be successful for modelling electrical machinery (Dlala, 2008).

Rotational single sheet testers (RSST) reproduce the magnetic flux patterns in an electrical steel sheet in the x-and y-directions. The dimensions of such devices are usually small, between 50 mm and 150 mm (e.g. Nakata et al., 1993 and Tumanski et al. 2001). Nencib et al. (1995) tested a larger vertical yoke system and concluded that the larger the yoke, the greater the uniformity in the sample. Two types of RSST are suggested for the measurements of magnetic properties: the horizontal type and the vertical type. As demonstrated by Nakata et al. (1993), with the vertical yoke type, higher magnetic flux densities are achieved and this yoke type reproduces the material properties with more accuracy. For this reason this configuration will be used later in this work. Further details regarding these setups are discussed, for

example, in Krismanic (1995) and in Sievert (1996), where the authors emphasised different methods to measure magnetic material properties with the aim of obtaining rotational power losses.

Models that characterise the magnetic properties of materials create suitable and efficient measurement setups. The subject is, however, vague and further literature discussion is found, for example, in Ivanyi (1997) and Berttotti (1998). The aim of this dissertation is to measure magneto-mechanical properties, mainly magnetostriction under pre-stresses.

2.3.2 Effect of applied stress on microstructure and power losses

Dijkstra (1953) first observed the changes in domain patterns under an applied stress up to plasticity on grain-oriented silicon steel. This research was inspiring for Corner (1964), who detailed a mechanism for the changes in the domains and successfully compared a theoretical approach and measurements made by applying tensile stress along the [110] and [100] directions on a microscopic domain level.

Yamamoto et al. (1972) studied the effect of tensile stress on losses on a single sheet tester. They measured and analysed the effect of applying external tensile stress in the rolling direction of a specimen and concluded that a similar tensile stress induced by surface coating might reduce losses. Later, Banks (1976) discussed the influence of normal stresses on magnetostriction.

Foster et al. (1984) investigated the dependence of the Steinmetz coefficient on small applied tensile stresses up to 8 MPa through measurements of oriented and non-oriented steels on an Epstein frame. How the stress was applied remains unclear; however, the results present an increase in the Steinmetz coefficient with increasing stress. In the case of non-oriented steels, the hysteresis losses decreased with increasing tensile stress.

Dąbrowski et al. (1989) applied longitudinal stress to a magnetised Fe-Si sample and observed that a compressive stress of 5 N/mm^2 or more affected the magnetisation curve significantly, increasing the total power losses. However, tensile stresses up to 15 N/mm^2 had the opposite effect.

Pitman et al. (1990) described the behaviour of B-H characteristics under stress by measuring B-H loops with a permeameter system. They presented the B-H characteristics under different stresses. For large compressive stresses, the saturation of the material occurs at lower magnetic fields than for null stresses.

These observations were later verified by LoBue et al. (1999), LoBue et al. (2000), and Pulnikov et al. (2004). Those works indicated a significant correspondence between the power losses and the stress applied. The loss increase

was noted as being around 50% for an increase in compressive stress of 20 MPa. Furthermore, Pulnikov et al. (2004) considered hysteresis losses under higher tensile stresses. The measurement presented a decrease of those losses until 50 MPa and then an increase. The 1-D measurement setup used for this purpose is described in detail in Pulnikov et al. (2004), Permiakov et al. (2005), and Permiakov et al. (2006).

It was established that under uni-axial stress loading, the properties of electrical steels deteriorate more under rotating than under alternating fields. Additionally, the calculated power losses from the measured B-H loops were much higher (Permiakov et al., 2004).

2.3.3 Techniques for magneto-mechanical measurements

Several techniques have been used to measure magnetostriction in electrical steel sheets. A brief overview is presented below.

Among those techniques, the strain gauge method, the capacitance method, the piezo-electric pick-up, and differential transformers are the most common ones in the case of a direct or semi-direct contact between the test specimen and the sensor. Optical techniques, such as the laser Doppler vibrometer, have also been developed. All these techniques are reviewed, for example, in Yastrebov et al. (1987) and, later, in Yabumoto (2009). The choice of one against another depends on the type of yoke preferred in the measurements, the sensitivity to magnetostriction, the specimen size, and the appropriate accuracy. In ribbons and wires, the field dependence of the shear modulus is usually measured by the pendulum method and the field dependence of the Young's modulus is measured by the magneto-mechanical resonance method or the vibrating reed method (Squire et al., 1996). Bozorth (1953) explored experimentally the phenomenon of magnetostriction for a Ni-Fe alloy. The strain gauge method was used to obtain the parameters for the simple model of magnetostriction described in detail in du Trémolet de Lachaisserie (1993). Because they are commonly accepted as accurate methods for measuring force, and hence magnetostriction, the strain gauge and the piezo-electric methods are adopted in this work. Another advantage of both is that they are easily accessible and can be put into place almost effortlessly.

As no standard is available yet, the different measurement setups that were developed to apply stress to a magnetised material are described below. Moreover, the techniques used to acquire the different quantities are presented.

In order to measure magnetostriction in 1-D with and without pre-stress, several setups have been recommended. Anderson et al. (2000) designed a system that allows cut samples to be inserted into a Tufnol former, closing the magnetic path by an

appropriate yoke, and applying external uni-axial stress with a cylinder whose pressure is controlled by electro-pneumatic valves. Mohammed et al. (2004a, b) measured the direct and inverse magnetostriction effect of electrical steel sheets with a specially designed setup that was inserted into a magnet and the sample was stressed. However, the application of the external stress remained vague. Belahcen (2004) modified the traditional Epstein frame to apply stress onto the samples and added load cells and used a force transducer to sense the magnetostriction. Hilgert et al. (2005) used a single sheet tester to magnetise the sample and applied external uni-axial stress by means of force cells. They measured the resulting deformation with strain gauges. For now, both methods to acquire the deformation in electrical steel sheets cannot be compared and critically analysed because of their inherent differences. In both cases, the authors depicted their measuring procedures carefully.

Measurement setups for characterising the properties of electrical steel sheets under biaxial stress have been discussed by many research studies. Among others, Utsunomiya et al. (1991) and Kashiwaya (1991) used cruciform specimens and developed non-destructive techniques to evaluate the stress in steels. The first authors acquired the magnetic field with a search coil placed around the magnetising yoke and magnetic field strength with a hall sensor. Kashiwaya (1991) designed a special procedure to measure additionally the magnetisation perpendicular to the surface. Previously, Langman (1990) applied stress by bending specimens of a similar shape held between two crosses made of Bakelite. Holes were drilled in the centre of the sheet to acquire the magnetic flux density. Langman et al. (2003) put forward a method to magnetise a specimen in the *z*-direction while stressing it in the *x*-and *y*-directions. The setup was composed of a magnetic circuit, a stressing rig, vanes, and coils placed at the desired positions. Hubert et al. (2005) conducted experiments on a redesigned cruciform sample placed into a tri-axial tensile and compressive machine and magnetised.

Under no applied external stress, researchers investigated the influence of a rotating magnetic field on the magnetostriction. Enokizono et al. (1990) and Enokizono et al. (1995) built a horizontal yoke system and measured the so-called "*dynamic rotating magnetostriction*". From these, Enokinozo et al. (1995) and, later, Pfützner et al. (1996) concluded that the magnetostriction in non-oriented steel sheets is higher under a rotating magnetic field, and also depends on the axis ratio.

In 1999, Lundgren measured 2-D magnetostriction responses from the excitation of a vertical yoke system. In his work, he used a laser interferometer, which gave acceptable results. Recently, measurements under a rotational flux have been investigated more carefully by Somkun et al. (2010). Their conclusions were similar to the previous ones.

2.3.4 Conclusion

Although much research has been conducted in the field of measuring the magnetic properties of magnetic materials, little is known regarding the accuracy of the results. Within this dissertation, attempts will be made to compare two measuring devices, the Epstein frame and the vertical yoke system, and two measuring methods, the strain gauge method and the force transducer. The need for measurements is a natural outcome of the formulation of the coupled model. Thus, the Epstein frame as modified by Belahcen (2004) is adopted for the measurements.

Following the idea of Lundgren (1999), measurements will be compared on a vertical yoke system built for the purposes of the study, based on the design and conclusions on a similar setup by Krah (2004).

2.4 Summary

The literature study presented above intended to provide a concise survey of the previous research. The first section reviewed the importance of the study of stress on iron. The second one examined the main achievements in the field of modelling the magneto-mechanical effect from a theoretical point of view. The third one explored research works regarding the computation of the phenomenon for electrical machinery. Finally, the fourth part enumerated the different approaches to force calculations.

Following the previous research described in this chapter, the topic of magneto-mechanical coupling has drawn a lot of attention from researchers all around the world for more than 100 years. The phenomenon of magnetostriction is due to the movement of domain walls and has a proven influence on the noise within the iron cores of transformers. Various measurement setups have been developed for 1-D magnetisation and uni-axial or bi-axial stresses; however, at the time of writing of this thesis, no standards are yet available. A clear lack of measurements of the behaviour of the properties of electrical steels sheets under 2-D magnetisation and biaxial stress has been noted. Such measurements would enable researchers to model the phenomena physically as accurately as possible.

Additionally, numerical schemes accounting for magneto-mechanical coupling are extensively available in the literature. Weakly coupled models offer the comfort of not requiring detailed constitutive equations. The approach of using magnetostrictive forces has been developed in a strong coupling scheme; however, they do not model the phenomenon accurately. Locally coupled magneto-mechanical

models for accounting for the phenomenon in electrical steel sheets, supported by the physical laws, are rarely presented.

On the basis of the literature review, this work will consider an original energy-based model for coupling the magnetic and mechanical quantities. This model will originate from the qualitative knowledge of the single-valued magnetisation curve on different pre-stresses and of the magnetostrictive strains on the pre-stress and magnetic field. The model should be identified from the experimental work and inserted into suitable finite element software.

Subsequently, such a method applied to the computation of the deformation of electrical machines requires verification using special devices. These verifications are usually inconsistent or even omitted in the literature. This is why, within this dissertation, the model is reinforced by experimental results on specifically built devices.

Chapter 3

Energy-based magneto-mechanical model

This chapter puts forward a way of modelling the magneto-mechanical properties of the material of steel laminations. In Section 3.1, the basic equations for the magnetic field, the electromagnetic stress tensor, and the equation of equilibrium of a magneto-elastic body are introduced. These will enable the model that is developed to be understood. The energy of the electromechanical system or the Helmholtz free energy is then derived. Consequently, the determination of the quantities needed, the magnetisation vector, and the Cauchy stress tensor is achieved. Section 3.2 describes how the model is implemented into a finite element scheme. FORTRAN-based software, which is primarily intended for the research and modelling of field problems in electrical machines, is used for this purpose.

Sections 3.3 and 3.4 supplement the work. In Section 3.3, the influence of the electromagnetic stress tensor in the air gap of electrical machines is added. In Section 3.4, the dynamic magneto-mechanical problem is formulated in such a way that the mass and damping of the mechanical system are considered.

3.1 Modelling the magneto-mechanical properties of electrical steel sheets

Among the approaches cited in Chapter 2, most of the constitutive relations were not coupled. Recently, Wan (2003) and Dorfmann (2005), for example, have introduced coupled models for solving general non-linear magneto-elastic solids. Dorfmann (2005) presented universal relations for coupling the magnetic field and the electrical field. Wan (2003) expressed a general non-linear constitutive model for piezo-

magnetism. In both cases, the approaches were interesting from a structural mechanics and computational point of view. The purpose here is to couple the magnetic and mechanical equations explicitly.

This section includes the development of the magneto-mechanical coupled model for finite element implementation. The balance equations for a magneto-elastic solid are derived, starting from the formulation of the Maxwell equations. The balance of linear momentum in continuum mechanics is then recalled. The constitutive equations of isotropic ferromagnetic materials are written on the basis of the Helmholtz free energy.

3.1.1 Magnetic field equations

The Maxwell equations govern the electric field and magnetic flux density and are expressed below for magnetic systems. In its differential form, Faraday's law of induction is

$$\nabla \times \mathbf{E} = -\frac{\partial \mathbf{B}}{\partial t} \tag{8}$$

and Ampere's circuit law

$$\nabla \times \mathbf{H} = \mathbf{J}_f + \frac{\partial \mathbf{D}}{\partial t}. \tag{9}$$

E is the electric field, **D** is the electric displacement, and $\mathbf{J}_f$ is the free current density. The right-hand term of (9) can be written with the help of **J**, which is the total current density, as

$$\mathbf{J} = \mathbf{J}_f + \frac{\partial \mathbf{D}}{\partial t}. \tag{10}$$

In this work, electromagnetic wave propagation is neglected. For this reason, in (9) the displacement current, $\partial \mathbf{D}/\partial t \simeq 0$. In addition, $\mathbf{J}_f$ is significantly larger than $\partial \mathbf{D}/\partial t$ in good conductors. The quasi-static approach of (9) is thus preferred.

In a vacuum, the electrical displacement is related to the electrical field through the permittivity of the vacuum, ε_0, and the magnetic flux density is related to the strength of the magnetic field through the magnetic permeability of the vacuum, μ_0

$$\mathbf{D} = \varepsilon_0 \mathbf{E} \tag{11}$$

$$\mathbf{B} = \mu_0 \mathbf{H}. \tag{12}$$

In a magnetised material the previous relation is not satisfied any more. The constitutive equations of the material are

$$\mathbf{B} = \boldsymbol{\mu}\mathbf{H} \tag{13}$$

$$\mathbf{J} = \gamma\mathbf{E}, \tag{14}$$

where $\boldsymbol{\mu}$ is the magnetic permeability tensor and γ is the conductivity of the material. In general, $\boldsymbol{\mu}$ is expressed with the magnetic susceptibility $\boldsymbol{\chi}$,

$$\boldsymbol{\mu} = \mu_0 \left(\mathbf{I} + \boldsymbol{\chi} \right). \tag{15}$$

$\boldsymbol{\chi}$ is positive for paramagnetic materials and negative for diamagnetic materials. It serves as the relationship between the magnetisation **M**, which is the quantity of magnetic moment per unit volume, and **H**, such that

$$\mathbf{M} = \boldsymbol{\chi}\mathbf{H}. \tag{16}$$

In ferromagnetic materials **M** is a nonlinear function of **H**. In addition, the phenomenon of hysteresis complicates (16). Here, a single-valued curve approach will be preferred because of its simplicity.

Finally,

$$\mathbf{B} = \mu_0 \left(\mathbf{H} + \mathbf{M} \right), \tag{17}$$

is obtained by injecting Equation (15) into (13) and taking (16) into account.

The Maxwell equations imply the existence of a vector potential **A**, and a scalar potential, ϕ, such that

$$\mathbf{B} = \nabla \times \mathbf{A} \tag{18}$$

$$\mathbf{E} = -\frac{\partial \mathbf{A}}{\partial t} - \nabla\phi. \tag{19}$$

A gauge convention is needed to assure the uniqueness of the potentials; a satisfactory one is the Coulomb gauge defined by

$$\nabla \cdot \mathbf{A} = \mathbf{0}. \tag{20}$$

3.1.2 Balance equations for a magneto-elastic solid

To deal with a magneto-mechanical problem, mechanical equations need to be coupled with the magnetic equations.

Omitting magnetic dependency for the moment, the general expression for the balance of linear momentum in continuum mechanics is

$$\rho\left(\frac{\partial \mathbf{v}}{\partial t} + \nabla\mathbf{v} \cdot \mathbf{v} \right) - \nabla \cdot \boldsymbol{\sigma} - \rho\mathbf{b} = 0, \tag{21}$$

where $\rho(\mathbf{x},t)$ is the mass density, $\mathbf{v}(\mathbf{x},t)$ is the velocity, $\boldsymbol{\sigma}(\mathbf{x},t)$ is the Cauchy stress, and $\rho\,\mathbf{b}$ is the body force density. In the case of a magneto-mechanical problem, the latter term is

$$\rho\mathbf{b} = \mathbf{f}_{\text{mag}} + \mathbf{f}_{\text{mec}} + \mathbf{f}_{\text{inert}}\,, \tag{22}$$

where $\mathbf{f}_{\text{mag}}$ is the electromagnetic body force, $\mathbf{f}_{\text{mec}}$ is the mechanical body force, and $\mathbf{f}_{\text{inert}}$ is the total inertial force. All three forces are expressed per unit volume in a domain V delimited by its boundary surface S.

In a stationary case, (21) becomes

$$-\nabla\cdot\boldsymbol{\sigma} - \rho\mathbf{b} = 0\,, \tag{23}$$

which is the system of equations of equilibrium for a magneto-mechanical material.

The electromagnetic body force is expressible as the divergence of the electromagnetic stress tensor, $\boldsymbol{\tau}_{\text{m}}$, in magnetised matter, under the hypothesis of a magneto-static problem such that

$$\mathbf{f}_{\text{mag}} = \nabla\cdot\boldsymbol{\tau}_{\text{m}}\,. \tag{24}$$

Besides its mathematical definition of being a second-order tensor, $\boldsymbol{\tau}_{\text{m}}$ is understood as being the stress tensor of an electromagnetic field. This brings us back to the definition of a stress tensor in Chapter 1. This tensor appears when the Lorentz force for an unknown charge distribution is written in terms of the electrical field, magnetic field, and strength of the magnetic field. This equation, defined for example in Kovetz, 2000, is

$$\boldsymbol{\tau}_{\text{m}} = \mu_0^{-1}\left(\mathbf{B}\otimes\mathbf{B} - \frac{1}{2}(\mathbf{B}\cdot\mathbf{B})\mathbf{I}\right) + (\mathbf{M}\cdot\mathbf{B})\mathbf{I} - \mathbf{B}\otimes\mathbf{M}\,. \tag{25}$$

The dyadic symbol $\otimes$ refers to the product of two vector fields resulting in a tensor. $\mathbf{I}$ is the identity tensor.

An essential point to emphasise is that neither the Cauchy nor the electromagnetic stress tensors within the material are symmetric. However, by summing both components, a symmetric total stress tensor $\boldsymbol{\tau}$, first defined by Tiersten (1960) is obtained:

$$\boldsymbol{\tau} = \boldsymbol{\sigma} + \boldsymbol{\tau}_{\text{m}}\,. \tag{26}$$

According to (24), Equation (23) is expressed as

$$-(\nabla\cdot\boldsymbol{\sigma} + \nabla\cdot\boldsymbol{\tau}_{\text{m}}) = \mathbf{f}_{\text{mec}} + \mathbf{f}_{\text{inert}}\,. \tag{27}$$

Considering the additive property of the divergence operator, the equation of equilibrium becomes

$$-\nabla \cdot \boldsymbol{\tau} = \mathbf{f}_{\text{mec}} + \mathbf{f}_{\text{inert}} . \tag{28}$$

Next, a formulation for $\boldsymbol{\sigma}$ and $\mathbf{M}$ will be sought.

3.1.3 Derivation of the energy function

Independent variables ought to be chosen in order to formulate the scalar energy density function per unit mass, ψ. In thermodynamics, this energy is the Helmholtz free energy. The chosen independent state variables are $\boldsymbol{\varepsilon}$ and $\mathbf{B}$. Stress $\boldsymbol{\sigma}$ and magnetization $\mathbf{M}$ are obtained from the local form of the Clausius-Duhem inequality by using the Coleman-Noll approach (Kovetz, 2000 -Chapter 15, section 53-), giving the expressions:

$$\boldsymbol{\sigma} = \rho \frac{\partial \psi}{\partial \boldsymbol{\varepsilon}} \tag{29}$$

$$\mathbf{M} = -\rho \frac{\partial \psi}{\partial \mathbf{B}} . \tag{30}$$

For isotropic solid the most general form of the free energy function depending on a second order tensor and a vector can be expressed by using the following six invariants:

$$I_1 = \text{tr}\boldsymbol{\varepsilon} \tag{31}$$

$$I_2 = \frac{1}{2}\left(\text{tr}\boldsymbol{\varepsilon}\right)^2 \tag{32}$$

$$I_3 = \frac{1}{3}\left(\text{tr}\boldsymbol{\varepsilon}\right)^3 . \tag{33}$$

The fourth invariant is chosen to represent the single-valued magnetisation curve. The fifth and sixth invariants account for the magnetostrictive curves as a function of the magnetic flux density

$$I_4 = \mathbf{B} \cdot \mathbf{B} \tag{34}$$

$$I_5 = \mathbf{B} \cdot \boldsymbol{\varepsilon} \cdot \mathbf{B} \tag{35}$$

$$I_6 = \mathbf{B} \cdot \boldsymbol{\varepsilon}^2 \cdot \mathbf{B} . \tag{36}$$

which form the integrity basis. The specific functional form in terms of these invariants is dictated by experimental results. The fourth invariant is crucial for describing the magnetization curve correctly; dependency from the fifth and sixth invariants determines the magnetostriction response. Assuming linear elastic behaviour, the energy should not depend on the third invariant I_3

$$\psi = \psi(I_1, I_2, I_4, I_5, I_6)\,. \tag{37}$$

The expressions for the Cauchy stress tensor (29) and the magnetisation vector (30) are

$$\boldsymbol{\sigma}=\rho \sum_{i=1,i\neq 3}^{6} \frac{\partial \psi}{\partial I_i}\frac{\partial I_i}{\partial \boldsymbol{\varepsilon}} \tag{38}$$

$$\mathbf{M}=\rho \sum_{i=1,i\neq 3}^{6} \frac{\partial \psi}{\partial I_i}\frac{\partial I_i}{\partial \mathbf{B}}\,. \tag{39}$$

After some manipulations the partial derivatives of the invariants are

$$\frac{\partial I_1}{\partial \boldsymbol{\varepsilon}} = \mathbf{I} \tag{40}$$

$$\frac{\partial I_2}{\partial \boldsymbol{\varepsilon}} = \boldsymbol{\varepsilon} \tag{41}$$

$$\frac{\partial I_5}{\partial \boldsymbol{\varepsilon}} = \mathbf{B}\otimes\mathbf{B} \tag{42}$$

$$\frac{\partial I_6}{\partial \boldsymbol{\varepsilon}} = \mathbf{B}\otimes\mathbf{B}\cdot\boldsymbol{\varepsilon} + \boldsymbol{\varepsilon}\cdot\mathbf{B}\otimes\mathbf{B} \tag{43}$$

$$\frac{\partial I_4}{\partial \mathbf{B}} = 2\mathbf{B} \tag{44}$$

$$\frac{\partial I_5}{\partial \mathbf{B}} = \mathbf{B}\cdot\boldsymbol{\varepsilon} \tag{45}$$

$$\frac{\partial I_6}{\partial \mathbf{B}} = \mathbf{B}\cdot\boldsymbol{\varepsilon}^2\,. \tag{46}$$

The following notation is used in later developments:

$$\frac{\partial \psi}{\partial I_i} = \psi_i\,. \tag{47}$$

Accounting for the derived partial derivatives, the Cauchy-like stress tensor and the magnetisation are

$$\frac{1}{\rho}\boldsymbol{\sigma} = \psi_1\mathbf{I} + \psi_2\boldsymbol{\varepsilon} + \psi_5\mathbf{B}\otimes\mathbf{B} + \psi_6\left(\mathbf{B}\otimes\mathbf{B}\cdot\boldsymbol{\varepsilon} + \boldsymbol{\varepsilon}\cdot\mathbf{B}\otimes\mathbf{B}\right) \tag{48}$$

and

$$-\frac{1}{\rho}\mathbf{M} = 2\psi_4\mathbf{B} + \psi_5\mathbf{B}\cdot\boldsymbol{\varepsilon} + \psi_6\mathbf{B}\cdot\boldsymbol{\varepsilon}^2\,. \tag{49}$$

The expression for the energy takes into account the hypothesis that, under no mechanical loading, the single-valued magnetisation curve is still obtained. Let us now substitute expressions (48) and (49) into (26) and (17) in order to obtain the expressions of the magnetic field strength

$$\mathbf{H} = \left(\mu_0^{-1} - 2\psi_4\right)\mathbf{B} - \psi_5 \mathbf{B}\cdot\boldsymbol{\varepsilon} - \psi_6 \mathbf{B}\cdot\boldsymbol{\varepsilon}^2 \tag{50}$$

and the total stress tensor

$$\begin{aligned}\boldsymbol{\tau} = {} & \rho\psi_1 \mathbf{I} + \rho\psi_2 \boldsymbol{\varepsilon} + \rho\psi_6 \left[\mathbf{B}\otimes\mathbf{B}\cdot\boldsymbol{\varepsilon} + \boldsymbol{\varepsilon}\cdot\mathbf{B}\otimes\mathbf{B}\right] \\ & + \left(\mu_0^{-1} + 2\rho\psi_4 + \rho\psi_5\right)\mathbf{B}\otimes\mathbf{B} - \left(\frac{1}{2}\mu_0^{-1} + 2\rho\psi_4\right)\left(\mathbf{B}\cdot\mathbf{B}\right)\mathbf{I} \\ & - \rho\psi_5\left(\mathbf{B}\cdot\boldsymbol{\varepsilon}\cdot\mathbf{B}\right)\mathbf{I} - \rho\psi_6\left(\mathbf{B}\cdot\boldsymbol{\varepsilon}^2\cdot\mathbf{B}\right)\mathbf{I} + \rho\psi_5\mathbf{B}\otimes\mathbf{B}\cdot\boldsymbol{\varepsilon} + \rho\psi_6\mathbf{B}\otimes\mathbf{B}\cdot\boldsymbol{\varepsilon}^2.\end{aligned} \tag{51}$$

The calculation of the trace of the total stress tensor

$$\mathrm{tr}\left(\boldsymbol{\tau}\right) = 3\rho\psi_1 + \rho\psi_2 I_1 - \left(\frac{1}{2}\mu_0^{-1} + 4\rho\psi_4 - \rho\psi_5\right)I_4 - 2\rho\psi_5 I_5 - 2\rho\psi_6 I_6 + 2\rho\psi_6 I_5 \tag{52}$$

sets constraints on the energy function.

Within this research, Fortino et al. (2007) and Belahcen et al. (2006) established a first version for the free energy, which has been finally slightly modified to get more accurate results. The chosen suitable form of the Helmholtz free energy function presented in (37) is (Belahcen et al. 2008)

$$\rho\psi = \frac{1}{2}\lambda I_1^2 + 2GI_2 + \frac{1}{2}\sum_{i=0}^{4}\frac{g_i(I_1)}{i+1}\left(\frac{I_4}{B_{\mathrm{ref}}^2}\right)^i I_4 + \frac{1}{2}\alpha_5 I_5 + \frac{1}{2}\alpha_6 I_6 . \tag{53}$$

The functions $g_i(I_1)$ with i= 1,...4 are obtained after some assumptions that will be discussed below. They are given in Equations (67) and (68). B_{ref} is a reference value for the magnetic flux density. The parameters α_5 and α_6 are material-dependent. Their values will be provided in the next chapter. The expressions for ψ_5 and ψ_6 are

$$\begin{aligned}\psi_5 &= \frac{1}{2\rho}\alpha_5 \\ \psi_6 &= \frac{1}{2\rho}\alpha_6 .\end{aligned} \tag{54}$$

Under the hypothesis of a purely elastic material with no magnetic loading, the matrix of elasticity should be recovered. The first Lamé parameter is

$$\lambda = \frac{E\upsilon}{\left(1+\upsilon\right)\left(1-2\upsilon\right)}, \tag{55}$$

and the shear modulus is

$$G = \frac{E}{2(1+\upsilon)}. \tag{56}$$

They are defined in the case of plane strain in (55) and (56) with the use of the material-dependent parameters E and υ. The modulus of elasticity E of an isotropic material is a measure of the stiffness of the material and υ is called the Poisson's ratio. Knowing the expression for ψ, a set of constraints on this energy is

$$\psi_1 = \frac{1}{\rho}\lambda I_1 + \tilde{\psi}_1(I_4) \tag{57}$$

and

$$\rho\psi_2 = 2G. \tag{58}$$

$\tilde{\psi}_1$ is such that the Maxwell reciprocal condition is verified

$$\frac{\partial\tilde{\psi}_1}{\partial I_4} = \frac{\partial\psi_4}{\partial I_1}.$$

Hence, ψ_4 is

$$\psi_4 = \frac{1}{2\rho}\sum_{i=0}^{4}\frac{g_i}{i+1}\frac{\partial I_4^{i+1}}{\partial I_4} \tag{59}$$

and $\tilde{\psi}_1$ is

$$\tilde{\psi}_1 = \frac{1}{2\rho}\sum_{i=0}^{4}\frac{1}{i+1}\frac{\partial g_i}{\partial I_1}I_4^{i+1}. \tag{60}$$

Small deformations are supposed throughout this work. Quadratic terms in the volumetric deformation (61) are thus omitted; (52) becomes

$$\mathrm{tr}(\boldsymbol{\tau}) = 3\lambda + 2\mu I_1 + 3\rho\tilde{\psi}_1 - \left(\frac{1}{2}\mu_0^{-1} + 4\rho\psi_4 - \rho\psi_5\right)I_4 - 2\rho\psi_5 I_5 + 2\rho\psi_6 I_5\ . \tag{61}$$

Under the same conditions of volume-preserving deformation in pure magnetic loading, the two set of constraints are extracted from (61)

$$3\rho\tilde{\psi}_1 - \left(\frac{1}{2}\mu_0^{-1} + 4\rho\psi_4 - \rho\psi_5\right)I_4 = 0 \tag{62}$$

and

$$-2\rho\psi_5 I_5 + 2\rho\psi_6 I_5 = 0. \tag{63}$$

Inserting (59) and (60) into (62), the identity

$$\frac{3}{2}\sum_{i=0}^{4}\frac{1}{i+1}\frac{\partial g_i}{\partial I_1}I_4^{i+1}=\left(\frac{1}{2}\mu_0^{-1}-\rho\psi_5\right)I_4+2\sum_{i=0}^{4}\frac{g_i}{i+1}\frac{\partial I_4^{i+1}}{\partial I_4}I_4, \tag{64}$$

is obtained and the set of two simple differential equations is extracted

$$\frac{\partial g_0}{\partial I_1}=\frac{2}{3}\left(\frac{1}{2}\mu_0^{-1}-\rho\psi_5\right)+\frac{4}{3}g_0 \tag{65}$$

$$\frac{\partial g_i}{\partial I_i}=\frac{4}{3}(i+1)\,g_i\text{, where } i=1,...4. \tag{66}$$

These enable the solution of each of them to be written as

$$g_0=\frac{3}{4}\alpha_0\exp(\frac{4}{3}I_1)-\frac{2}{3}\left(\frac{1}{2}\mu_0^{-1}-\rho\psi_5\right) \tag{67}$$

$$g_i=\frac{3(i+1)}{4}\alpha_i\exp(\frac{4(i+1)}{3}I_1)\text{, where } i=1,...4, \tag{68}$$

α_i with i= 0,...4, are five parameters depending on the properties of the material being studied.

The free energy is thus now fully defined.

3.1.4 Summary

The expressions of the total stress tensor and magnetic field strength have been derived. They are

$$\begin{aligned}\boldsymbol{\tau}(\mathbf{B},\boldsymbol{\varepsilon})=&\lambda I_1\mathbf{I}+\rho\tilde{\psi}_1(I_4)\mathbf{I}+2G\boldsymbol{\varepsilon}+\mu_0^{-1}\left(\mathbf{B}\otimes\mathbf{B}-\frac{1}{2}(\mathbf{B}\cdot\mathbf{B})\mathbf{I}\right)\\&+2\rho\psi_4\left(\mathbf{B}\otimes\mathbf{B}-(\mathbf{B}\cdot\mathbf{B})\mathbf{I}\right)\\&+\frac{\rho}{2}\alpha_5\left[\mathbf{B}\otimes\mathbf{B}\cdot\boldsymbol{\varepsilon}-(\mathbf{B}\cdot\boldsymbol{\varepsilon}\cdot\mathbf{B})\mathbf{I}\right]\\&+\frac{\rho}{2}\alpha_6\left[\mathbf{B}\otimes\mathbf{B}+\mathbf{B}\otimes\mathbf{B}\cdot\boldsymbol{\varepsilon}^2-(\mathbf{B}\cdot\boldsymbol{\varepsilon}^2\cdot\mathbf{B})\mathbf{I}+(\mathbf{B}\otimes\mathbf{B}\cdot\boldsymbol{\varepsilon}+\boldsymbol{\varepsilon}\cdot\mathbf{B}\otimes\mathbf{B})\right],\end{aligned} \tag{69}$$

and

$$\mathbf{H}(\mathbf{B},\boldsymbol{\varepsilon})=\mu_0^{-1}\mathbf{B}-2\rho\psi_4\mathbf{B}-\rho\frac{1}{2}\alpha_5\mathbf{B}\cdot\boldsymbol{\varepsilon}-\rho\frac{1}{2}\alpha_6\mathbf{B}\cdot\boldsymbol{\varepsilon}^2 \tag{70}$$

with the definitions of ψ_4 in (59) and $\tilde{\psi}_1$ in (60).

The complexity of these equations and the interdependency of the strain tensor and magnetic flux density make it logical to use the finite element method to solve them.

3.2 Magneto-mechanical finite element method

The primary purpose of this work is to discuss the coupled phenomenon for rotating electrical machines. When considering an uncoupled case, the finite element analysis of such devices is based on the approximation of the field solution. It is coherent to formulate the derived equations with the help of a numerical method based on the solution of the discrete system of equations.

3.2.1 Introduction

The Maxwell equations are recalled under the condition of quasi-static systems

$$\nabla \times \mathbf{E} = -\frac{\partial \mathbf{B}}{\partial t} \tag{71}$$

$$\nabla \times \mathbf{H} = \mathbf{J}\,. \tag{72}$$

The constitutive equations are non-linear; for this reason, the Newton-Raphson iteration is preferred so that (69) and (70) are written in the linear form

$$\mathbf{H}(\mathbf{B},\boldsymbol{\varepsilon}) = \mathbf{H}_0 + \frac{\partial \mathbf{H}}{\partial \mathbf{B}}\Delta\mathbf{B} + \frac{\partial \mathbf{H}}{\partial \boldsymbol{\varepsilon}}\Delta\boldsymbol{\varepsilon} + \mathrm{o}\left(\mathbf{H}\right) \tag{73}$$

$$\boldsymbol{\tau}(\mathbf{B},\boldsymbol{\varepsilon}) = \boldsymbol{\tau}_0 + \frac{\partial \boldsymbol{\tau}}{\partial \mathbf{B}}\Delta\mathbf{B} + \frac{\partial \boldsymbol{\tau}}{\partial \boldsymbol{\varepsilon}}\Delta\boldsymbol{\varepsilon} + \mathrm{o}\left(\boldsymbol{\tau}\right). \tag{74}$$

$\mathbf{H}_0$ and $\boldsymbol{\tau}_0$ are the initial values, $\Delta\mathbf{B}$ and $\Delta\boldsymbol{\varepsilon}$ are the iterative changes of the magnetic flux density and strain tensor, respectively, and $\partial\mathbf{x}(\mathbf{y},\mathbf{z})/\partial\mathbf{y}$ is the partial derivative of quantity $\mathbf{x}$ with respect to $\mathbf{y}$, assuming $\mathbf{z}$ to be constant. Finally, o(*****) stands for the higher-order terms of the quantity *****.

The solved nodal quantities for the finite element method are chosen to be the displacements in Cartesian coordinates (*x* and *y*-directions) or in polar coordinates (*r*- and θ-directions) and the magnetic vector potential. Hence, expressions (73) and (74) need to be expressed in the desired reference frame.

Those quantities are obtained from basic definitions from continuum mechanics and electromagnetics. First, the tensor field for a rigid deformation

$$\boldsymbol{\varepsilon} = \frac{1}{2}\left(\nabla \mathbf{u} + \nabla \mathbf{u}^{\mathrm{T}}\right) \tag{75}$$

is called the infinitesimal strain. $\nabla \mathbf{u}$ is the displacement gradient and is assumed to be small. A complete demonstration is found in Gurtin (1981). Second, the magnetic flux density is expressed as the rotational of a vector potential **A,** as discussed in Section 3.1.1:

$$\mathbf{B} = \nabla \times \mathbf{A}\,. \tag{76}$$

3.2.2 Variational formulation

The variational formulation of the coupled problem for the solution in the finite element method is now presented.

In magnetism, the weighted residual expression is obtained by multiplying Equation (72) by a weight function $\mathbf{w}$ and integrating it over a domain Ω:

$$\Re = \int_{\Omega} \left(\mathbf{w} \cdot \left(\nabla \times \mathbf{H}\right)\right) \mathrm{d}\Omega = 0\,. \tag{77}$$

Denoting **p** and **q** as vectors, the identity

$$\nabla \cdot \left(\mathbf{p} \times \mathbf{q}\right) = \mathbf{p} \cdot \left(\nabla \times \mathbf{q}\right) - \mathbf{q} \cdot \left(\nabla \times \mathbf{p}\right) \tag{78}$$

is applied to the integrand of (77), so that

$$\int_{\Omega} \left(\mathbf{H} \cdot \left(\nabla \times \mathbf{w}\right)\right) \mathrm{d}\Omega + \int_{\Omega} \left(\nabla \cdot \left(\mathbf{w} \times \mathbf{H}\right)\right) \mathrm{d}\Omega = 0\,. \tag{79}$$

Using the theorem of Gauss, (79) becomes

$$\int_{\Omega} \left(\left(\nabla \times \mathbf{w}\right) \cdot \mathbf{H}\right) \mathrm{d}\Omega + \int_{\partial\Omega} \left(\mathbf{w} \times \mathbf{H}\right) \cdot \mathrm{d}\mathbf{s} = 0\,. \tag{80}$$

This is the variational formulation of a field problem that has been derived extensively, for example in Silvester et al. (1983).

In mechanics, the principle of virtual displacements states that for any small virtual displacement on the body in equilibrium, the total internal virtual work equals the total external virtual work (e.g. Bathe, 1996). This is written in the following form:

$$\int_{\Omega} \hat{\boldsymbol{\varepsilon}}^{\mathrm{T}} \boldsymbol{\tau} \mathrm{d}\Omega = \int_{\Omega} \hat{\mathbf{u}}^{\mathrm{T}} \left(\mathbf{f}_{\mathrm{mec}} + \mathbf{f}_{\mathrm{inert}}\right) \mathrm{d}\Omega + \int_{\partial\Omega} \hat{\mathbf{u}}^{\mathrm{T}} \mathbf{f}_{\mathrm{surf}} \mathrm{dS}\,. \tag{81}$$

Replacing $\boldsymbol{\tau}$ and **H** by their linear expressions, (80) and (81) become

$$\int_\Omega \left((\nabla \times \mathbf{w}) \cdot \frac{\partial \mathbf{H}}{\partial \mathbf{B}} \Delta \mathbf{B} \right) \mathrm{d}\Omega + \int_\Omega \left((\nabla \times \mathbf{w}) \cdot \frac{\partial \mathbf{H}}{\partial \boldsymbol{\varepsilon}} \Delta \boldsymbol{\varepsilon} \right) \mathrm{d}\Omega = -\int_\Omega \left((\nabla \times \mathbf{w}) \cdot \mathbf{H}_0 \right) \mathrm{d}\Omega - \int_{\partial\Omega} (\mathbf{w} \times \mathbf{H}_0) \cdot \mathrm{d}\mathbf{s} \tag{82}$$

and

$$\int_\Omega \hat{\boldsymbol{\varepsilon}}^{\mathrm{T}} \frac{\partial \boldsymbol{\tau}}{\partial \mathbf{B}} \Delta \mathbf{B} \mathrm{d}\Omega + \int_\Omega \hat{\boldsymbol{\varepsilon}}^{\mathrm{T}} \frac{\partial \boldsymbol{\tau}}{\partial \boldsymbol{\varepsilon}} \Delta \boldsymbol{\varepsilon} \mathrm{d}\Omega = -\int_\Omega \hat{\boldsymbol{\varepsilon}}^{\mathrm{T}} \boldsymbol{\tau}_0 \mathrm{d}\Omega + \int_\Omega \hat{\mathbf{u}}^{\mathrm{T}} \left(\mathbf{f}_{\mathrm{mec}} + \mathbf{f}_{\mathrm{inert}} \right) \mathrm{d}\Omega + \int_{\partial\Omega} \hat{\mathbf{u}}^{\mathrm{T}} \mathbf{f}_{\mathrm{surf}} \mathrm{dS} \,. \tag{83}$$

These formulations are ready to be discretised.

3.2.3 Solution by the finite element method in 2-D

In Voigt notation, the strain tensor is simplified to a vector and in this work is named $\bar{\boldsymbol{\varepsilon}}$, such that

$$\bar{\boldsymbol{\varepsilon}} = \begin{bmatrix} \varepsilon_x & \varepsilon_y & 2\varepsilon_{xy} \end{bmatrix}^{\mathrm{T}}. \tag{84}$$

ε_x and ε_y are the normal strains in the *x*-and *y*-directions, respectively, and ε_{xy} is the shear strain.

Accordingly, (75) is rewritten in 2-D as

$$\bar{\boldsymbol{\varepsilon}} = \mathcal{L}\mathbf{u} \tag{85}$$

with the differential operator

$$\mathcal{L} = \begin{bmatrix} \frac{\partial}{\partial x} & 0 & \frac{\partial}{\partial y} \\ 0 & \frac{\partial}{\partial y} & \frac{\partial}{\partial x} \end{bmatrix}^{\mathrm{T}}. \tag{86}$$

Positioning the problem at an element level, the displacement vector has its two components in the *x*-direction (u_x) and *y*-direction (u_y)

$$\mathbf{u} = \begin{bmatrix} u_x & u_y \end{bmatrix}^{\mathrm{T}}. \tag{87}$$

The approximate solution $\mathbf{u}_k \approx \mathbf{u}$ of the displacements in one element is a linear combination of the matrix containing *n* basis functions $\mathbf{N}_i$:

$$\mathbf{u}_k = \sum_{i=1}^{n} \mathbf{N}_i \tilde{\mathbf{u}}_i \,, \tag{88}$$

where $\tilde{\mathbf{u}}_i = \begin{bmatrix} u_{x,i} & u_{y,i} \end{bmatrix}^{\mathrm{T}}$ are the nodal values of the displacement corresponding to the nodal point *i*. The basis functions are composed of polynomials in a piecewise fashion. In matrix notation, (88) is similar to

$$\mathbf{u}_k = \left(\mathbf{N}\tilde{\mathbf{u}}\right)^{\mathrm{T}}, \tag{89}$$

where **N** and $\tilde{\mathbf{u}}$ are:

$$\mathbf{N} = \begin{bmatrix} N_1 & N_2 & \cdots & N_n \end{bmatrix} \tag{90}$$

$$\tilde{\mathbf{u}} = \begin{bmatrix} u_{x1} & u_{x2} & \cdots & u_{xn} \\ u_{y1} & u_{y1} & \cdots & u_{yn} \end{bmatrix}^{\mathrm{T}}. \tag{91}$$

The approximated strain tensor becomes

$$\bar{\boldsymbol{\varepsilon}}_k = \mathcal{L}\left(\mathbf{N}\tilde{\mathbf{u}}\right)^{\mathrm{T}}. \tag{92}$$

A comparable approach is adopted for the magnetic vector potential. In 2-D, **A** is reduced to its *z* component. The following notation will be used: $\mathbf{A} = \mathbf{a} = a\mathbf{e}_z$.

With the help of an operator $\mathcal{L}'$ defined as

$$\mathcal{L}' = \begin{bmatrix} \dfrac{\partial}{\partial y} & -\dfrac{\partial}{\partial x} \end{bmatrix}^{\mathrm{T}}, \tag{93}$$

Equation (76) becomes

$$\mathbf{B} = \mathcal{L}'a. \tag{94}$$

Likewise, the approximated solution of the magnetic vector potential in one element is a linear combination of the matrix containing *n* basis functions N_i:

$$a_k = \sum_{i=1}^{n} N_i \tilde{a}_i. \tag{95}$$

In matrix notation, Equation (95) is

$$a_k = \mathbf{N}\tilde{\mathbf{a}}. \tag{96}$$

where $\tilde{\mathbf{a}}_i$ are the nodal values of the magnetic vector potential corresponding to the nodal point *i*

$$\tilde{\mathbf{a}} = \begin{bmatrix} a_1 & a_2 & \cdots & a_n \end{bmatrix}^{\mathrm{T}}. \tag{97}$$

The approximated magnetic flux density is such that

$$\mathbf{B} = \mathcal{L}'\mathbf{N}\tilde{\mathbf{a}}. \tag{98}$$

The Galerkin method is convenient for the solution of such variational problems; see, for instance, Bastos et al. (2003). Therefore, the basis functions are used as the weight functions, such that in 2-D

$$\nabla \times \mathbf{w} = \left(\mathcal{L}'\mathbf{N}\right)^{\mathrm{T}}. \tag{99}$$

Following these notations, (82) and (83) are handled. Under the hypothesis that the surface integrals vanish, they become

$$\int_{\Omega}\left(\left(\nabla\times\mathbf{w}\right)\cdot\frac{\partial\mathbf{H}}{\partial\mathbf{B}}\Delta\mathbf{B}\right)+\left(\left(\nabla\times\mathbf{w}\right)\cdot\frac{\partial\mathbf{H}}{\partial\boldsymbol{\varepsilon}}\Delta\boldsymbol{\varepsilon}\right)\mathrm{d}\Omega=-\int_{\Omega}\left(\left(\nabla\times\mathbf{w}\right)\cdot\mathbf{H}_0\right)\mathrm{d}\Omega \tag{100}$$

and

$$\int_{\Omega}\hat{\boldsymbol{\varepsilon}}^{\mathrm{T}}\left(\frac{\partial\boldsymbol{\tau}}{\partial\mathbf{B}}\Delta\mathbf{B}+\frac{\partial\boldsymbol{\tau}}{\partial\boldsymbol{\varepsilon}}\Delta\boldsymbol{\varepsilon}\right)\mathrm{d}\Omega=-\int_{\Omega}\hat{\boldsymbol{\varepsilon}}^{\mathrm{T}}\boldsymbol{\tau}_0\mathrm{d}\Omega\,. \tag{101}$$

Rewriting those equations according to the previously defined notations, these equations are

$$\int_{\Omega}\left[\left(\left(\mathcal{L}'\mathbf{N}\right)^{\mathrm{T}}\frac{\partial\mathbf{H}}{\partial\mathbf{B}}\mathcal{L}'\mathbf{N}\right)\Delta\tilde{\mathbf{a}}+\left(\left(\mathcal{L}'\mathbf{N}\right)^{\mathrm{T}}\frac{\partial\mathbf{H}}{\partial\boldsymbol{\varepsilon}}\mathcal{L}\mathbf{N}\right)\Delta\tilde{\mathbf{u}}\right]\mathrm{d}\Omega=-\int_{\Omega}\left(\left(\mathcal{L}'\mathbf{N}\right)^{\mathrm{T}}\mathbf{H}_0\right)\mathrm{d}\Omega \tag{102}$$

and

$$\int_{\Omega}\left[\left(\left(\mathcal{L}\mathbf{N}\right)^{\mathrm{T}}\frac{\partial\boldsymbol{\tau}}{\partial\mathbf{B}}\mathcal{L}'\mathbf{N}\right)\Delta\tilde{\mathbf{a}}+\left(\left(\mathcal{L}\mathbf{N}\right)^{\mathrm{T}}\frac{\partial\boldsymbol{\tau}}{\partial\boldsymbol{\varepsilon}}\mathcal{L}\mathbf{N}\right)\Delta\tilde{\mathbf{u}}\right]\mathrm{d}\Omega=-\int_{\Omega}\mathcal{L}\mathbf{N}\boldsymbol{\tau}_0\mathrm{d}\Omega\,. \tag{103}$$

In the basic theory of numerical methods, a discretised non-linear system is expressed, in the general form, as

$$\mathcal{Y}(\tilde{\mathbf{x}})\equiv 0\,. \tag{104}$$

This may be solved only iteratively. In this work, the Newton-Raphson method is adopted. The principle of this method is to correct the nodal values vector $\tilde{\mathbf{x}}_i$

$$\mathcal{Y}(\tilde{\mathbf{x}}_i+\Delta\tilde{\mathbf{x}}_i)=\mathcal{Y}(\tilde{\mathbf{x}}_i)+\left(\frac{\mathrm{d}\mathcal{Y}(\tilde{\mathbf{x}})}{\mathrm{d}\tilde{\mathbf{x}}}\right)_i\Delta\tilde{\mathbf{x}}_i\,, \tag{105}$$

where $\dfrac{\mathrm{d}\mathcal{Y}(\tilde{\mathbf{x}})}{\mathrm{d}\tilde{\mathbf{x}}}$ represents a tangential matrix. Hence, the improved value "$\tilde{\mathbf{x}}_i+\Delta\tilde{\mathbf{x}}_i$" is obtained by evaluating

$$\Delta\tilde{\mathbf{x}}_i=-\left(\frac{\mathrm{d}\mathcal{Y}(\tilde{\mathbf{x}})}{\mathrm{d}\tilde{\mathbf{x}}}\right)_i^{-1}\mathcal{Y}_i\,. \tag{106}$$

In the problem being considered, the tangential matrix can be straightforwardly expressed as

$$\frac{\mathrm{d}\mathcal{Y}(\tilde{\mathbf{x}})}{\mathrm{d}\tilde{\mathbf{x}}} = \int_{\Omega} \begin{bmatrix} \mathcal{L}'\mathbf{N} & 0 \\ 0 & \mathcal{L}\mathbf{N} \end{bmatrix}^{\mathrm{T}} \begin{bmatrix} \dfrac{\partial \mathbf{H}}{\partial \mathbf{B}} & \dfrac{\partial \mathbf{H}}{\partial \boldsymbol{\varepsilon}} \\ \dfrac{\partial \boldsymbol{\tau}}{\partial \mathbf{B}} & \dfrac{\partial \boldsymbol{\tau}}{\partial \boldsymbol{\varepsilon}} \end{bmatrix} \begin{bmatrix} \mathcal{L}'\mathbf{N} & 0 \\ 0 & \mathcal{L}\mathbf{N} \end{bmatrix} \mathrm{d}\Omega \,. \tag{107}$$

The solved quantities $\Delta\tilde{\mathbf{x}}$ and the residual vector $\mathcal{Y}(\tilde{\mathbf{x}}_i)$ are

$$\Delta\tilde{\mathbf{x}} = \begin{bmatrix} \Delta\tilde{\mathbf{a}} & \Delta\tilde{\mathbf{u}} \end{bmatrix}^{\mathrm{T}} \tag{108}$$

$$\mathcal{Y}(\tilde{\mathbf{x}}_i) = \int_{\Omega} \begin{bmatrix} \left(\mathcal{L}'\mathbf{N}\right)^{\mathrm{T}} & \mathcal{L}\mathbf{N} \end{bmatrix} \begin{bmatrix} \mathbf{H}_0 \\ \boldsymbol{\tau}_0 \end{bmatrix} \mathrm{d}\Omega \,. \tag{109}$$

The system is now fully discretised. However, this model is considered in iron only. Parts of electrical machines are made of materials such as copper, solid steels, aluminium and air. Other issues to be included are presented in the next section.

3.2.4 Overall system of equations

In the case of rotating electrical machines, the system of equations to be solved appears to be rather more intricate. Circuit equations are solved together with the magnetic and mechanical equations. A Crank-Nicolson time-stepping scheme is adopted to discretise the system, which is solved iteratively with the Newton-Raphson method (Figure 3.1). This system of equations is in matrix form

$$\begin{bmatrix} \boldsymbol{\Phi} & \mathbf{D}_{\mathrm{r}}^{\mathrm{T}} & \mathbf{D}_{\mathrm{s}}^{\mathrm{T}}\mathbf{W}^{\mathrm{T}} \\ \mathbf{D}_{\mathrm{r}} & \mathbf{C}_{\mathrm{r}} & 0 \\ \mathbf{W}\mathbf{D}_{\mathrm{s}} & 0 & \mathbf{G}_{\mathrm{s}} \end{bmatrix} \begin{bmatrix} \boldsymbol{\xi}^{k+1} \\ \mathbf{v}_{\mathrm{r}}^{k+1} \\ \mathbf{i}_{\mathrm{s}}^{k+1} \end{bmatrix} = \mathbf{h} \,. \tag{110}$$

$\boldsymbol{\xi}^{k+1}$ is the column vector of nodal values of the magnetic vector potential and nodal values of the displacements in x ($\mathbf{u}_x^{k+1}$) and in y ($\mathbf{u}_y^{k+1}$) direction at time step k+1, such that

$$\boldsymbol{\xi}^{k+1} = \begin{bmatrix} \mathbf{a}^{k+1} \\ \mathbf{u}_x^{k+1} \\ \mathbf{u}_y^{k+1} \end{bmatrix} . \tag{111}$$

$\mathbf{v}_{\mathrm{r}}^{k+1}$ is the column vector of the bar potential differences and $\mathbf{i}_{\mathrm{s}}^{k+1}$ is the column vector of the stator currents. Finally, **h** is the column vector that contains quantities from time step *k* and source terms from time step *k*+1. Matrices $\mathbf{C}_{\mathrm{r}}$, $\mathbf{G}_{\mathrm{s}}$, $\mathbf{D}_{\mathrm{r}}$, and $\mathbf{D}_{\mathrm{s}}$ couple the magnetic vector potential and the voltages and currents in the windings (Arkkio, 1987). Matrices $\mathbf{D}_{\mathrm{r}}$ and $\mathbf{D}_{\mathrm{s}}$ are extended with zeros in appropriate locations. **W** describes the type of connection of the stator winding. Indices r and s refer to the rotor and stator reference frames, respectively. The formulation of matrix $\boldsymbol{\Phi}$ cannot be expressed explicitly. In Section 3.2.3, this matrix has been indirectly discussed for elements in iron and in Section 3.2.4 for elements with nodes connecting air and iron. For elements in any other kind of material, the conventional assembly matrix **S** (Bastos et al., 2003), is included in $\boldsymbol{\Phi}$. Its expression at element level is

$$\mathbf{S} = \left[S_{ij} \right] = \int_{\Omega} \mu_0^{-1} \nabla N_i \cdot \nabla N_j \mathrm{d}\Omega . \tag{112}$$

Geometrical boundary conditions for the problem and the variables to be solved should be specified. They will be used to initialise the finite element procedure shown in Figure 3.1. The nodes with no degrees of freedom, which are the three nodal values (magnetic vector potential, and displacements in the x- and y-directions), are not going to be solved. These prescribed boundary conditions respectively, *a**, *u** and *v** are set in each of the examples presented later in the work and handled as in Bathe, 1996.

Finally, it should be specified that a switch between polar and Cartesian coordinates with the rotational matrix is enforced because the boundary conditions for the displacements are commonly specified in the radial and tangential or circumferential directions. This change is usual in mechanical problems and the procedures are discussed thoroughly for example in Bathe (1996) and Zienkiewicz (1967). Following this change in coordinates and considering a rotating electrical machine, an acceptable way to set the boundary conditions is to allow the outer edge of the stator to move in the radial direction and prevent it from rotating around the centre of the machine (Belahcen, 2004). In addition, it can be assumed that the rotor shaft is fixed in any direction.

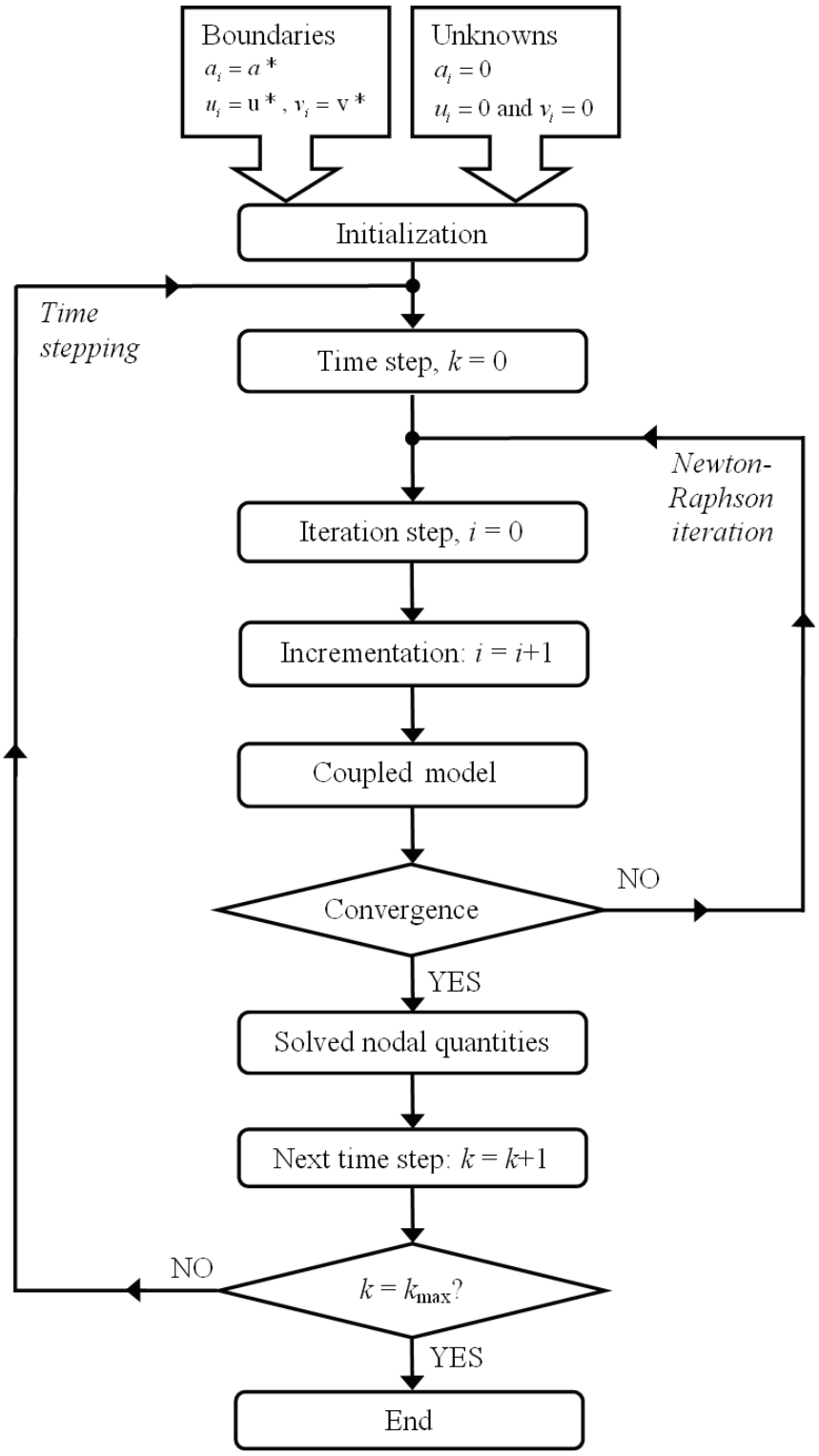

Figure 3.1: Flowchart of the finite element procedure.

3.3 Dynamic case

Under dynamic conditions, the displacements depend on the mass and damping of the system, which are trivially time-dependent. The matrices, $\mathcal{M}$ and $\mathcal{C}$, are, respectively, the total system mass matrix and the total system viscous damping matrix. The system of equations is

$$\mathcal{M}\frac{\mathrm{d}^2\mathbf{u}}{\mathrm{d}t^2}+\mathcal{C}\frac{\mathrm{d}\mathbf{u}}{\mathrm{d}t}+\mathcal{K}\,\mathbf{u}=-\mathbf{f}_{\mathrm{tot}} \tag{113}$$

with the initial conditions

$$\begin{aligned}\mathbf{u}(0)&=\mathbf{u}_0\\ \dot{\mathbf{u}}(0)&=\mathbf{v}_0.\end{aligned} \tag{114}$$

Particularly, $\mathcal{M}$ is the sum of integrations over the volume of all finite elements:

$$\mathcal{M}=\sum_{\#elements}\int_{\Omega}\left(N_i\rho N_j\right)\mathrm{d}\Omega, \tag{115}$$

ρ is the mass density of one element, Ω is the volume of one element. From Zienkiewicz (1967), the total damping matrix is written as

$$\mathcal{C}=c_1\mathcal{M}+c_2\mathcal{K}, \tag{116}$$

of which the parameters c_1 and c_2 have been discussed in Belahcen (2004), for instance. $\mathcal{K}$ was discussed in Section 3.2.

Applying the weighted residual method to Equation (113) and assuming that the working domain is that of one element, defining suitable shape functions normalised to a time interval, the recurrence formulation, derived by Newmark and rewritten in Zienkiewicz (1967)

$$\begin{aligned}&\left(\mathcal{M}+\tilde{\gamma}\Delta t\mathcal{C}+\tilde{\beta}\Delta t^2\mathcal{K}\right)\mathbf{u}^{k+1}\\ &+\left(-2\mathcal{M}+\left(1-2\tilde{\gamma}\right)\Delta t\mathcal{C}+\left(\frac{1}{2}-2\tilde{\beta}+\tilde{\gamma}\right)\Delta t^2\mathcal{K}\right)\mathbf{u}^{k}\\ &+\left(\mathcal{M}-\left(1-\tilde{\gamma}\right)\Delta t\mathcal{C}+\left(\frac{1}{2}+\tilde{\beta}-\tilde{\gamma}\right)\Delta t^2\mathcal{K}\right)\mathbf{u}^{k-1}=-\mathbf{f}_{\mathrm{tot}}\Delta t^2\end{aligned} \tag{117}$$

is obtained. The superscripts k–1, k, and k+1 refer to the second-to-previous, previous, and current time step, respectively. The parameters $\tilde{\gamma}$ and $\tilde{\beta}$ are chosen such that

$$\tilde{\gamma} = \frac{\int_{-1}^{1} W\left(\zeta + \frac{1}{2}\right) \mathrm{d}\zeta}{\int_{-1}^{1} W \mathrm{d}\zeta} \tag{118}$$

$$\tilde{\beta} = \frac{1}{2} \frac{\int_{-1}^{1} W\zeta\left(\zeta + 1\right) \mathrm{d}\zeta}{\int_{-1}^{1} W \mathrm{d}\zeta}, \tag{119}$$

where W are the weight functions for a three-point recurrence formula and $\zeta = t/\Delta t$. Details of the calculations are presented in Zienkiewicz (1967). Symmetric weight functions are preferred, so that $\tilde{\gamma} = 1.5$. Backward formulation is adopted (by definition, $\tilde{\beta} = 1$). It should, however, be noticed that this formulation is numerically damped. With this formulation it is possible to study the dynamic behaviour of steel plates and electrical machines.

The overall system of equations is similar to the one presented in Section 3.2.4, except for vector **h** that contains terms related to the second-to-previous time step. In addition, matrix $\mathbf{\Phi}$ includes $\mathcal{M}$ and $\mathcal{C}$.

3.4 Importance of the electromagnetic stress tensor in air

From the literature review in Chapter 2, reluctance forces translated in terms of surface stresses acting at the iron-air boundary are known to be preponderant in electrical machines. These forces are usually taken into account at the early stage of the development of a model. Because they are the major ones, other side effects such as magnetic forces and magetostriction are sometimes omitted. The approach through this work does not aim at minimizing the importance of the resulting forces due to the transition from air to iron, however the treatment of this effect does not require a complex approach. For this reason, it is considered only at this stage of the study.

Until now, the focus of the thesis was the modelling of the magneto-mechanical behaviour in the material. Indeed, in Section 3.2, the finite element method mainly took into account elements in iron. However as presented in the overall system of equations in Section 3.2.4, electrical machines present several parts that are not filled with magnetic material. Examples of these are the slots, which contain copper windings, and the air gap between the rotor and the stator, where the elements are thus in air.

This section briefly presents the methodology followed to take into account the forces acting between air and iron. Indeed, the electromagnetic stress tensor defined in (69) is recalled:

$$\boldsymbol{\tau}_{\mathrm{m}} = \mu_0^{-1}\left(\mathbf{B}\otimes\mathbf{B} - \frac{1}{2}(\mathbf{B}\cdot\mathbf{B})\mathbf{I}\right) + (\mathbf{M}\cdot\mathbf{B})\mathbf{I} - \mathbf{B}\otimes\mathbf{M}. \tag{120}$$

In air $\mathbf{M} = \mathbf{0}$, so that this tensor becomes trivially

$$\boldsymbol{\tau}_{\mathrm{m}}^{\mathrm{air}} = \mu_0^{-1}\left(\mathbf{B}\otimes\mathbf{B} - \frac{1}{2}(\mathbf{B}\cdot\mathbf{B})\mathbf{I}\right). \tag{121}$$

The previously defined total stress tensor in Equation (69) is used only in iron. Since the magnetic flux density penetrates into the air in the air-gap region, the electromagnetic stress tensor defined in (121) is added to this total stress tensor in the total stiffness matrix for those elements with a common air-iron boundary. The total stress tensor for these nodes is

$$\boldsymbol{\tau} = \boldsymbol{\sigma} + \boldsymbol{\tau}_{\mathrm{m}} + \boldsymbol{\tau}_{\mathrm{m}}^{\mathrm{air}}. \tag{122}$$

The areas to be considered are illustrated in Figure 3.2. In Figure 3.2 (a), the bold lines delimit the slots in the stator and rotor and the air-gap region is in grey. In this case there is only one layer of elements. Figure 3.2 (b) is a zoom on the air-gap elements and iron elements close to the air gap, where, "Fe,*i*" is the element *i* in iron and "Air,*i*" is the element *i* in air. The total stress tensor in (122), is evaluated in those nodes only.

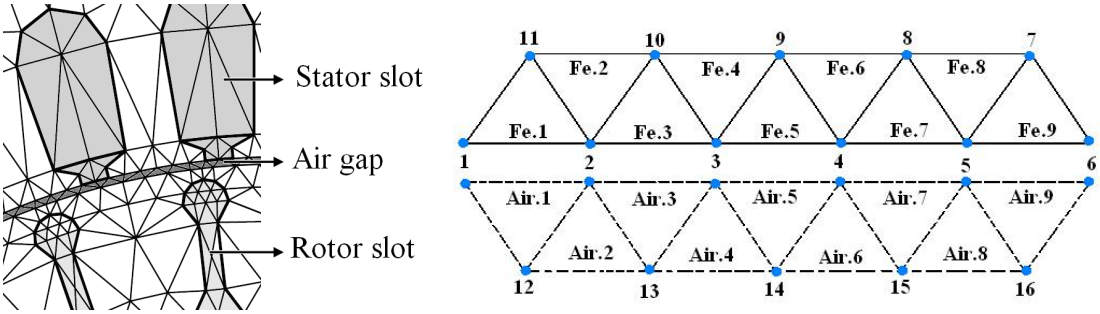

(a) (b)

Figure 3.2: Zoom of the mesh of the air gap of an electrical machine.

3.5 Summary

This chapter dealt with the energy-based magneto-mechanical model, integrated into a 2-D finite element analysis, for simulating electrical machines. The model has been theoretically presented through a suitable form of the Helmholtz free energy and the material constitutive equations have been derived. Additionally, the insertion of the electromagnetic stress tensor for elements close to the air gap has been discussed. To account for the mass and damping of a structure, the overall system of equations is derived following Zienkiewicz (1967). The results from the implementation of the finite element method are analysed later, in Chapter 5, where the method is suitably verified.

In Chapter 4, the parameters for the model are identified and the present and next chapter are consequently conjoined. Indeed, the derived Helmholtz free energy is straightforwardly established on the measured stress-dependent magnetostrictive and single-valued magnetisation curves.

Chapter 4

Measurements and identification of magneto-mechanical properties of materials

Inside electrical machines, the magnetic flux density can be either rotating, for example in the yoke of the stator, or alternating, in the teeth of the machine. As precise local measurements inside these machines are difficult to perform, rotational single sheet testers are mostly used to identify the properties of one electrical steel sheet and extrapolate the results for larger devices.

1-D and 2-D measurements are covered in this chapter through single sheet testers. The first one is a modified Epstein frame, the second one, a vertical yoke system. The latter one was designed and built for an introductory study of magnetostriction at no stress from which uni-axial measurements are compared with those from the Epstein frame. From the literature review conducted earlier, many uncertainties have been spotted regarding suitable methods for measuring stress and strains in electrical steel sheets under applied pre-stresses.

Different types of methods are commonly used to measure the effect of magnetostriction in electrical steels, among others strain gauges, piezo-electric sensors, lasers, and accelerometers. The first two methods are chosen in this work for acquiring the magnetostrictive strains resulting from the applied magnetic field and stress.

The model for magneto-mechanically coupled problems presented previously requires parameter identification. Therefore, magnetostriction is measured under different pre-stresses and magnetic flux densities on the modified Epstein frame. The model in Chapter 3 is identified from the obtained beam of curves.

4.1 The modified Epstein frame

4.1.1 Measurements and data treatment

The device in Figure 4.1 was built following the IEC 60404-2 standard, and modified to apply a mechanical pre-stress to the iron strips (Belahcen, 2004). The square-shaped frame comprises two types of windings: a primary winding and a secondary winding. The first one consists of the feeding coils, and the second one serves to acquire the voltage to evaluate the magnetic flux density. Parameters for the setup and sample sheets are given in Appendix A. Four load cells are attached to four corners of the frame, while the other corners are fixed. The load cells are connected by means of screws on the strips to a measuring device that acquires the force that is applied. At equilibrium, the strips are magnetically excited and the resulting force is acquired with a piezo-electric sensor directly connected to the data acquisition card.

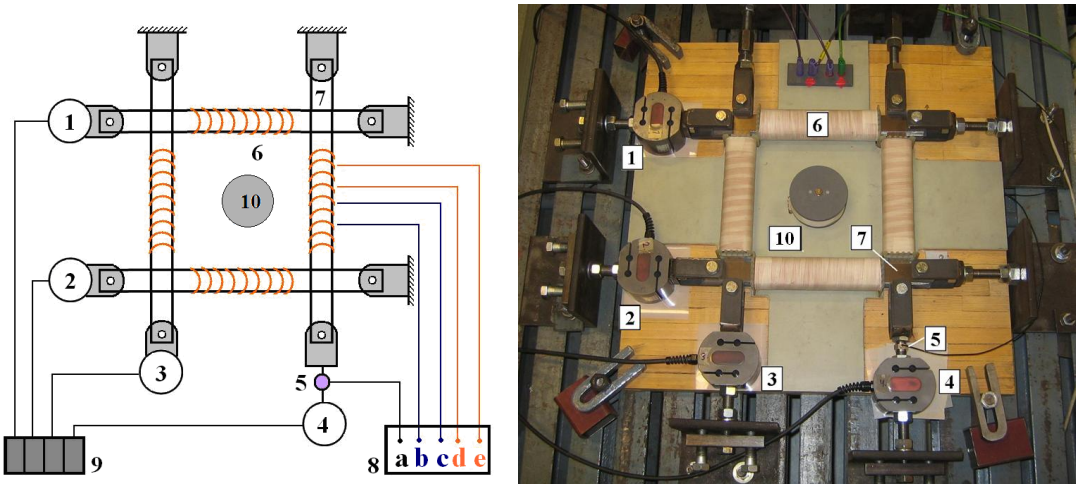

(a) Schematic view and picture of the Epstein frame.

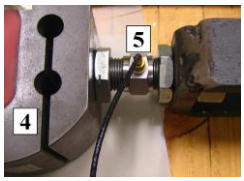

(b) Zoom of the piezo-electric sensor.

1-4: load cells, 5: piezo-electric sensor, 6: feeding coils and B coils,
7: test samples, 8: PC, 9: force meters, 10: air-flux compensating coil.

Figure 4.1: Views of the modified Epstein frame.

The spring constants of the iron strip, the force transducer, the load cell, and the support in Figure 4.2 (a and b) are, respectively, k_{iron} =1.7E+8 N/m, k_{FT} =1E+8 N/m, k_{LC} =5E+8 N/m, and $k_{support}$ =5E+6 N/m. The constants have been evaluated in Belahcen (2004). The piezo-electric force transducer is connected to a charge pre-amplifier.

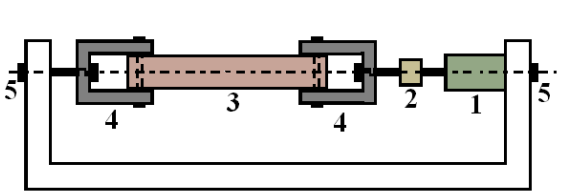

(a) Lateral schematic view of one limb of the setup, where the piezo-electric sensor is put into place.

1: load cell (actuator), 2: piezo-electric force transducer (sensor), 3: sample, 4: support, 5: screws.

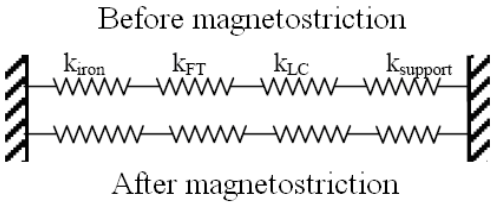

(b) Equivalent representation.

Figure 4.2: Details of the lateral view of the setup for the calculation of the magnetostrictive elongation (Belahcen 2004).

The piezo-electric force transducer measures the force F_{piezo}, parallel to the applied magnetic flux in the sample sheets at equilibrium

$$F_{piezo} = -\left(\frac{1}{k_{iron}} + \frac{1}{k_{FT}} + \frac{1}{k_{LC}} + \frac{1}{k_{support}} \right)^{-1} \Delta l_{ms}. \qquad (123)$$

The displacement, Δl_{ms} is the equivalent magnetostrictive elongation resulting from the presence of the external magnetic field and pre-stress. The measurements were conducted at a supply frequency of 5 Hz.

In Figure 4.3 the magnetostrictive hysteresis loops, also called butterfly loops, are illustrated before the data treatment. Similar measurements have been observed in previous studies, such as in Lundgren (1999). Only the DC component was added, so that the loops originate from zero. In fact, the phenomenon of magnetostriction is non-linear, testifying to the change of sign that is influenced by the magnetic field and pre-stress. Hence, for fitting the data, a single-valued curve is calculated by a least-squares procedure from these double-valued strain curves. Figure 4.4 shows the corresponding measured hysteresis loops at different pre-stresses, where a region of the loop is zoomed to observe the effect better. However, for the range of pre-stresses applied, the differences are very small. Examining the measurements in Figure 4.3, it could be deduced that magnetostrictive strain varies in a quadratic way with the magnetic flux density, omitting the behaviour at saturation (over 1.5 T). The model

presented in Chapter 3 accounts for this phenomenon and the importance of each of the parameters is discussed in the next section.

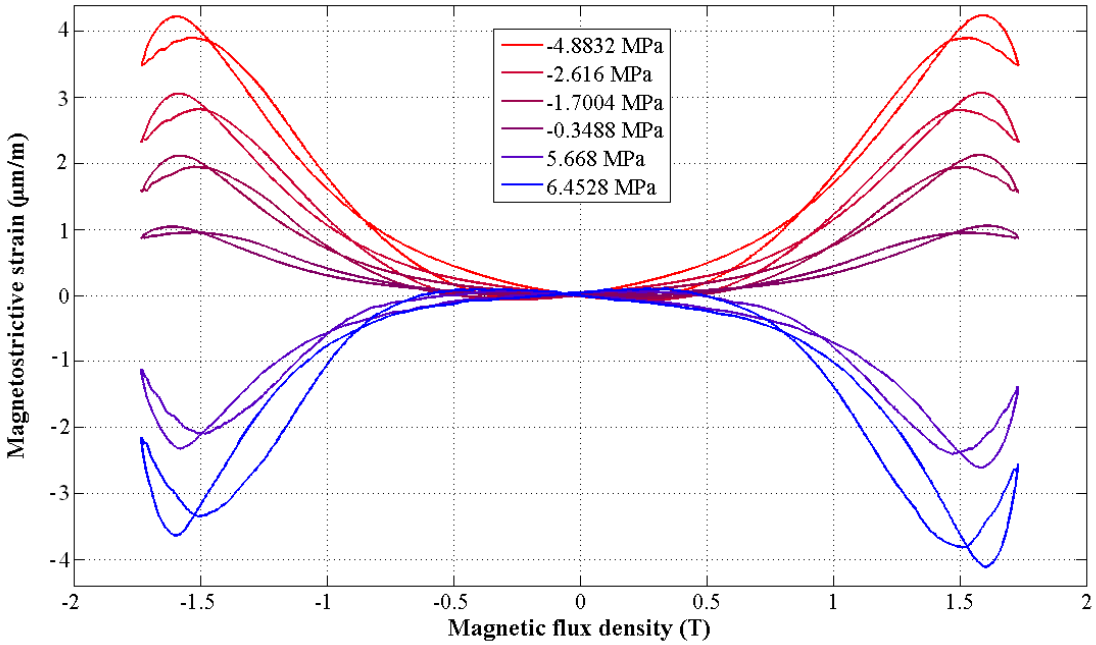

Figure 4.3: Measured magnetostriction curves at different values of the applied tensile and compressive stress.

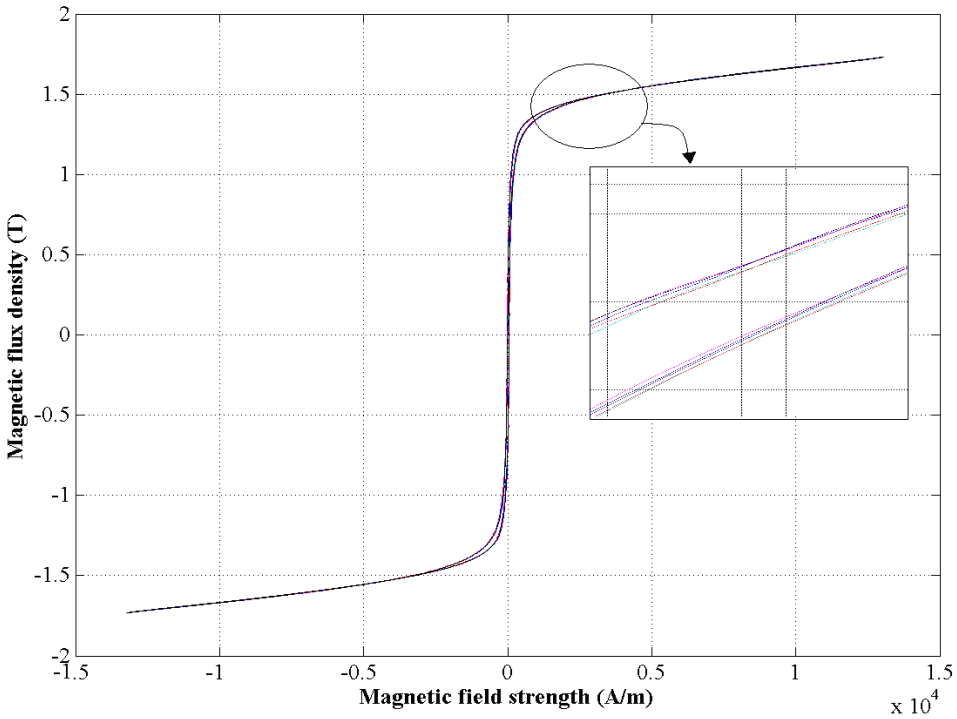

Figure 4.4: Hysteresis loops at different values of applied stress.

4.1.2 Identification of the parameters

The measurements were performed on a modified Epstein frame. The calculated single-valued curves are presented in Figure 4.5 and Figure 4.6. The experimental results are used to identify the model derived in Chapter 3 for a magnetised sample under magnetic stress.

The Helmholtz free energy function, and hence the constitutive equations, depends on the set of five invariants (I_1, I_2, I_4, I_5, and I_6), which depend on the magnetic and mechanical fields. The six dimensionless parameters to be identified are immerged within the expression of $\boldsymbol{\sigma}$, (124), and $\mathbf{M}$, (125).

$$\boldsymbol{\sigma}=\rho \sum_{i=1,i\neq 3}^{6} \frac{\partial \psi}{\partial I_i} \frac{\partial I_i}{\partial \boldsymbol{\varepsilon}} \tag{124}$$

$$\mathbf{M}=\rho \sum_{i=1,i\neq 3}^{6} \frac{\partial \psi}{\partial I_i} \frac{\partial I_i}{\partial \mathbf{B}} \tag{125}$$

The parameters are evaluated by fitting the experimental data of magnetisation and magnetostriction obtained with the described modified Epstein device.

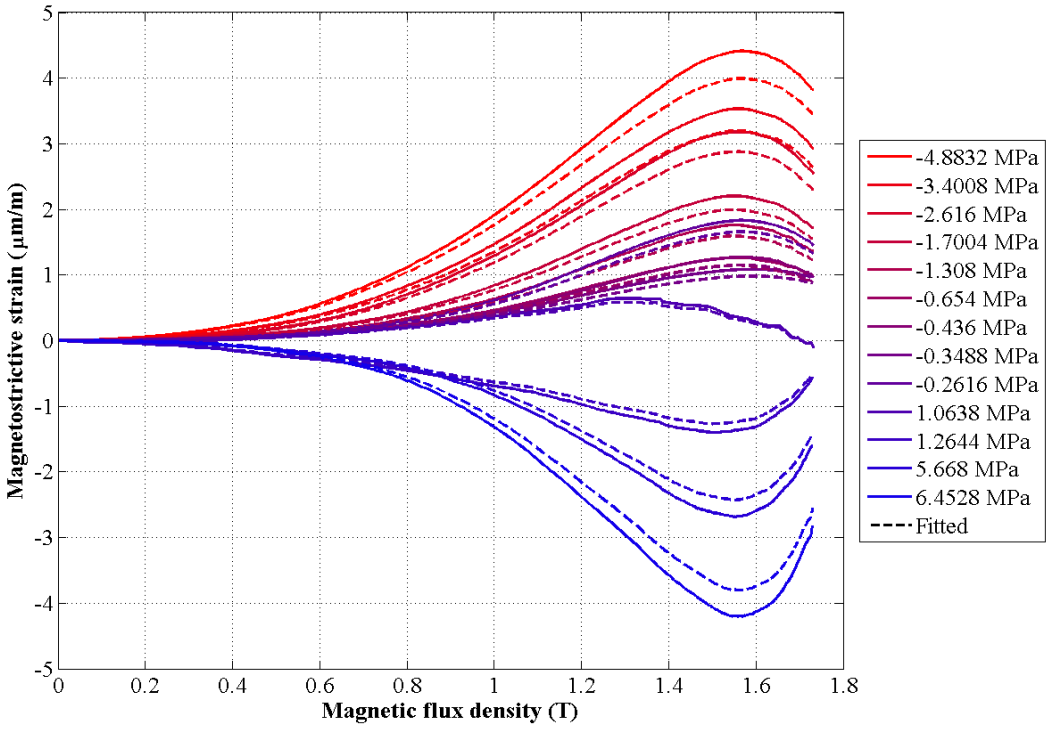

Figure 4.5: Experimental and fitted average magnetostrictive strains as function of the magnetic flux density under compressive (negative sign) and tensile pre-stresses (positive sign).

The identification is performed using the MATLAB® solver for non-linear least-squares problems. Initial guesses and manual adjustment of the parameters are of great help. Table 1 presents the values of the dimensionless parameters of the model that were identified from the measurements on the modified Epstein frame.

Moreover, the two additional mechanical parameters required for the model are the modulus of elasticity E and the Poisson's coefficient, set to 183 GPa and 0.34 respectively. These were not obtained experimentally but were assumed to be acceptable within this framework.

To identify the magnetic material model, the static hysteresis loops were measured at different values of pre-stresses (Figure 4.4). Two methods are commonly adopted to obtain a single-valued curve (Ivanyi, 1997). The first one is the evaluation of the fundamental magnetisation curve. This curve is obtained by connecting the tips of the hysteresis loops at different amplitudes of the alternating field. The second method involves calculating numerically the average between the ascending and descending parts of the hysteresis loop. The latter approach seems appropriate in this case, as measurements are performed at 5 Hz. At that frequency, the area of the hysteresis loop is small enough for it to be considered that both methods would provide similar results. The resulting experimental and fitted curves at zero stress are plotted in Figure 4.6.

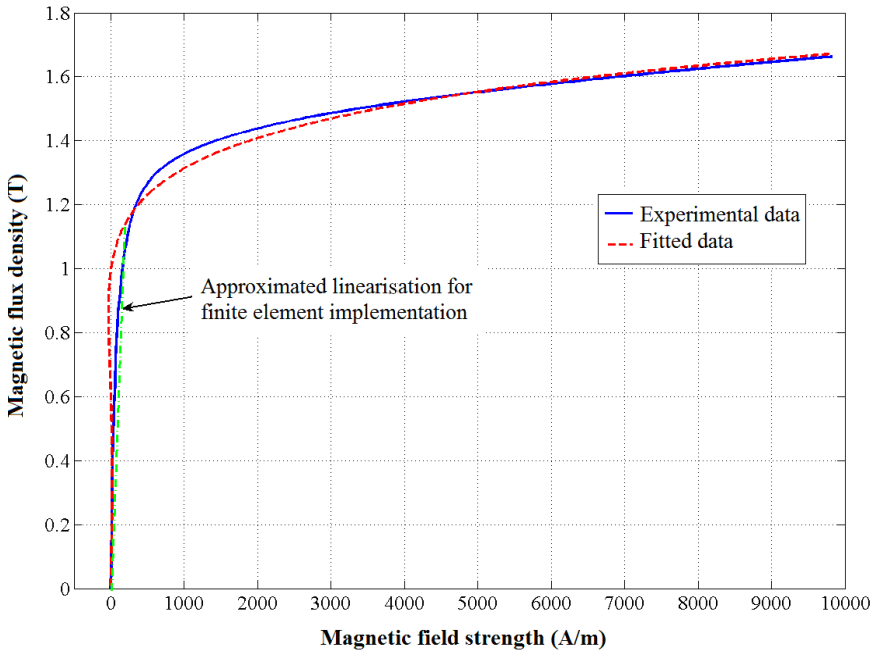

Figure 4.6: Experimental and fitted single-valued magnetisation curve.

The estimation of invariant 4 through the polynomial expansion gives an approximate description of the single-valued magnetisation curve. The saturating part is fitted

approximately correctly; however, the model fails to give a correct approximation of the linear part of the single-valued curve. This is due to the fact that this curve is approximated by a polynomial. This fitted curve will induce instability in the Newton-Raphson method. To circumvent convergence problems within this area, an approximated linearisation is thus considered, as in Figure 4.6, for the implementation into the finite element code.

From the model that is derived, coefficients α_0, α_1, α_2 and α_3 are those of a polynomial expansion such as defined in Chapter 3. Coefficient α_4 characterises the effect of magnetostrictive strain saturation when the magnetic saturation is reached. Invariant 5 is necessary in order to account for the positive and negative magnetostriction in electrical steel. Invariant 6 gives a measure of the distance between the maximum of the upper magnetostrictive curve and the minimum of the lower magnetostrictive curve, as in Figure 4.7. The estimated parameters for the model are reported in Table 1. These results show that the energy-based model defined in Chapter 3 is accurate enough to account for the phenomenon of magnetostriction.

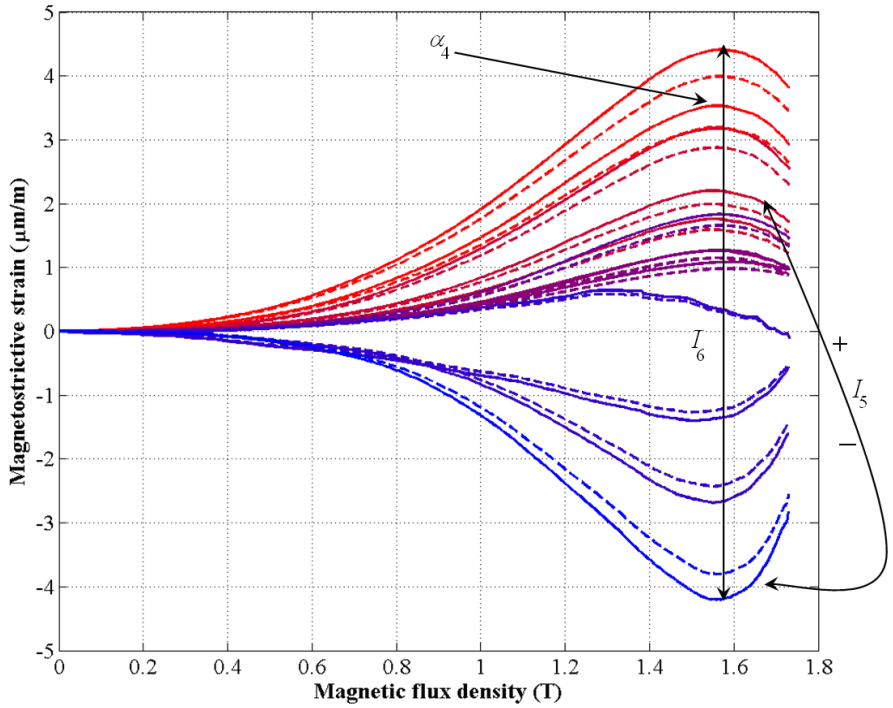

Figure 4.7: Explanation of the parameters.

Table 1 Values of the dimensionless parameters identified from the measurements.

Parameter	α_0	α_1	α_2	α_3	α_4	α_5
Values	-1.99	$-1.21\cdot10^{-3}$	$4.09\cdot10^{-4}$	$8.82\cdot10^{-5}$	-0.38	-0.71

4.1.3 Dependence of magnetostriction on the frequency

The purpose here is to show that magnetostriction is a frequency-dependent phenomenon. Measurements were conducted on the described setup at 20 Hz and 50 Hz and at zero applied stress. At higher supply frequencies, the hysteretic behaviour is more dominant, as illustrated in Figure 4.8. However, the average peak-to-peak magnetostrictive strain remains constant, regardless of whether the measurements were conducted at 5 Hz, 20 Hz, or 50 Hz.

The extrapolated single-valued curves for the dependence of the magnetostrictive strain as a function of the magnetic flux density are, however, more difficult to obtain from measurements at 20 Hz or 50 Hz. This is the reason why the identification of the parameters was performed on the set of curves presented in Figure 4.3, which were treated simply by taking an average over five measured butterfly curves.

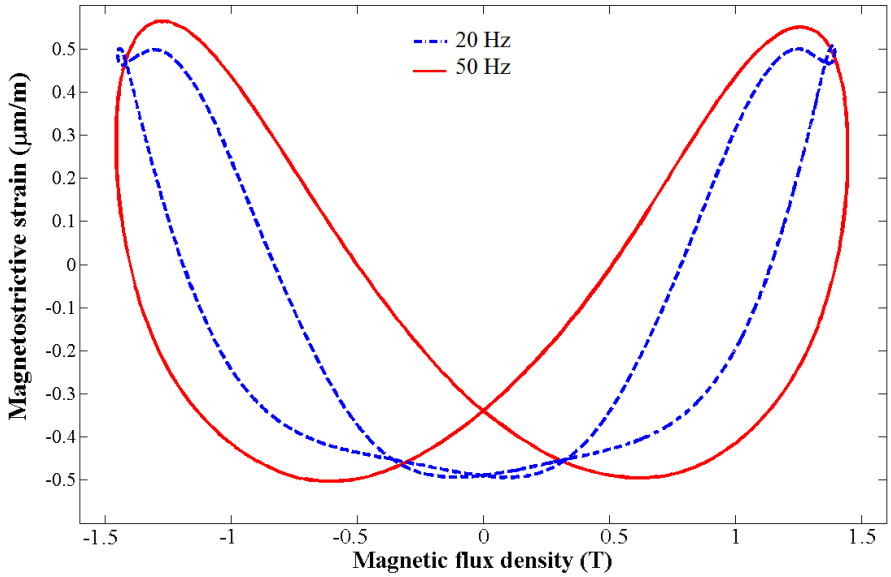

Figure 4.8: Butterfly loops.

4.2 The vertical yoke system

As presented in Chapter 2, various setups for a rotational magnetic field in electrical steel sheets have been developed over the years. The design within this work was pioneered by Bergqvist (1994), modified and adapted by Krah (2004), and again rethought in the frame of this research. The experimental setup for acquiring the 2-D magnetic flux density and field strength inside an electrical steel sheet is detailed first. The measurements of the magnetostrictive curves are then described.

4.2.1 Introduction

In Figure 4.9, the symmetric yoke system is composed of two similar geometries superposed onto each other, the upper yoke and the lower yoke. The test electrical steel sheet is placed between them. In order to prevent leakage fluxes though perpendicular yokes, they were laminated and approximately 50 % of the sheets are steel sheets and 50% are a non-magnetic material such as “Mylar” polyester. More information regarding this device can be found in Krah (2004) and Fonteyn et al. (2008, 2009a).

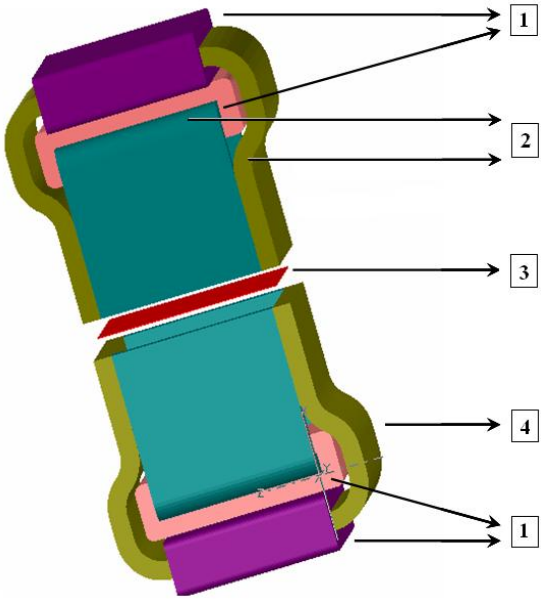

1: exciting coils, 2: upper yoke, 3: steel sheet, 4: lower yoke.

Figure 4.9: Design of the vertical yoke system

The assembled sheets have been impregnated into resin to guarantee the solidity and durability of the system. The limbs, which are touching the electrical steel sheets to be tested, have been polished to obtain the best possible surface. The upper copper windings and the lower copper windings are using almost all the available volume between the inner and outer yokes and are fed from a sinusoidal waveform generator.

The vertical yoke system in its symmetric and non-symmetric configurations was first simulated by means of the MAXWELL® software. The results are discussed in Fonteyn et al. (2008). In that research, six simulations were performed with a symmetric yoke system and a non-symmetric yoke system. The results were achieved as part of the design of the measuring setup to confirm that the configuration and geometry of the yoke that are presented bring acceptable results. Figures 4.10 and 4.11 present the numerical results obtained with the MAXWELL® software when the lower yokes were excited.

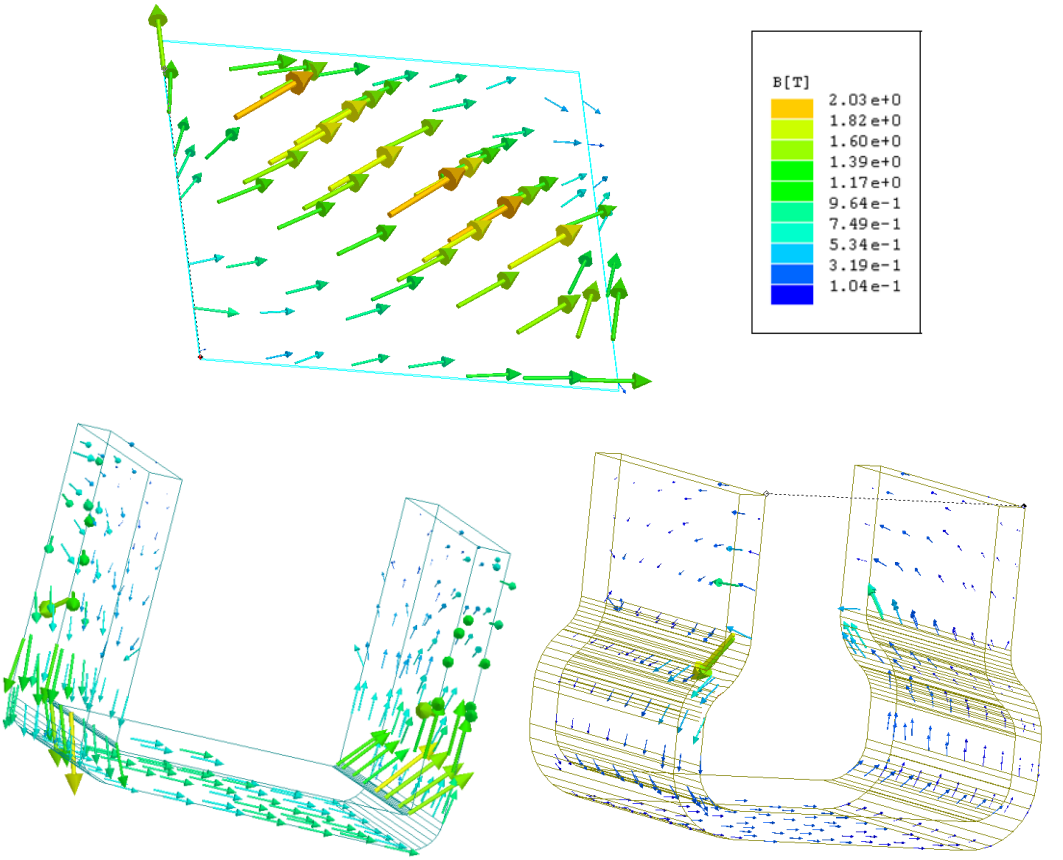

Figure 4.10: Simulated magnetic flux density distribution in the yoke and in the sheet (arrow plot).

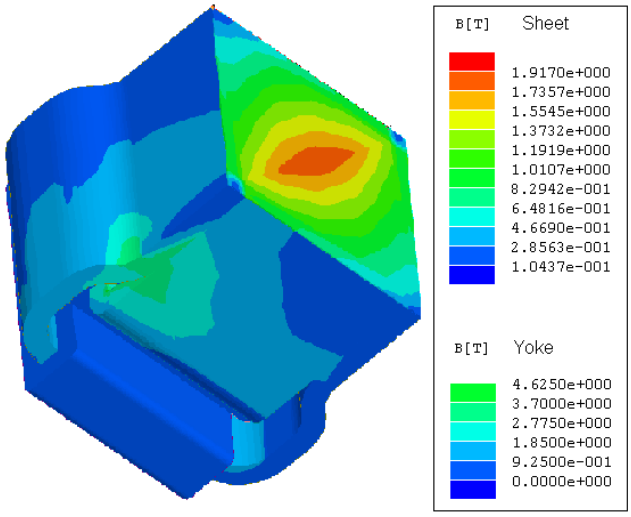

(a) Magnetic flux density in the sheet and in the yoke.

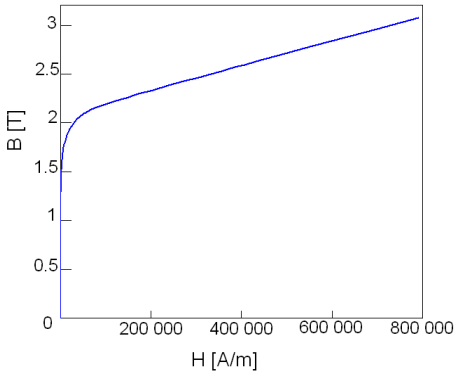

(b) B-H curve of the sheet used for the simulations from MAXWELL®.

Figure 4.11: Simulations for the vertical yoke system.

The maximum flux density inside the sheet is nicely uniform only over approximately 5% of the total area of the sheet, as shown in Figure 4.11 (a). The uniformity of the magnetic flux density in the electrical steel sheet is fundamental not only for the positioning of the field sensors, but also for the strain gauges. The single-valued B-H curve for the steel type of the simulated sheet is as in Figure 4.11 (b). The data treatment software used is LabVIEW®. Data are acquired with an NI PCI-7831R card from National Instruments, using four analogue inputs for the signals from the coils and two analogue outputs for sending the input waveform to the exciting coils. The signals from the sensors are sent to the DAQ card, which memorises the input and sends it back to the computer. From there, the different analyses are processed.

Additional information about the measurement procedures and extended results are provided in Alkar (2007), Fonteyn et al. (2008, 2009a), Belkasim (2008), Dlala (2008) and Dlala et al. (2009). Additional data for the vertical yoke system are presented in Appendix B.

4.2.2 Dependence of the magnetostriction on the supply frequency.

The described experimental apparatus was adopted for the measurements of magnetostrictive strain resulting from 1-D and 2-D magnetic fields under three supply frequencies. A view of this setup is provided in Figure 4.12.

Two strain gauges are glued to both sides of the electrical steel sheet in the centre, as can be seen in Figure 4.13. The strain gauges were chosen to be as insensitive as possible to external magnetic fields varying in the range of the measurements and they were connected to a Wheatstone bridge. The change of resistance induced by a change of length within the specimen is measured. The temperature effect is minimised thanks to a dummy resistance. Strains parallel and perpendicular to the magnetic field are acquired.

First, 1-D measurements at three different frequencies were obtained at different peak magnetic flux densities. Although the study in this work is limited to the single-valued dependence of magnetostriction on the magnetic field, it seemed essential to remember that, like many other physical problems, magnetostriction is a hysteretic phenomenon that depends on the supply frequency. Some attempts to account for this behaviour in the models have recently been investigated in Hilgert (2008).

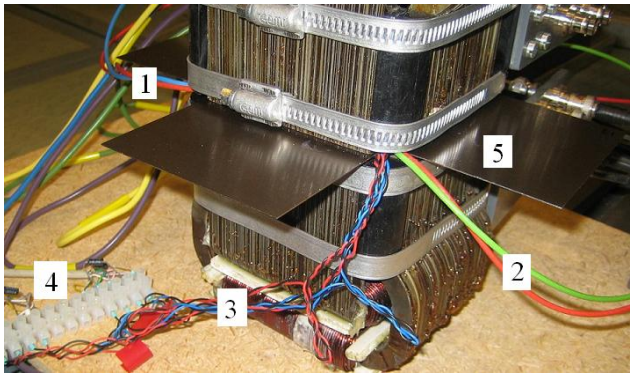

1: wires for H-coils, 2: wires for B-coils, 3: wires for strain gauge,
4: bridge connection for the strain gauge, 5: electrical steel sheet.

Figure 4.12: Vertical yoke system.

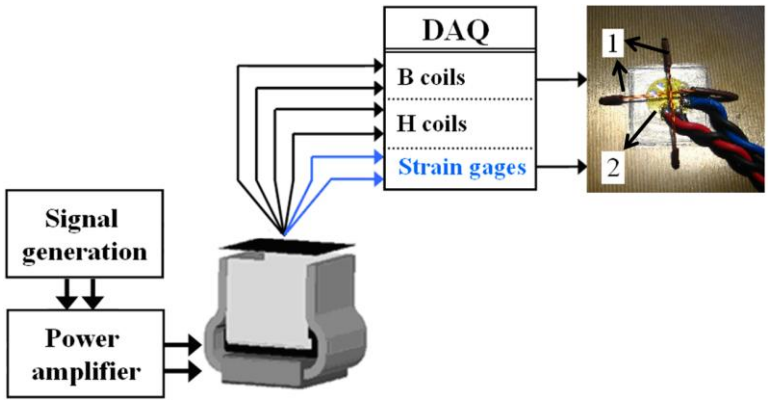

1: B-coils, 2: strain gauge.

Figure 4.13: Schematic view of the setup.

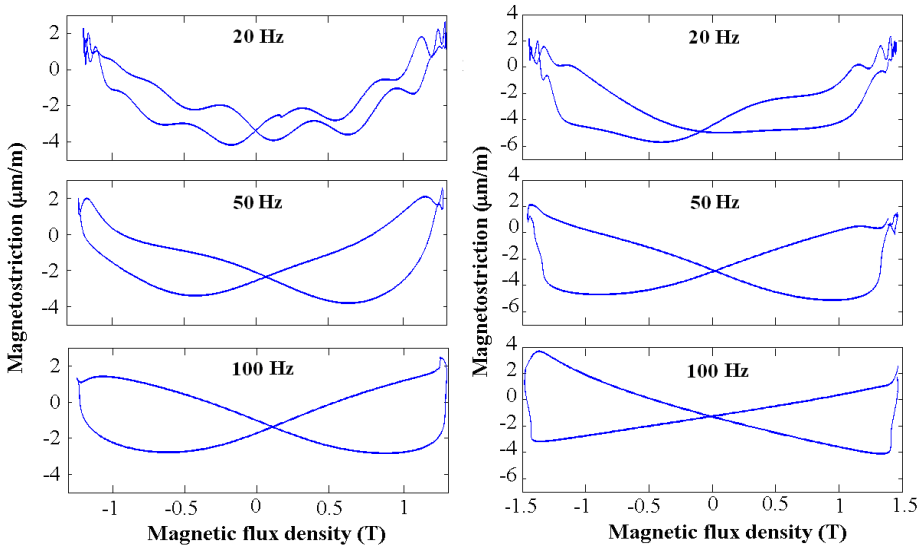

(a) B_{peak}= 1.25 T (b) B_{peak}= 1.5 T

Figure 4.14: Magnetostrictive strain in the direction parallel to the excitation at different frequencies.

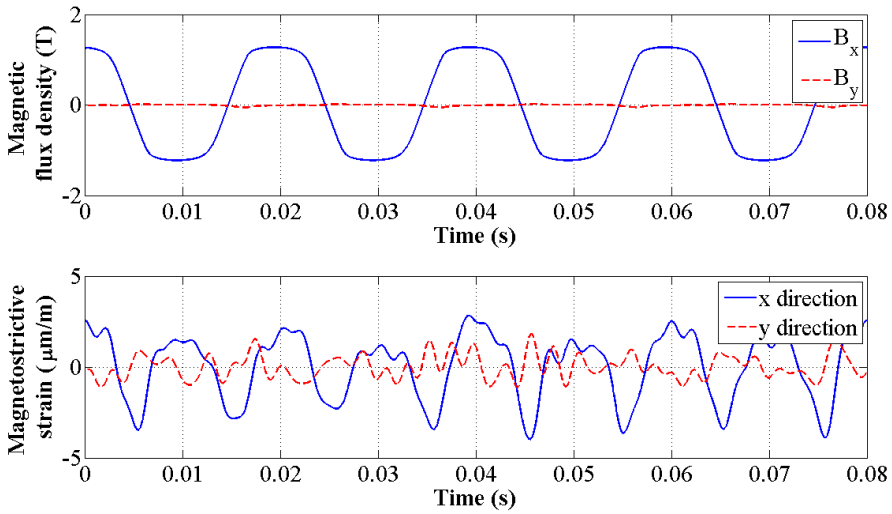

Figure 4.15: Time-dependent magnetic flux density in the centre of the device and corresponding magnetostrictive strains.

The measurements, over three frequencies (20 Hz, 50 Hz and 100 Hz) are presented for constant peak magnetic flux densities of 1.25 T and 1.5 T. Therefore, the frequency dependence of the butterfly loops is shown in Figure 4.14.

The peak-to-peak magnetostriction has a range of about 6 μm. As expected, the area of the loop grows with higher frequencies. The time dependence of the measured magnetic flux density and magnetostriction is presented in Figure 4.15 for a supply frequency of 50 Hz.

4.2.3 Measurements of dynamic magnetostriction at zero stress under rotating field.

Among others, Enokizono et al. (1990), Pfützner et al. (1996), and Hilgert (2008) have discussed the influence of the rotating field on magnetostriction. The term "*rotational magnetostriction*" is defined as "*the magnetostrictive behaviour of a soft magnetic sheet which is subject to rotational magnetisation, characterised by arbitrary rotations of the induction* ***B***" (Pfützner et al., 1996). Both the setups and the measurements presented here are challenging as regards the topic of the thesis. The purpose is to present limitations to the developed model and discuss accuracy in measurements. The purpose is to present the limitations of the model that was developed and discuss the accuracy of the measurements.

Displacements under magnetic loading are directly measured on the electrical steel sheet and the magnetic flux density is acquired in the same region. Those results

should have a higher precision, regardless of the sensitivity of the strain gauge. However, strain gauges are known to be sensitive to external magnetic fields.

In Figure 4.16 and Figure 4.17, the measured magnetostriction as a function of time under a rotating magnetic flux density is illustrated. Measurements were performed under a supply frequency of 50 Hz. The B-coil and the strain gauges acquire the signals at exactly the same time. Symmetry is somehow present in the butterfly loop measurements in Figure 4.17. Although the field was the same in both directions, the butterfly loops are not identical in the *x*-and *y*-directions. This is due to a possible privilege direction of grain orientation.

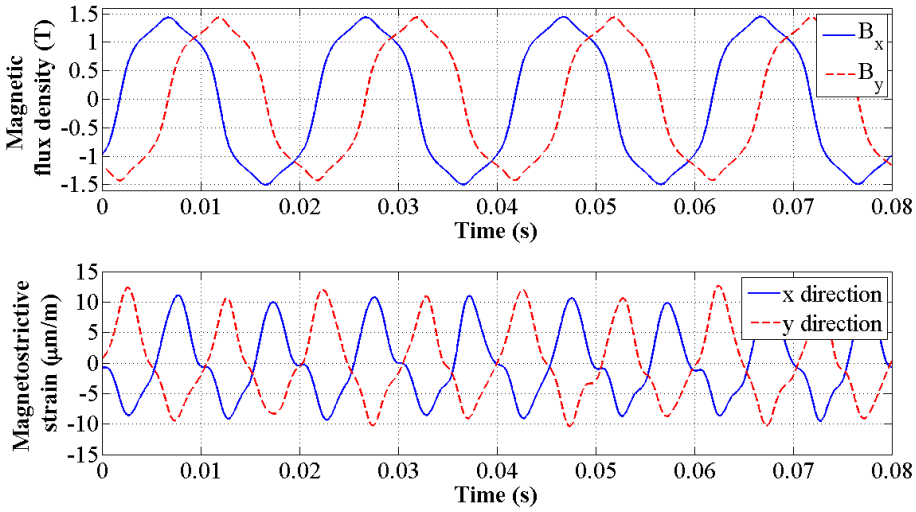

Figure 4.16: Measured time-dependent magnetic flux density in the centre of the device and corresponding magnetostrictive strains.

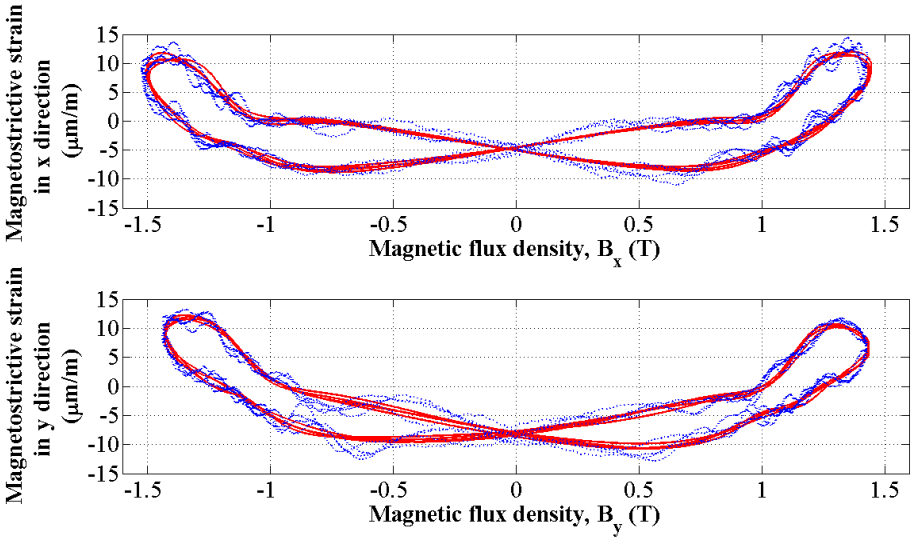

Figure 4.17: Butterfly loops. Measured signal (dotted) and filtered signal (plain).

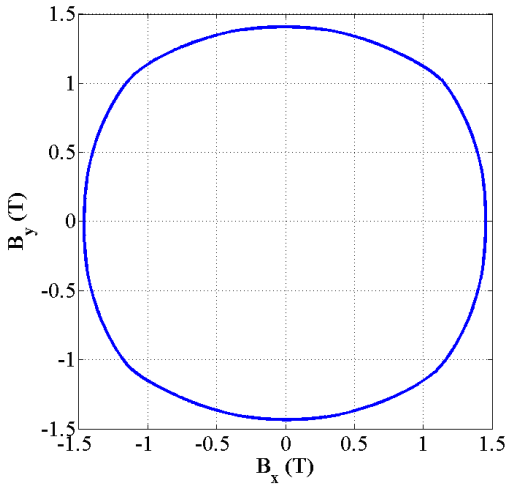

Figure 4.18: Measured rotating magnetic flux density in the centre of the sheet.

When $B_x = B_y$ or $B_x = -B_y$ in Figure 4.16, the corresponding strains reach their maximum and minimum values respectively. Under the condition that the derivative $\mathrm{d}B_x/\mathrm{d}t$ reaches its maximum over the time period and $\mathrm{d}B_y/\mathrm{d}t = 0$ or vice versa, both measured ε_x and ε_y are equal to zero.

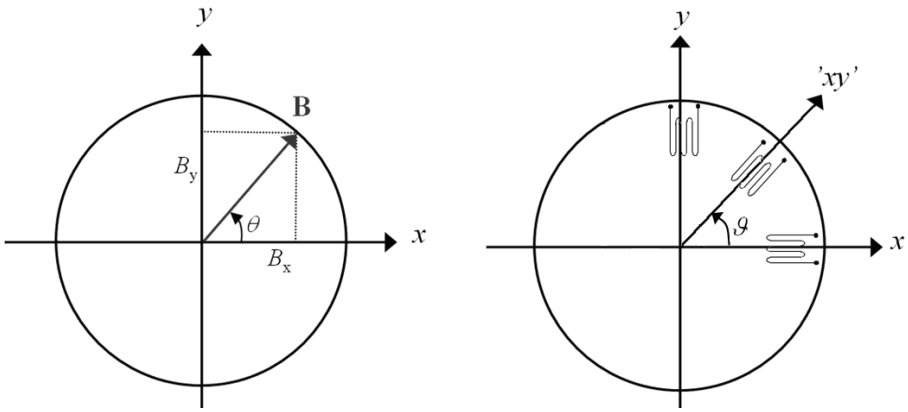

Figure 4.19: Placements of the strain gauge.

The deformations in the *x*-, *y*- and *'xy-'* directions are known to be

$$\lambda_x = \varepsilon_x \tag{126}$$

$$\lambda_y = \varepsilon_y \tag{127}$$

$$\lambda_{xy} = \frac{1}{4}\left(\varepsilon_x + \varepsilon_y\right) - \varepsilon_{xy}\,. \tag{128}$$

The total elongation, λ_e, and contraction, λ_c, are obtained from

$$\lambda_{e,c} = \frac{\varepsilon_x + \varepsilon_y}{2} \pm \frac{1}{2}\sqrt{\varepsilon_x^2 - 2\varepsilon_x\varepsilon_y + \varepsilon_y^2 + \frac{1}{2}\left(\varepsilon_x + \varepsilon_y - \varepsilon_{xy}\right)}. \quad (129)$$

Within this work, the total elongation as a function of time cannot be known because the shear strain, the strain in the ε_{xy} direction, has not been measured. A schematic view of the rotating magnetic flux density and placement of the strain gauge is shown in Figure 4.19.

The measurements gathered in this section were conducted as critical attempts to assess the validity of the work. Notwithstanding the accuracy in the measuring methods and setups, the experimental results from both the setups require special attention, and thus they are discussed below.

4.3 Comparisons and discussions

Comparisons of the results in Section 4.1 and 4.2 are obtained for both cases at zero stress under uni-axial magnetisation in the direction of magnetisation, because there is no mechanical loading of the sample in the vertical yoke. The advantages and drawbacks of the piezo-electric force transducer method are compared to the strain gauge method. The advantages and drawbacks of both setups, the modified Epstein frame (setup 1) and the vertical yoke system (setup 2), are also discussed.

The measurements at supply frequencies of 20 Hz and 50 Hz and after the filtering process are illustrated in Figure 4.20. The positioning of the curves with respect to each other is random, as the differences needed to be stressed out at best. The measurements from the Epstein frame are 10 times smaller than the results from the vertical yoke system for both cases. The magnetostrictive strain from the Epstein frame has been magnified for a better comparative view.

In the case of setup 2, the internal strains on one sheet only were considered. The placement of the strain gauge in the centre of the sample covers a wide range of magnetic domains, as its diameter is 0.5 mm. The first and main reason for the anticipated overestimation of the strain gauges is their sensitivity to external magnetic fields. Another drawback of the vertical yoke system is the pressure introduced when the magnetic circuit is closed by pressing the upper yoke onto the plate. The sheet is then unable to move totally freely, although a tiny air gap is naturally present because of the roughness of the yoke limbs. The same problem is present in setup 1 because the screws and the support, although freed from any loading, produce pressure on the stack of samples. The repeatability of the measurements for setup 1 is challenging.

The four screws should be manually adjusted before each measurement. The load cells have to be calibrated and zero stress is difficult to achieve.

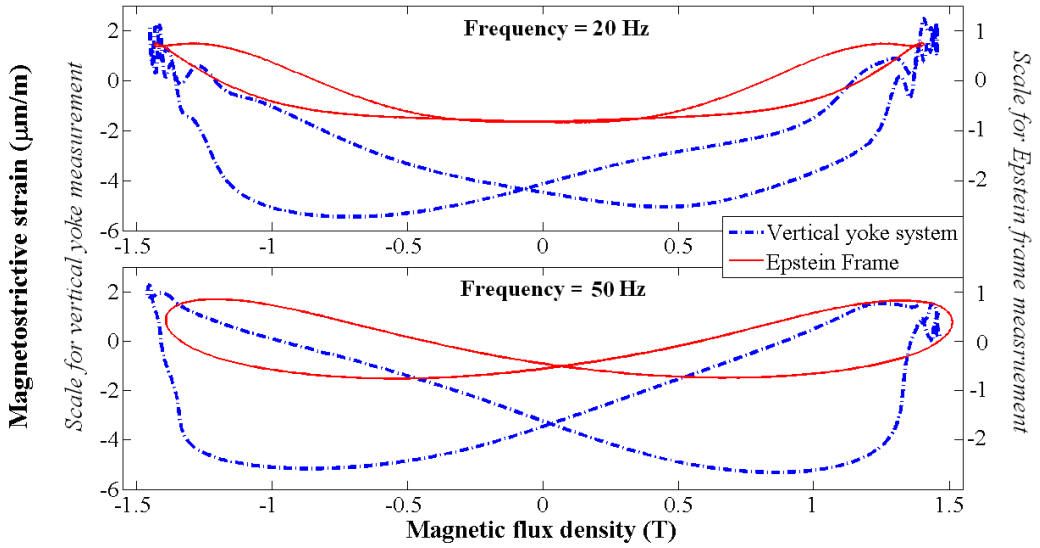

Figure 4.20: Comparison of the two measurement techniques.

Recently, Somkun et al. (2010) measured rotational magnetostriction in non-oriented electrical steels. Their experimental results showed that the peak-to-peak magnetostriction at 50 Hz, with a circular magnetic field of peak value, 1.3 T equals approximately 10 μm/m. The area of the butterfly loop was, however, smaller, which leads us to suppose that the material that was studied was different.

Regarding the acceptability of the strain gauge method, identical measurements presented in Hilgert (2008) and Ghalamestani (2010) concluded that the strain gauge method seems to lead to higher magnetostrictive strains compared to the dual heterodyne laser interferometers. The authors measured the displacements on a vertical single sheet tester.

4.4 Summary

The results presented in this chapter are essential for the investigation of magneto-mechanical properties in electrical steel sheets. Two measuring devices have been presented: a vertical rotational single sheet tester and a modified Epstein frame. The first one provided an insight into the study of the internal stresses induced by a 2-D magnetisation of electrical steel. The theoretical model was compared with the measurements. Taking into account external noise problems and the inadequate

magnetic insulation of the strain gauges, the results were satisfactory at zero stress. The coupled model defined in Chapter 3 was identified from the same electrical steel sheets as will be used later on to build a test device. The comparison of the measurements from the two different types of devices at zero stress and the discussion of similar results obtained from previous researchers establish that it is the measuring technique, and not the measurement setup, that causes a large difference in the magnetostrictive strain. However, the results from the strain gauge technique are relatively too high.

Reducing the phenomena of magnetostriction to a single-valued curve is acceptable. The general behaviour is a good approximation within the present research work. Nevertheless, some extra measurements are presented to depict the full idea of the phenomena and suggest possible further investigations.

This comparative study obviously necessitates a deeper investigation of the measurement techniques of magnetostriction, measurement setups and their standardization. These measurements show the difficulties arising when modelling the magnetostrictive effect in electrical steel sheets.

Chapter 5

Verification and analysis of the coupled model

This chapter presents the verification and results of the developed model. In the past, very few test devices accounting for the phenomenon of magnetostriction have been proposed. Models may be verified on the RSST or SST, but, as the parameters for the models have been identified on those, the use of the same setup for verification is not acceptable.

First, the different steps from the design to the final building of a test device for the verification part are illustrated. The aim is to observe the displacements of the outer boundary of the machine under a rotating magnetic field. The measured values are therefore compared with the simulated ones and discussed. Second, as shown in Section 3.3, a discussion based on experimental results on a test asynchronous machine is provided to account for the displacements originating from the penetration of the magnetic flux into the air gap of electrical machines. Third, simulated results from two rotating electrical machines are approached. Finally, the dynamic model, including damping and mass effects is studied briefly.

5.1 Verification with a test device

This section provides the different steps from the design to the final constructed test device. The aim is to focus on the measurements of the displacements of the machine outer boundary under a rotating magnetic field. Test devices for the same purpose have been developed earlier. Låftmann (1995) worked with a wound hollow cylinder made of electrical steel sheets. This stator had the disadvantage of taking into account all the forces, including the ones caused by possible leakage fluxes penetrating from one tooth to another one. Later, Cester (2002), together with Belahcen (2004), built a plain device that offered promising results, even though the magnetic flux density

was not well distributed over the geometry. Here the design and measurement results from an enhanced version of the latter device are presented.

In the present study, the design offers a homogeneous magnetic flux density in the 2-D cross-section. Results from the measurements and simulations are discussed. More details can be found in Appendix C, Pyhäranta (2009), and Fonteyn (2009).

5.1.1 Structure of the new device

In electrical machines the forces acting on the boundaries between the rotor and the stator are the reluctance forces. Made of non-oriented Fe-Si discs piled onto each other, this device has no air gap through so that only the deformations resulting from magnetostriction and the electromagnetic stress tensor in iron are observed. Slots were laser-cut at a suitable distance from the centre of the sheets beforehand. The sheets were transposed, or more precisely rotated by an angle equal to one over the total number of slots, in order to prevent anisotropy and remove the preferred direction of magnetisation, also known as the rolling and transverse directions.

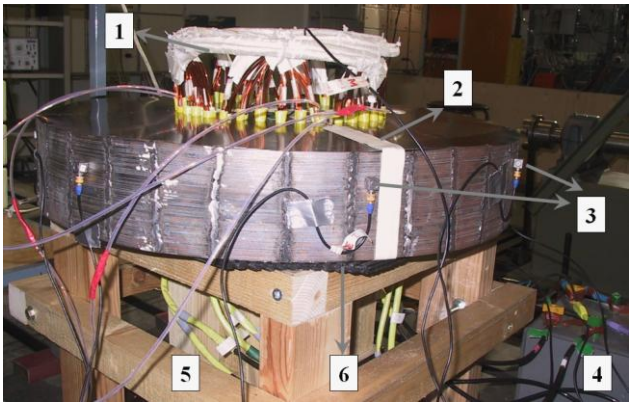

(a) Side view of the device.
1: windings, 2: search coils, 3: accelerometers,
4: connecting box, 5: wooden support,
6: vibration absorption plate.

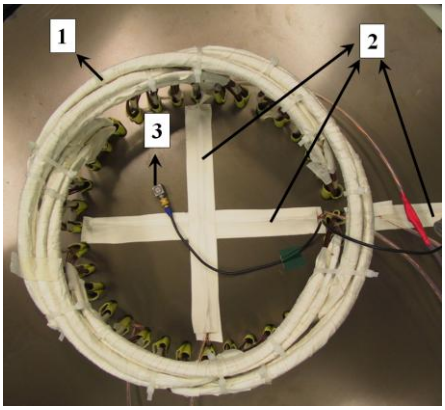

(b) Positioning of the reference accelerometer and sensing coils.
1: windings, 2: search coils,
3: reference accelerometer.

Figure 5.1: Test device ready for measurements.

To assist the design stage, numerical simulations were conducted to obtain a uniform magnetic flux density in the centre, as well as in the yoke of the machine. These helped in the adjustment of the position of the slots. The shape of the slots is small in order to avoid unnecessary left-over air, but large enough to insert the windings, which were insulated beforehand. Additionally to these, search coils for measuring the magnetic flux densities were squeezed into the slots. Five of these

were wound around the iron in the central part, as well as on the yoke and the teeth. The resistance of the phase windings is similar for three phases. Figure 5.1 (a and b) shows the final apparatus, welded and ready for measurements. As can be seen in this figure, the device is separated from its wooden support by a rubber plate in order to absorb the external vibrations. A fan is used to cool down the structure after each set of measurements. Eight accelerometers, in addition to the reference accelerometer, are placed on the outer boundary of the device. The reference accelerometer (Ref.), positioned in the central part, as shown in Figure 5.2, is necessary in order to get the relative displacement of each sensor with respect to it.

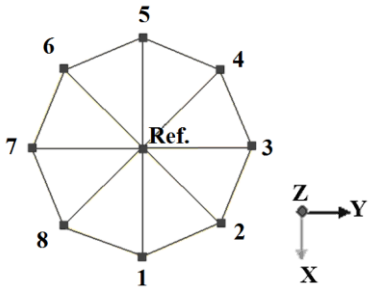

Figure 5.2: Schematic view of the placement of the accelerometers.

5.1.2 Experimental results

A setup as in Figure 5.3 is introduced for measuring these displacements at a supply frequency of 50 Hz. A root mean square value of magnetic flux density varying from 0.2 T to 1.1 T is reached in the centre of the device. The accelerometers are connected to their control unit. They are fixed using insulated magnets for better accuracy in the results on the outer surface. Those magnets do not have an influence on the results; they just serve as a support for the accelerometers. The input line current and voltage are measured with a power analyser. The input voltage is controlled in order to obtain the desired magnetic flux density in the central part.

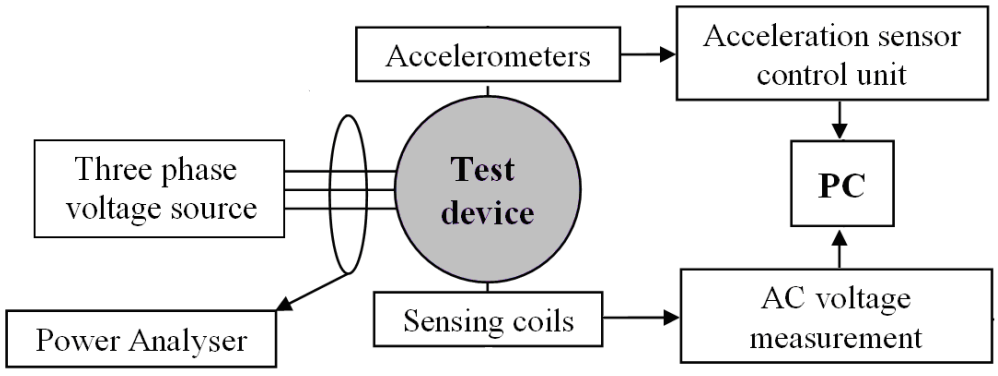

Figure 5.3: Experimental setup.

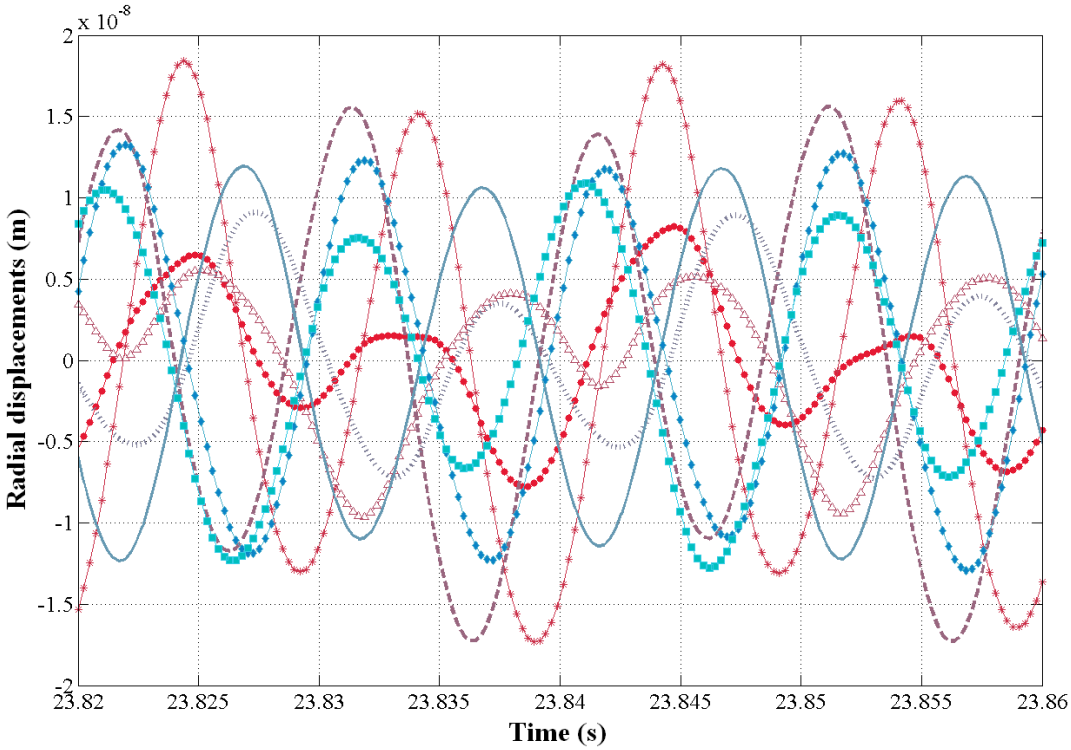

Case 1, measured for **B** = 0.4 T.

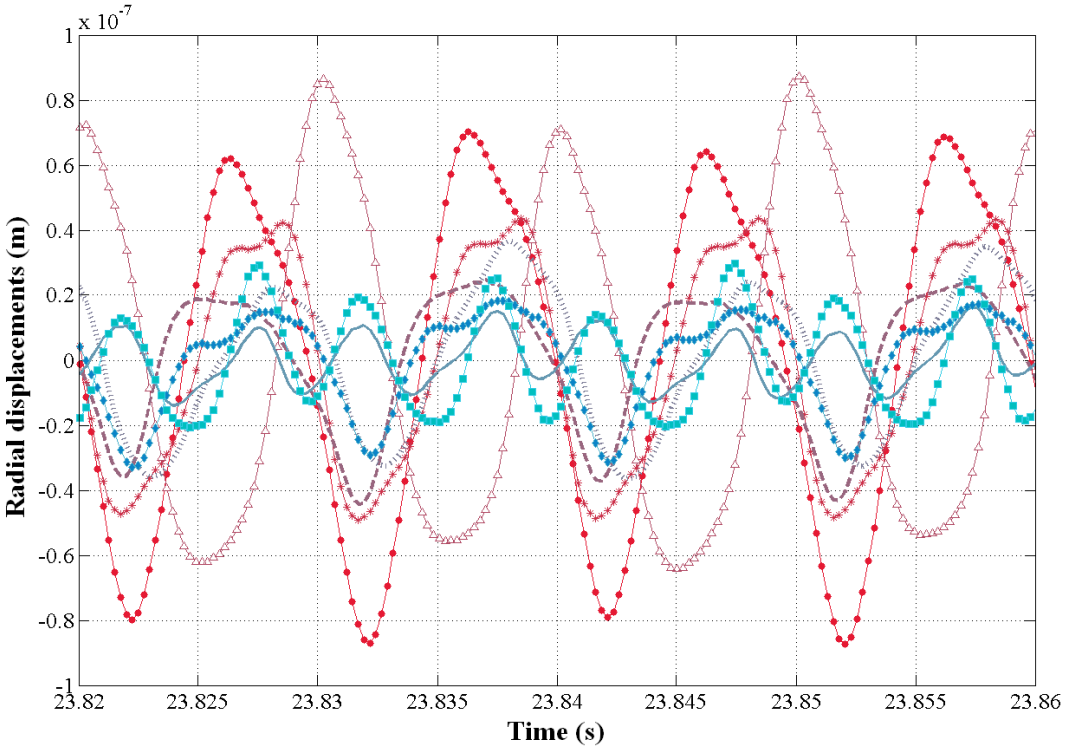

Case 2, measured for **B** = 1.1 T.

Figure 5.4: Measured radial displacements; each dataset represents the displacement from one accelerometer, results at 50 Hz.

Displacements from the eight accelerometers are shown in Figure 5.4 for two different input voltages. In the first case, “Case 1”, the peak value of the magnetic flux density in the centre of the device is 0.4 T. The measured line voltage and line current are 85 V and 0.9 A. In Case 2 the peak value of the magnetic flux density is 1 T. The measured line voltage and line current are 162 V and 17 A. The results are discussed below.

In Case 1, the radial displacements vary from 0.018 μm up to 0.038 μm. In Case 2, the peak-to-peak displacements vary from 0.035 μm up to 0.17 μm. Four out of the eight sensors measured displacements from 0.055 μm to 0.078 μm. The results show a difference between the different sensors. Indeed, in an ideal symmetric case, i.e. a symmetric magnetic field, perfect windings, perfectly stacked sheets, and no preferred direction of magnetisation in the sheets, there would probably not have been such differences. The measured voltages in the perpendicular coils in the centre of the device are illustrated in Figure 5.5. As can be seen from the rectangular shape in this figure, the material starts to saturate in “Case 2”, while in “Case 1” the magnetic flux density is still sinusoidal.

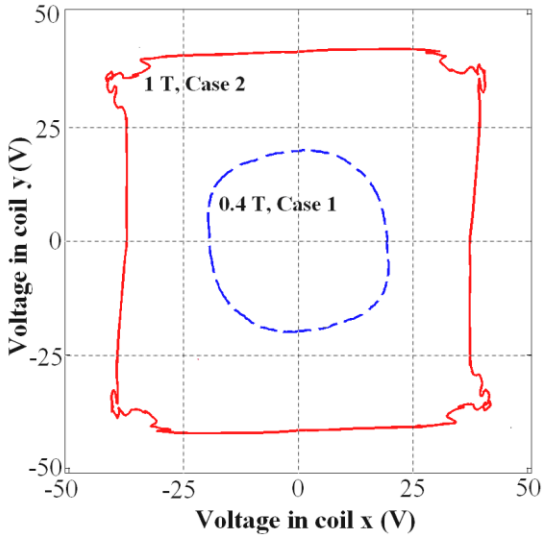

Figure 5.5: Voltage measured in the perpendicular coils in the centre of the device.

On the basis of these measurements, the following observations are pointed out.

(1) The device is placed on a wooden structure, which creates the possibility that damping may increase. Moreover, the asymmetric positioning of the machine can certainly lead to greater stiffness in one direction than in the other one.

(2) The core is loose because of the lack of axial compression and thus high structural damping is evident. The hammer test method was used to get the

fundamental frequency of the structure. However, clear results were difficult to get because of this high damping.

(3) The sensors are attached to the boundary with specially insulated magnets. Hence two problems arise. First, the influence of the external magnetic field on the accelerometers should in theory be weak; anyhow, the measuring accuracy of these is known to be influenced by external magnetic fields. In particular, the reference accelerometer was positioned in the centre of the device, where the magnetic flux density is the highest. This leads us to the next point.

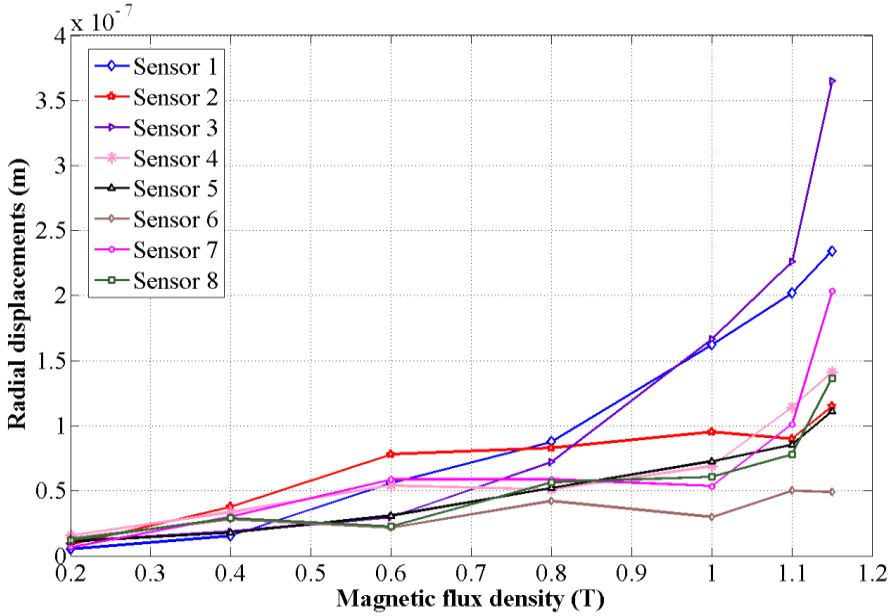

Figure 5.6: Differences between the eight sensors.

(4) Comparisons between the measurements in Case 1 and Case 2 show that the outputs of the sensors vary randomly with the magnetic flux density. For this reason, the measurements were performed at magnetic flux densities in the centre of the device from 0.2 T to 1.1 T with steps of 0.2 T. These results, for a supply frequency of 50 Hz, are illustrated in Figure 5.6. The radial displacements are the peak-to-peak values. From these, it can be established that there is no single sensor that acquires higher displacements than all the others for each value of **B**. The differences between the measurements are ostensibly large over 0.8 T. Besides in most cases the radial displacement logically increases with an increasing input **B**. Considering one value of **B**, higher than 0.2 T, the minimum measured point is always approximately two to four times lower than the maximum one. For this specific reason, a clear dependency on the accuracy cannot be directly deduced.

In the next section, the computed results are compared with the measured ones. Conclusions on these results will be drawn, with the previous discussions being kept in mind.

5.1.3 Computed results and discussion

Simulations with a 50 Hz sinusoidal supply of 160 V and 280 V are performed (Figure 5.7). One period of the magnetic flux density is 20 ms, so that 2.5 periods are presented. As shown in Figure 5.7, the peak-to-peak radial displacement of one node on the outer boundary for Case 1 is 0.02 μm, and for Case 2, it is 0.038 μm. If the magnetic flux density is 2.5 times larger, correspondingly the displacements experience an increase by a factor of 1.9. The fundamental harmonic in Figure 5.7 is 100 Hz, which is twice the supply frequency. The parameters for the model are those identified from the beam of curves in Figure 4.5, on the same type of material as the sheets of the device.

Figure 5.8 (a) shows the mesh of the test device at zero magnetic flux density. The mesh is prepared with COMSOL® and exported into the finite element software, which contains the coupled model. Figure 5.8 (b) presents the same mesh at a specific time step that corresponds to the magnetic flux density distribution in Figure 5.9. At this point it should be noticed that the displacements are always calculated from the original mesh. Since the displacements are small enough (less than 10 μm), this hypothesis is acceptable.

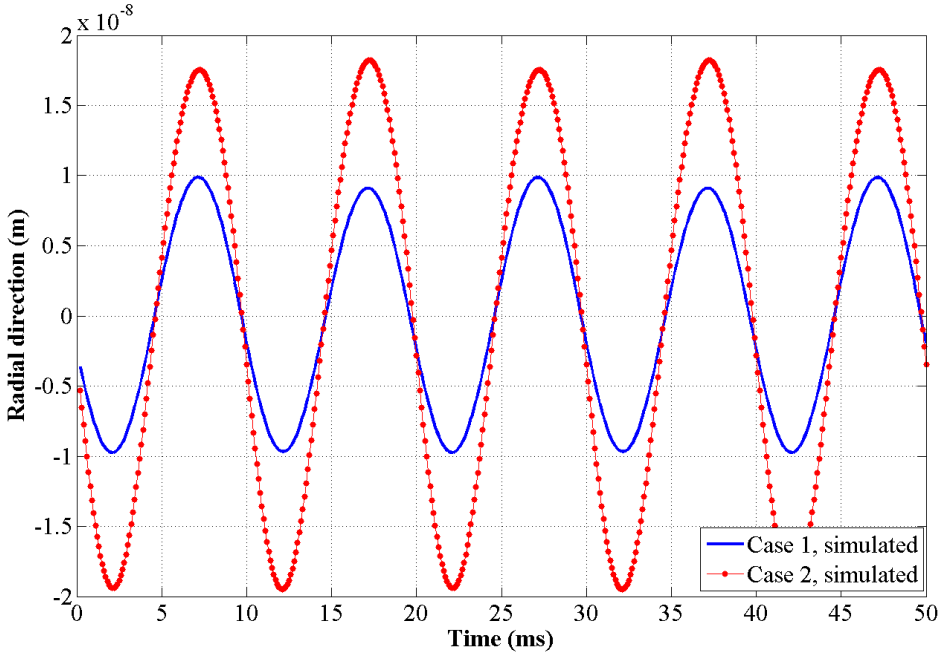

Figure 5.7: Simulated displacements of one node on the outer boundary.

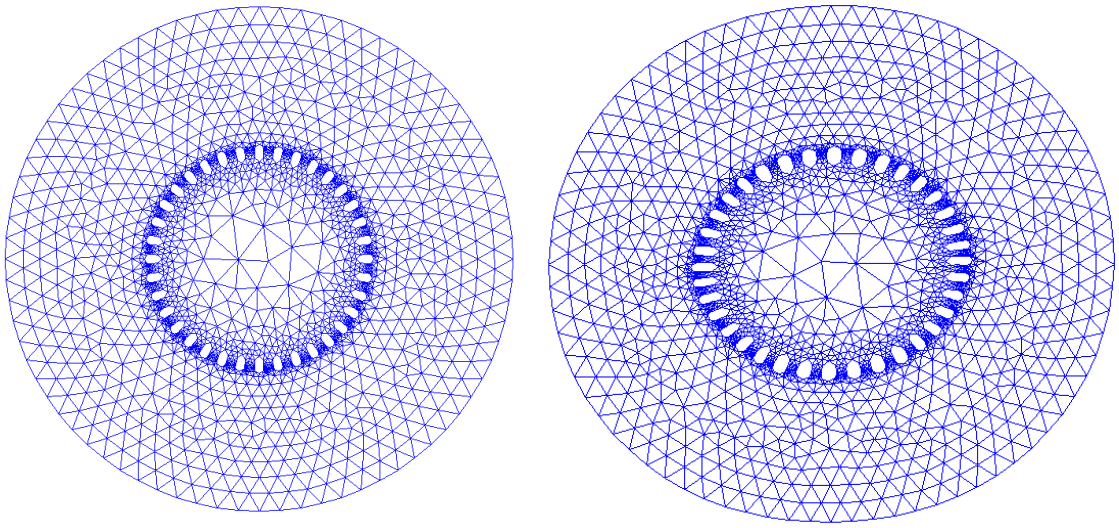

(a) Non-deformed case. (b) Deformed case. Scale X 20000.

Figure 5.8: Mesh of the test device, 5604 nodes, 11064 first-order elements.

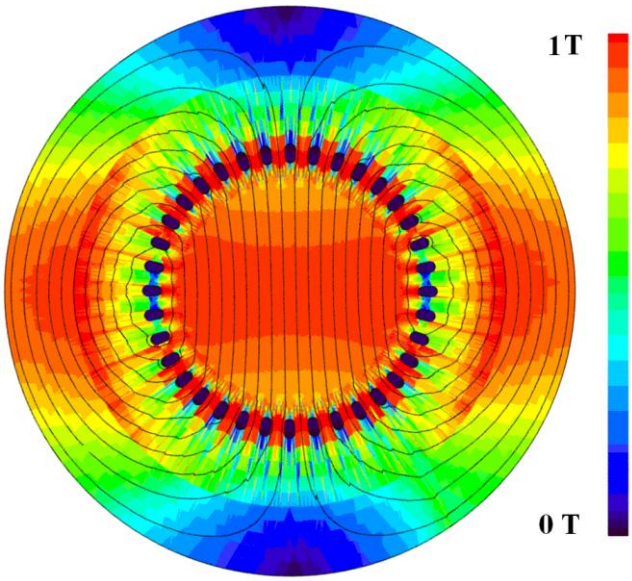

Figure 5.9: Simulated magnetic flux density distribution in the test device.

On the basis of these figures, it is clear that the structure tends to expand under the magnetic loading, especially in its centre. The computed results, compared with the experimental ones, are presented in Figure 5.10. They reveal the following points.

(1) For Case 1, the sensors measure peak-to-peak radial displacements between 0.03 μm and 0.015 μm. The simulations predict the value as being 0.019 μm. For this case, the computed results are within the same range as the measured values.

(2) For Case 2, the sensors measured a peak-to-peak radial displacement between 0.175 μm and 0.025 μm. The simulations predict the value as being 0.039 μm. The computed results are within the same range as the measured ones. However, they are much closer to the lower limit.

(3) The measured displacements in the axial or *z*-direction were the highest ones. They were not presented here because they are not supposed to be due to magnetostriction. However, they might have a slight effect on the high values obtained by some sensors in both cases.

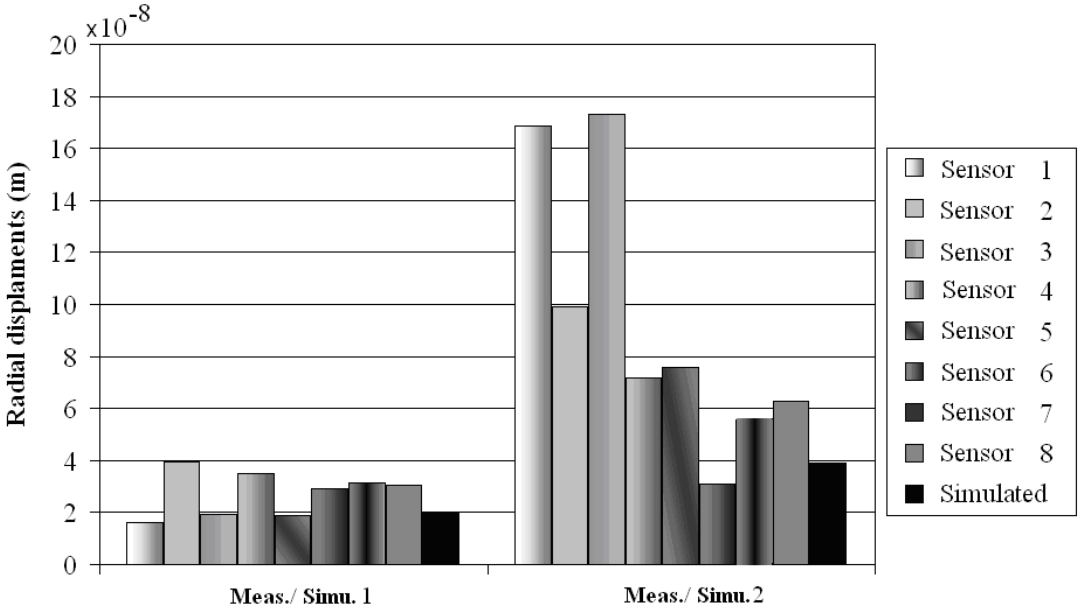

Figure 5.10: Comparison between the measured values and simulated ones.

The results displayed here are compared to previous work. Indeed, Låftman (1994) assessed displacements as ranging from 0.2 to 0.35 μm under a frequency of 50 Hz and a magnetic flux density in the yoke of 1.5 T. The measurements were conducted on a hollow machine. These values are 10 times higher than those presented above. Belahcen (2004) observed, at 50 Hz and 1 T displacements of 0.04 μm. In both cases, the measurements were performed by acquiring the velocity with a laser, and in both cases there was no information about the material type of the electrical steel.

5.2 Verification with an asynchronous machine

The method presented in Chapter 3, Section 3.4 accounts for the Maxwell stress in air. In this section, results from measurements and simulations are compared.

First, a simple case geometry is examined and the computed results using the coupled method are compared with those from commercial software. The second verification method consisted in running an asynchronous machine at locked rotor operation. This test machine has been built by Hirvonen (1983) in the Unit of Electromechanics of the Helsinki University of Technology. Its geometry and the absence of a stator outer frame allow placing sensors on the outer boundary, between the windings to measure the displacements.

5.2.1 Implementation of the method to a simple square geometry

In this section, electrical steel with an air gap is simulated as an example. In Chapter 3, the approach, albeit not traditional, in the present work has been justified. It is known that the stress acting on the air-iron boundary deforms the most the structure. Although, the resulting reluctance forces acting on the air-iron boundary have been primarily considered in the literature, the major aim in this subsection is to validate numerically on a simple case the implementation of the developed model in iron and the importance of the Maxwell stress at the boundary. This sample geometry is a way of assessing whether the numerical method that was developed can be used for larger geometries. Consequently, it will be extended later in this chapter to the case of electrical machines.

The dimensions of the square sample are 0.6 m x 0.6 m and the air gap is 0.6 m long and 0.05 m wide. For the sake of simplicity the outer boundaries of the test sample cannot deform. Only the region close to the air gap can experience a displacement. In all the simulations a constant magnetic flux density of 2 T is applied to the whole geometry, in the *y*-direction in Figure 5.11 (a, c, and e) and in the *x*-direction in Figure 5.11 (b, d, and f). As expected, the displacements in Figure 5.11 (a, c, and e) and in Figure 5.11 (b, d, and f) are of opposite signs. Results for those simulations are divided into three parts.

In the first case the coupled magneto-mechanical model defined in Equations (69) and (70) was taken into account in iron It should be noticed that this case is not physically acceptable. However, these results enable the understanding of the influence of the magnetostriction and electromagnetic stress tensor inside iron. In the second case, the simulations shown in Figure 5.11 (c and d) take the electromagnetic stress tensor in the elements in air into account. All four of these simulations are performed within the finite element software where the model is implemented. In the third and last case, the geometry is exported into COMSOL and analysed within the software.

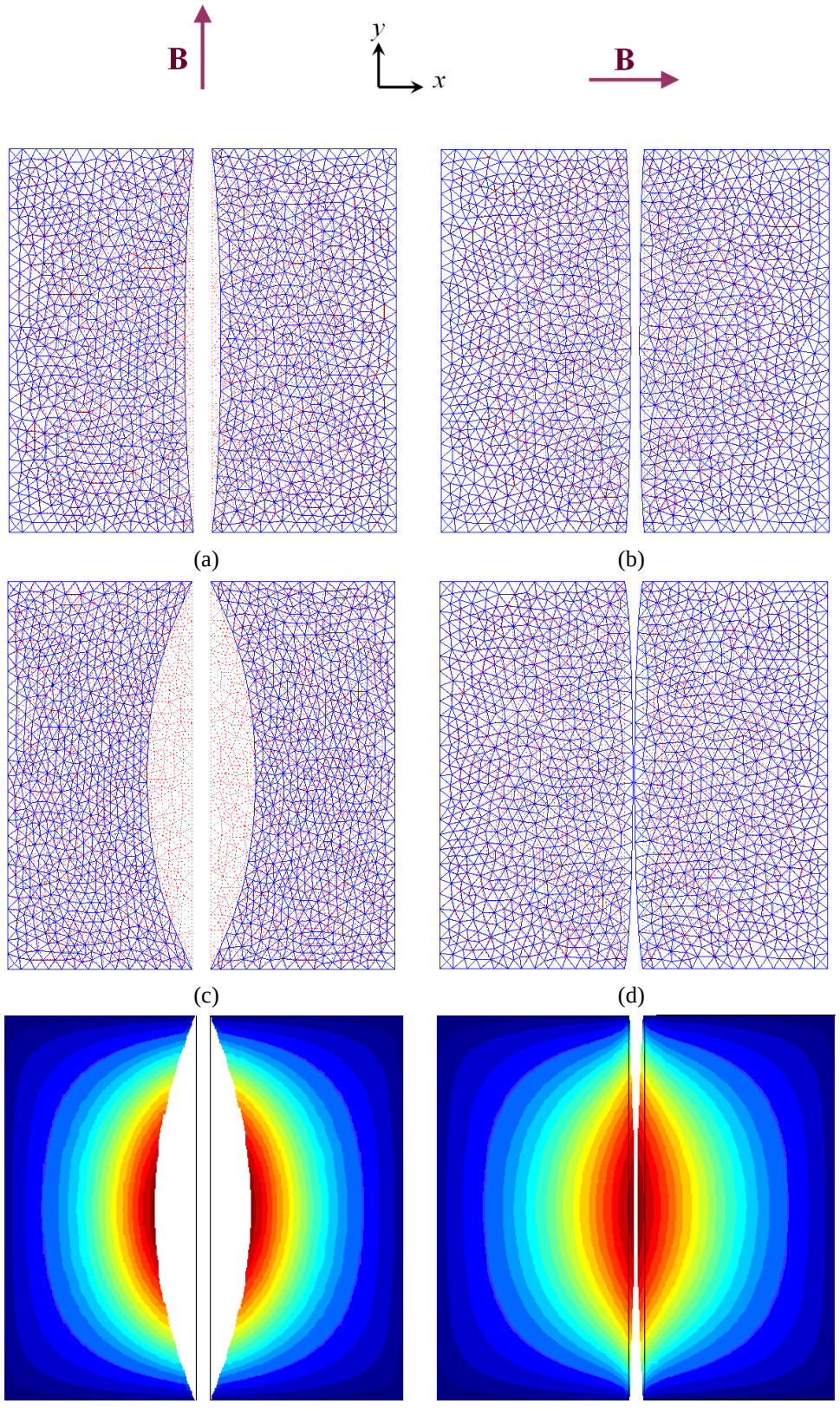

Figure 5.11: Deformed meshes of the test geometries, scale $\times 10^5$ and $\times 2 \cdot 10^5$.

All the external boundaries are fixed mechanically and the magnetic boundary conditions are set in the same fashion so as to reproduce those in the previous simulations. A distributed load is added at the iron-air boundary that is equal to the electromagnetic stress tensor evaluated in air. This is calculated in the post-processing. The scales are similar to those in Figure 5.11 (c, d, e, and f).

As anticipated, Figure 5.11 (a and b) depicts a smaller displacement than Figure 5.11 (c, d, e, and f). The configuration in Figure 5.11 (d and f) resembles that of a stator and rotor boundary of an electrical machine in the sense that the magnetic flux lines traverse the air gap perpendicularly, omitting, by hypothesis, all kinds of fringing or flux leakages.

5.2.2 Experimental results for the machine

The device in 1: rotor, 2: stator, 3: windings, 4: search coils, 5: supporting grips.
Figure 5.12 is an asynchronous machine, where only the stator has been wound. The machine is directly fed with a sinusoidal voltage from the grid and fixed to a support frame by six grips. The windings were connected in a star. The dimensions of the machine and the mesh used later for the finite element computation are presented in Appendix D. More information regarding the design and building of the device is provided by Hirvonen (1983).

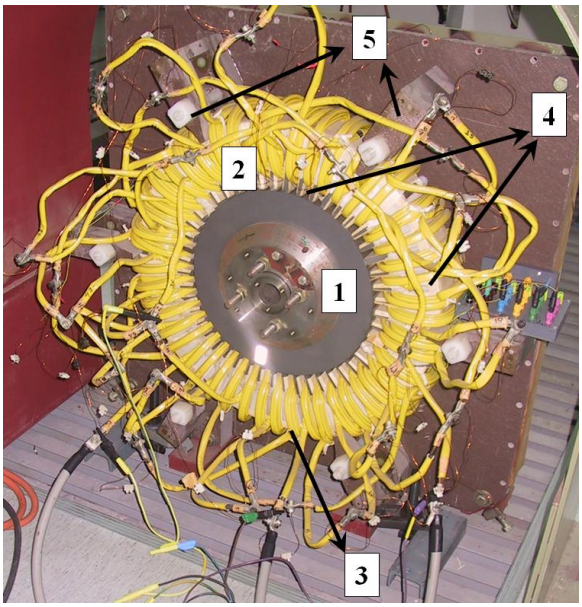

1: rotor, 2: stator, 3: windings, 4: search coils, 5: supporting grips.

Figure 5.12: Side view of the machine.

The measurements are run in a similar way as in the previous section. The outer stator boundary of the machine is more difficult to access because of the windings, and so

only three accelerometers are positioned. The magnetic flux density is acquired thanks to search coils around the stator yoke and on the teeth. The rotor is kept locked during the measurements because of a noticeable eccentricity in the air gap. The simulations will not take any eccentricity into account. Measurements were conducted at 100 Hz. Indeed, the accelerometers appeared to be sensitive to the disturbance from external magnetic flux density at a supply frequency of 50 Hz. The input frequencies, currents, and voltages are provided in Table 2. There, the peak magnetic flux density in the stator yoke is given as a reference. The three measured magnetic flux densities as functions of time are plotted in Figure 5.13.

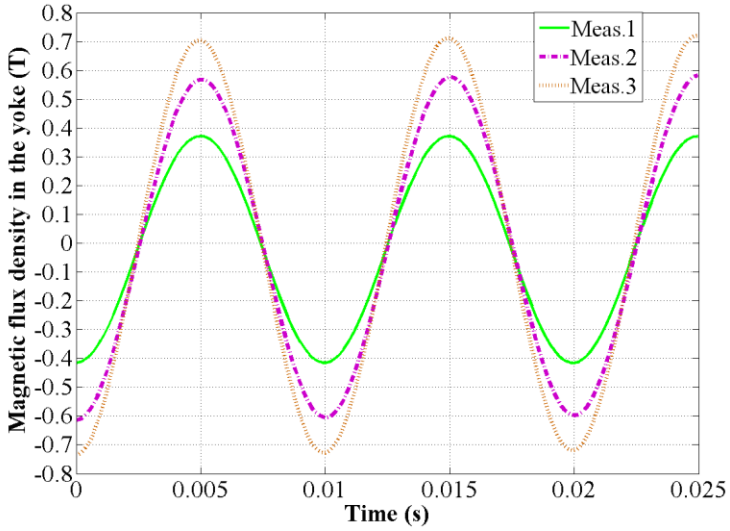

Figure 5.13: Measured magnetic flux density in the yoke.

In Figure 5.14, measurements at 100 Hz are presented in the radial and tangential directions for each measurement configuration (Meas. 1, 2, and 3).

The peak-to-peak radial displacements vary in Meas. 1 from 0.025 to 0.055 μm, in Meas. 2 from 0.05 to 0.065 μm, and in Meas. 3 from 0.06 to 0.088 μm. On the other hand, the tangential displacements are higher. In Meas. 1 they vary from 0.04 to 0.075 μm, in Meas. 2 from 0.06 to 0.1 μm, and in Meas. 3 from 0.05 to 0.1 μm. The latter two results are very close to each other, for no significant understandable reason.

In general, the radial displacements seem to depend on the position of the accelerometer on the stator. It is highly likely that the windings, wound like in a toroïd, induce extra stresses and thus higher frequencies in the displacements. The rotor, for instance, is not placed perfectly symmetrically. The experimental results indicate that the displacements resulting from the magnetic stresses in the stator of an asynchronous machine are close to 0.1 μm on the outer boundary of the stator for

higher magnetic flux densities. Extra measurements could be conducted by putting special accelerometers or strain gauges on the inner boundary of the stator. This kind of setup could help in acquiring the acceleration of a region on the stator tooth.

In the next section, the displacements of the stator teeth as predicted by the model are depicted. However, no certainty about those can be established, as discussed above.

Table 2: Inputs for the measurements.

	Frequency [Hz]	**Line current [A]**	**Line voltage [V]**	**B_{peak} in yoke [T]**
Meas. 1	100	29	100	0.37
Meas. 2	100	45	150	0.57
Meas. 3	100	53	185	0.75

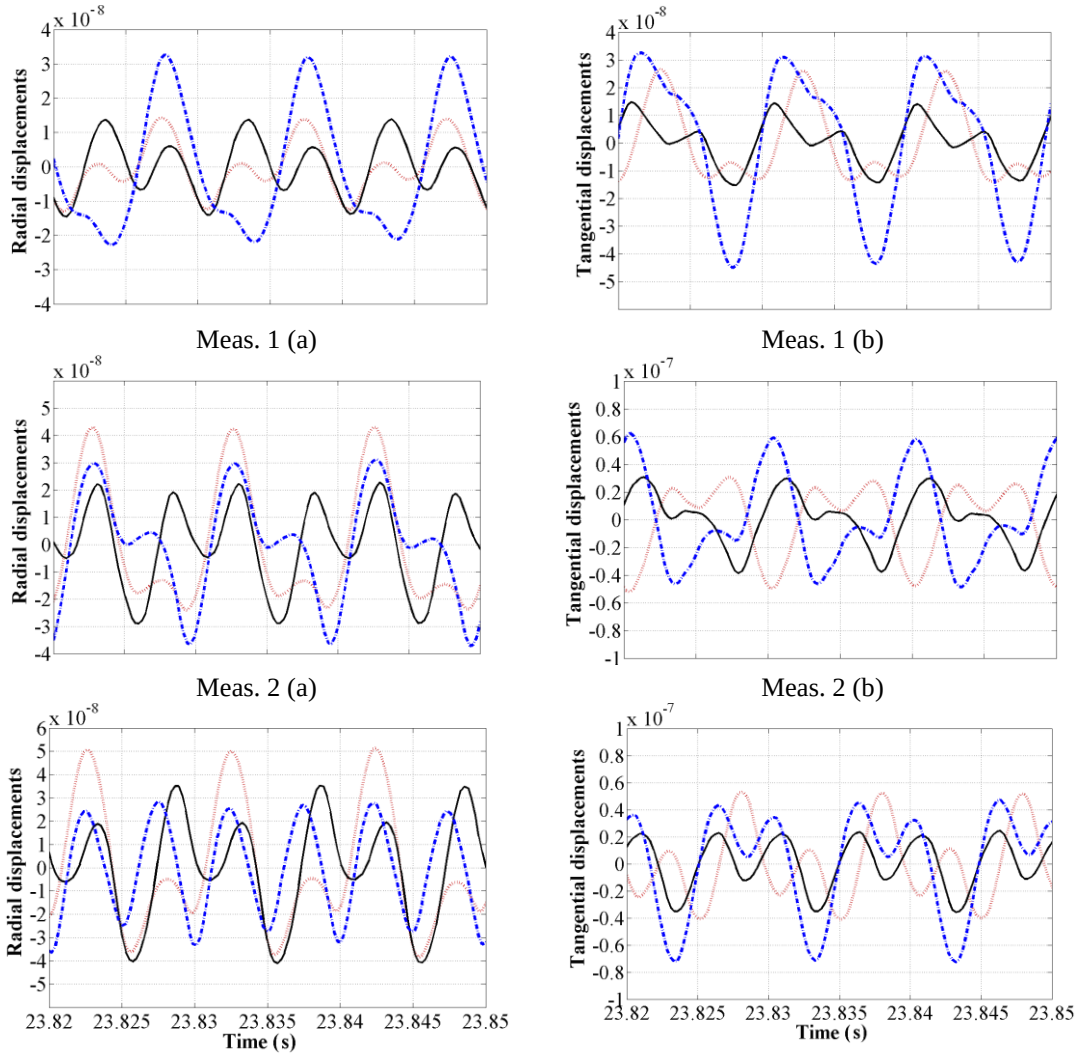

Figure 5.14: Measured displacements of three sensors.

5.2.3 Computed results and discussion

The computed results use the values from Table 3 as inputs. The number of time steps per period is 800, and 3 periods are simulated. Regarding the speed of the calculation, it took approximately 2 hours, with a PC to simulate in this specific case the first-order element geometry. This is fairly acceptable on an industrial level, but for the purpose of the study, it is considered to be more than fine. The results are gathered in Figure 5.15. The corresponding radial and tangential displacements are denoted as Simu. 1 (a) (simulation 1) and Simu. 1 (b). The corresponding input values of Simu. 1 are gathered in Table 3. The outer stator boundary is free to move in the radial and tangential directions, except for six regions that are holding the structure, as shown in Figure 5.16 (a). In practice, for the computation, selected nodes and elements close to the marked black dots in Figure 5.16 (a) are chosen to be fixed. Figure 5.16 (b) offers a zoom of one quarter of the structure, in the normal and deformed cases. The arrows illustrate the direction of the displacements and their magnitude with respect to each other. The rotor is free to move, except for its shaft, as it is fixed. Figure 5.16 (c and d) show the magnetic flux density distribution in the 2-D cross section of the machine, in the whole machine, and in one quarter of the machine.

The radial displacements of three nodes on the outer boundary are plotted. The displacements are five times higher in the second case. The displacements of one stator tooth are analysed in Figure 5.17. The results from this latter figure, as well as from Figure 5.16 (a and b), show that the structure is pushed towards the air gap. Displacements in the teeth have a significant value, which lies between 50% and 67%, higher than those on the outer boundary. The tangential displacements are high too.

In the radial direction the computed values are slightly different from the measured ones but remain within the range of the measurements. In the simulations, the shape of the stator slots was deduced approximately since these data could not be found from Hirvonen (1983). Further, the rotor was locked during the measurements. Rotating it would have required complicated adjustments because of the condition of the machine. These anomalies in the measurements can probably be accounted for by errors in the correct data of the electrical machine. Moreover, there is a strong possibility that the properties of the electrical steel sheets in the verification induction machine are different from those identified. However, as will be discussed later, these parameters remain within a similar range because there is a reasonable match between the results from the computations and those from the measurements. Nevertheless, for a strict scientific approach, the model should be identified with the parameters from the same electrical steel sheets as the one used in the machine.

Table 3: Inputs for the simulations.

	Frequency [Hz]	Line current [A]	Line voltage [V]
Simu. 1	100	36	100
Simu. 2	100	52	150
Simu. 3	100	66	185

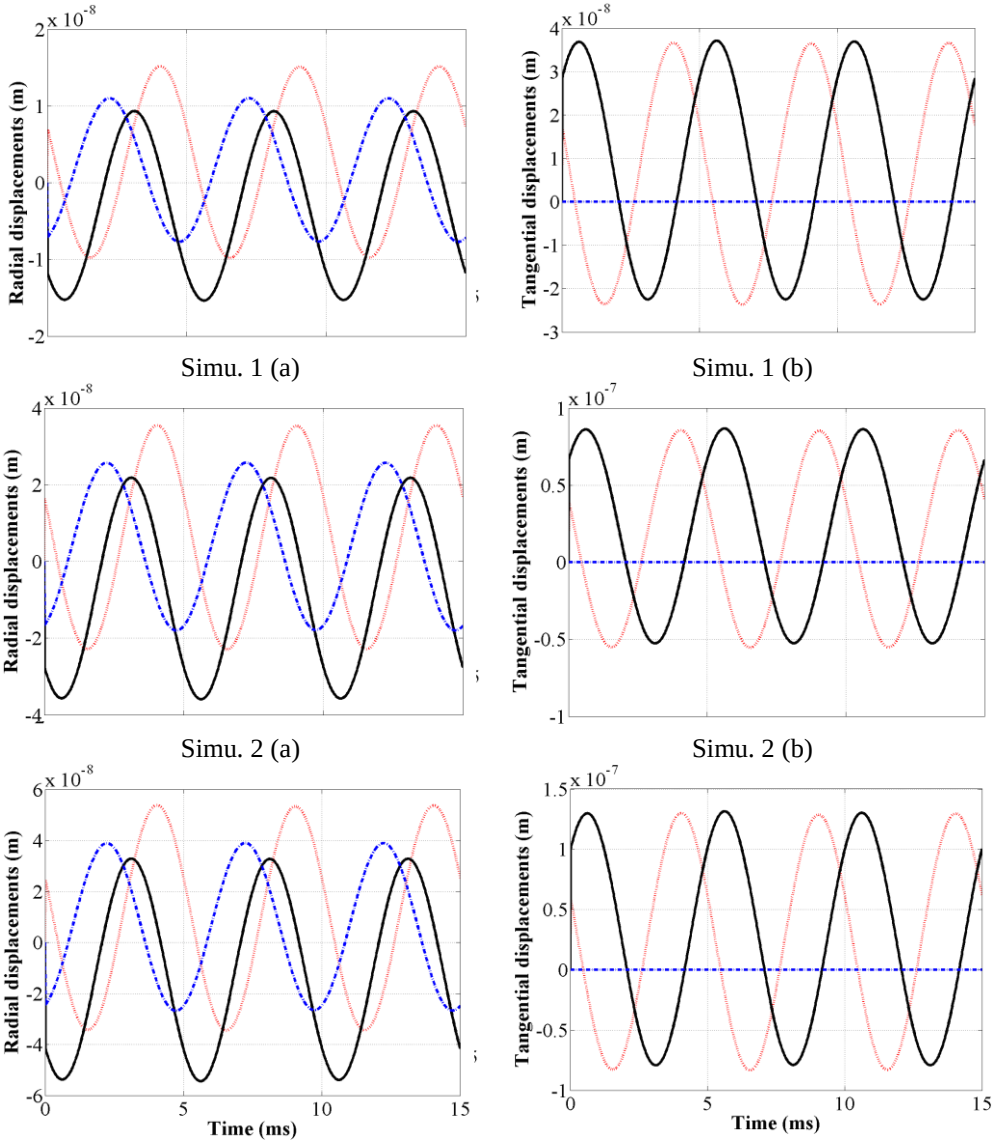

Simu. 1 (a) Simu. 1 (b)

Simu. 2 (a) Simu. 2 (b)

Simu. 3 (a) Simu. 3 (b)

Figure 5.15: Simulated displacements of three sensors.

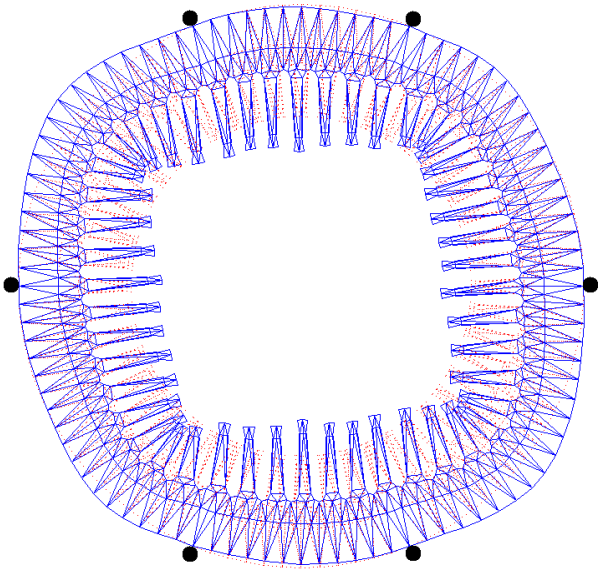

(a) Deformed stator geometry, when the electromagnetic stress tensor in air is taken into account.

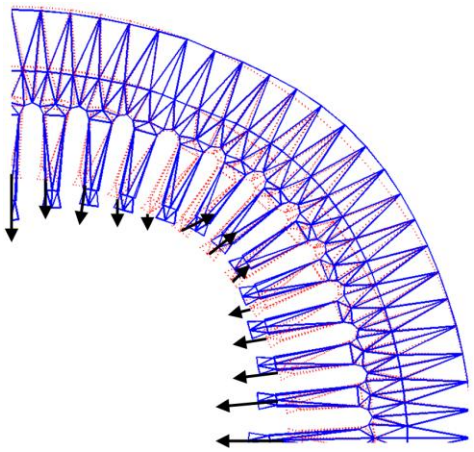

(b) Zoom (X 10^4) of the teeth of the stator.

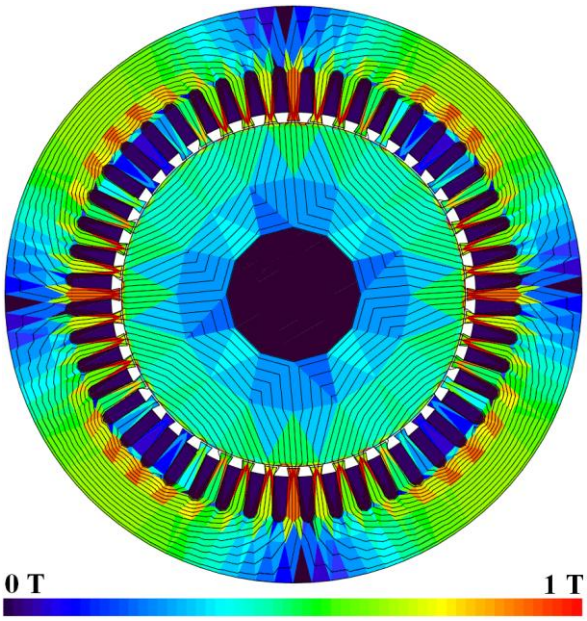

V_{line} = 150 V, whole machine.

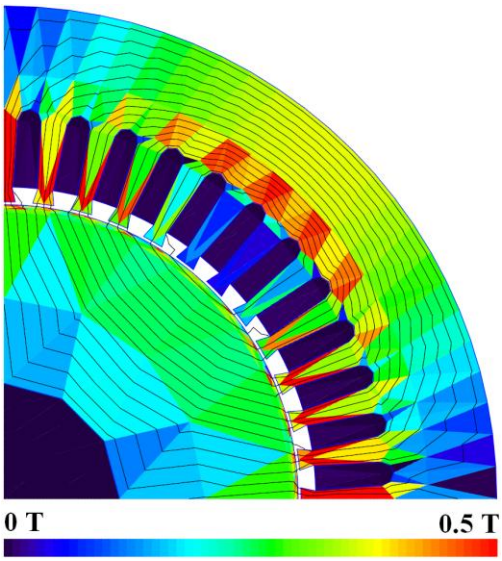

V_{line} = 100 V, one quarter of the machine.

(c) Magnetic flux density distribution.

Figure 5.16: Simulated results.

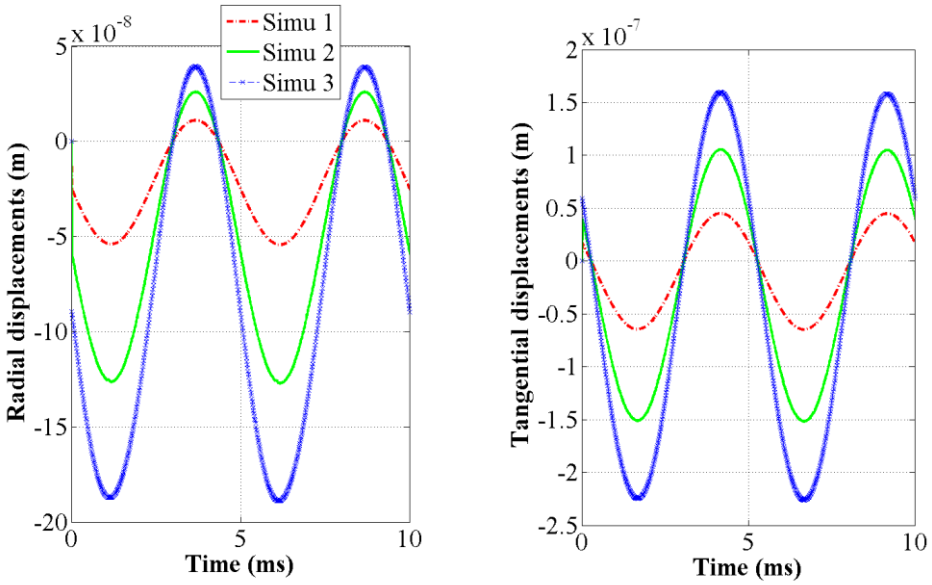

Figure 5.17: Radial and tangential displacements of one node on the stator tooth.

For better comparison, the collected peak-to-peak values of the displacements in the radial and tangential directions are presented in Figure 5.18. The maximum and minimum over all the accelerometers and the simulated results are remarkably good in the radial direction. However in the tangential direction, the model overestimates the displacements in 2 and 3. In 1, the results are fairly acceptable.

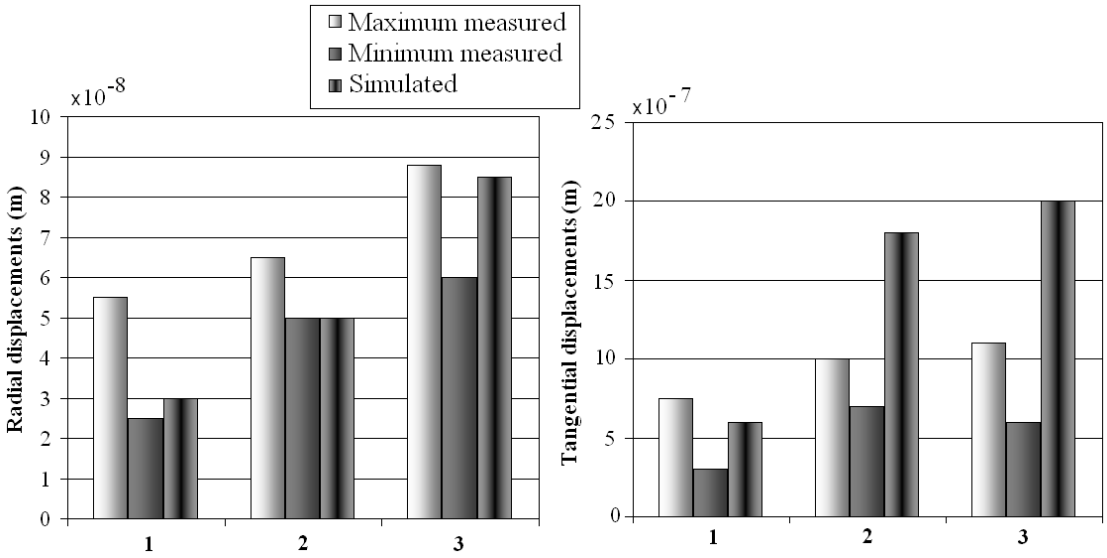

Figure 5.18: Measurements and simulated results compared for each of the three measurements.

Figure 5.19 and Figure 5.17 serve as an introduction to Section 5.3, where the influence of the electromagnetic stress tensor in air and the displacements of the teeth

will be studied thoroughly. From the geometry in Figure 5.19, the deformed shape is clearly different from the one in Figure 5.16 (a).

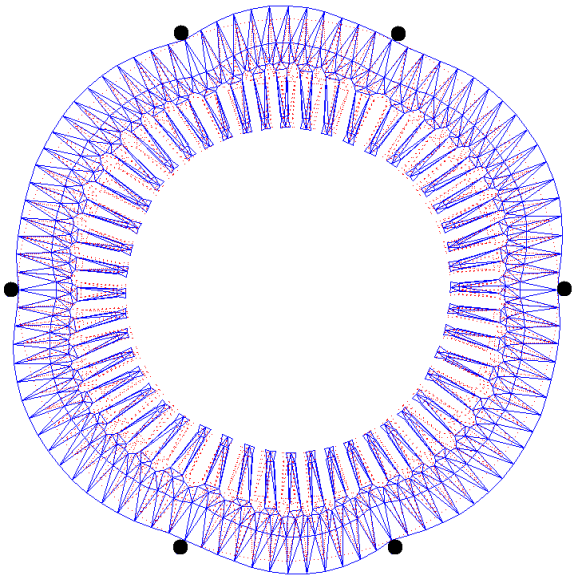

Figure 5.19: Deformed stator geometry when the electromagnetic stress tensor in air is not taken into account.

5.3 Analysis of the energy-based model

The magneto-mechanical coupled methods described in Chapter 3 and later generalised by taking the electromagnetic stress tensor in air into account were applied to a simple square geometry with an air gap, as well as to two different electrical machines. On the basis of the previous results from Section 5.1 and 5.2, the model is assumed to be acceptable for the study. The results of the deformation of the structures are presented in the following sub-sections.

5.3.1 Introduction

Here, the numerical problem discussed in Chapter 3 is solved in the finite element software and analysed. As previously stated, the model requires parameter identification, and thus knowledge of the material properties. For the simulated machines, these data are unavailable. For this reason, the parameters presented in the table below are used as a hypothesis, as these parameters are valid only for one type of material.

The necessary parameters, (α_0, ..., α_6) for the model were identified from unidirectional magnetostrictive stress measurements from the modified Epstein frame on the samples used in Belahcen (2004) as presented in Chapter 4. The difference between Figure 4.5 and Figure 5.20 lies in the type of electrical steel sheet and thus the magnetostrictive strain response for those.

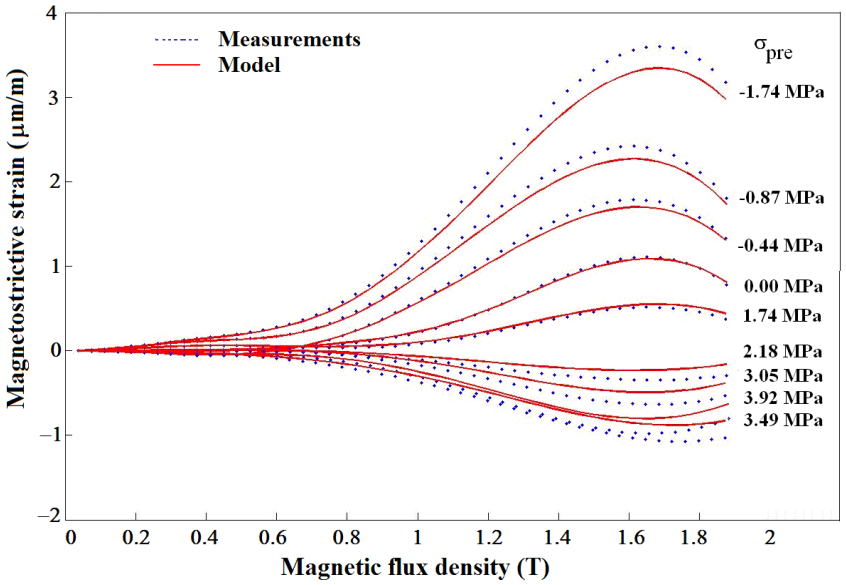

Figure 5.20: Magnetostrictive curves at different stress states.

The measured magnetostrictive strain that was obtained and the corresponding results from the model for both cases of compressive and tensile mechanical pre-stresses are presented in Figure 5.20. The best-fitted curve corresponds to no mechanical pre-stress. The parameters gathered in Table 4 used are those identified from the beam of curves in Figure 5.20.

Table 4: Values of the dimensionless parameters identified from the Epstein frame.

Parameter	α_0	α_1	α_2	α_3	α_4	α_5
Values	-0.9994	$-1.2\cdot10^{-3}$	$4.0857\cdot10^{-4}$	$8.8242\cdot10^{-5}$	-0.028	-0.052

The following results are intended to present an approximate idea of what the solution might look like if the material characteristics were correctly identified. However, the discussion will be based on relative and not quantitative values of displacements.

5.3.2 Application to two- and four-pole electrical machines

This section concentrates on the effects of the different terms within the model. Efficient computation is possible because the 2-D magnetic field and displacement are solved simultaneously and the different single-valued stress-dependent magnetisation curves do not need to be evaluated one by one. Furthermore, the actual influence of the electromagnetic stress within iron cores is studied. The simulated machines attest to the acceptability of the model for a 2-D mesh of a rotating electrical machine.

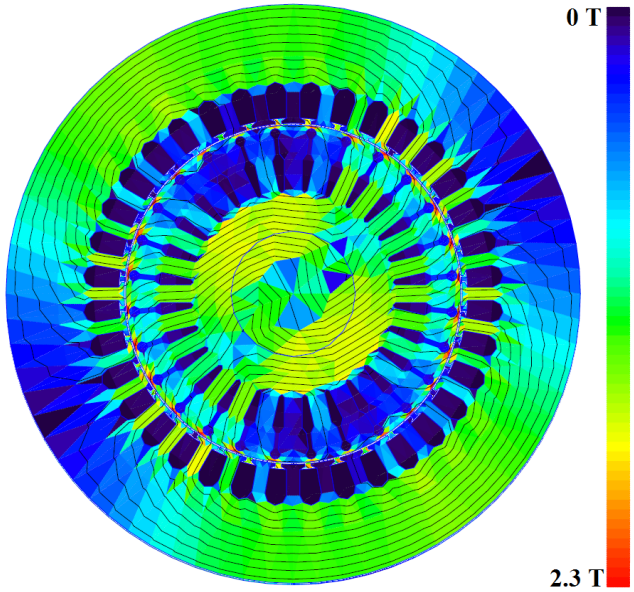

Machine I

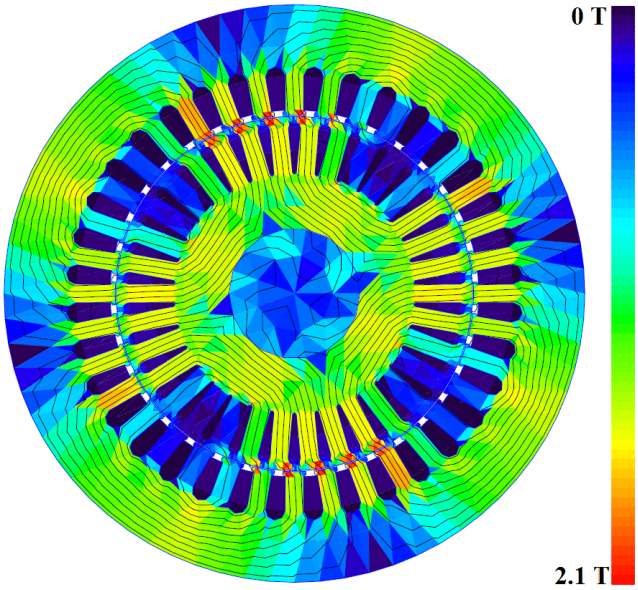

Machine II

Figure 5.21: Simulated flux density distribution.

The coupled model was applied in the case of two asynchronous machines. Both test motors are squirrel-cage induction motors. The first one, referred to as “Machine I”, is a 30-kW machine with two stator poles, and the second one, referred to as “Machine II”, is a 15-kW machine with four stator poles. Appendix D provides detailed data for these machines. The reason for choosing these machines is mainly the different numbers of pole pairs and slots in the stator and rotor in order to study whether the model can predict displacements in both cases.

Six simulations are performed, each of them in a steady state. An initial magnetic state for the time-stepping analysis is computed from the results of a time-harmonic formulation. This enables the behaviour of the machine to be simulated away from any transient phenomena. The machines are supplied with a sinusoidal voltage at the rated values. The first set of simulations involves analysing the influence of the elastic stress tensor and magnetostriction only on the displacements of the structure. The second set of simulations accounts for the previous terms and for the electromagnetic stress in *iron*. The third set takes into account the influence of the electromagnetic stress tensor in *air*. Magnetic flux-density distributions at an arbitrary time step are shown in Figure 5.21. The corresponding original and displaced 2-D stator and rotor geometries are presented in the following pages, in Figures 5.22, 5.24, 5.26, and 5.28. The differences between the last four figures are specifically discussed below.

As described in the previous sections, the boundary conditions are set to be such that the outer boundary of the machine is fixed in the tangential direction but free to move in the radial direction. Furthermore, the shaft is fixed in both directions in order to fix the boundaries on the rotor. Another assumption is that the welding of the outer boundary of the machine is not taken into account in the simulations, but its influence is assumed to be small.

As explained above, the displacements of each node of the mesh are known at every time step, thanks to the numerical method that was developed. The results indicate that the magnetostrictive effect is attenuated by the contribution of the electromagnetic stress within the simulated electrical steel sheet, as in Figures 5.23 and 5.27. According to Figures 5.23, 5.25, 5.27, and 5.29, the contribution of magnetostriction and magnetic stress in iron tends to expand the shape of the machine. The radial and tangential displacements when the electromagnetic stress tensor in iron is taken into account (or not) are now discussed. The general observation is that the addition of electromagnetic stress to the computation slightly reduces the peak-to-peak amplitudes of the displacements. However, the DC component is reduced by 20% for Machine I and by 25% for Machine II. The ripples in the displacements are more dominant for Machine II. Radial displacements in

Machine II are higher than in Machine I because the magnetic flux density is higher. The effect of the electromagnetic stress is small with respect to the deformations resulting from the magnetostriction. The tangential displacements are three times smaller than the radial displacements on the tooth of the stator.

On the other hand, the inclusion of the electromagnetic stress tensor in air into the computation has a considerable influence on the displacements of the stator and the rotor. Figures 5.25 and 5.29 suggest that the displacements are increased 2.5 to 4 times, depending on the number of pole pairs and the magnitude of the magnetic flux density. The deformations resulting from the addition of this stress to the computation are shown in Figures 5.24 and 5.26 for both machines.

Finally, one node in the centre of the stator tooth is studied in Figures 5.25 (a) and 5.29 (a). When compared to the displacements on the outer boundary – Figures 5.25 (b) and 5.29 (b) – it can be established that the displacements on the teeth in the radial direction have a higher amplitude than the ones on the outer boundary of the stator. The displacements in the tangential directions are also relatively high, as the peak-to-peak displacements range from 0.4 to 1.2 μm. These results are plotted in Figures 5.25 (c) and 5.29 (c).

According to the computed results the following conclusions are established.

(1) On the basis of the knowledge of the parameters of the material, the model is suitable for predicting the displacements in a radial-flux rotating electrical machine.

(2) The displacements, when accounting for the Maxwell stress tensor in air, are significantly high. In Machine II, the outer boundary of the stator undergoes a displacement of 0.5 μm peak-to-peak.

(3) The model can predict tangential displacements.

(4) Displacements on the stator teeth are 15% higher than those on the outer boundary of the stator. For small air gaps, for example 1 mm, as a result of these deformations, the rotor and the stator come closer by 0.2%.

(5) As an extrapolation, sudden changes in the magnetic flux density can be detected numerically.

(6) There is a need for measurements of the acceleration, and hence the displacements of the outer boundary of rotating electrical machines, for the verification of the method. Even better, the measurements of those on the teeth of such machines could create even greater trust in this method.

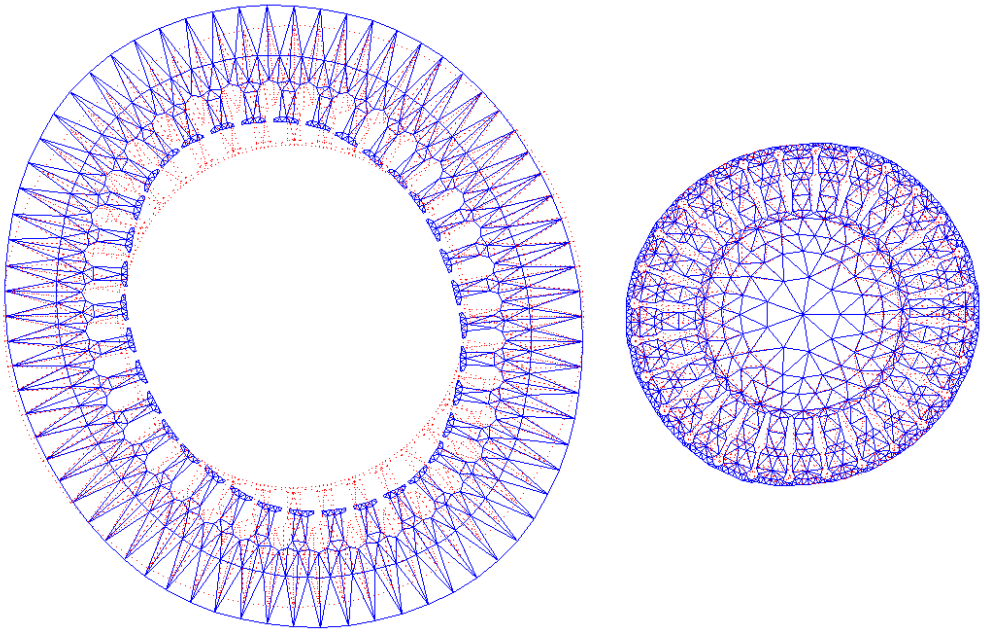

Figure 5.22: Machine I: Deformation of stator (left) and rotor (right), the electromagnetic stress tensor in the air gap is not taken into account.

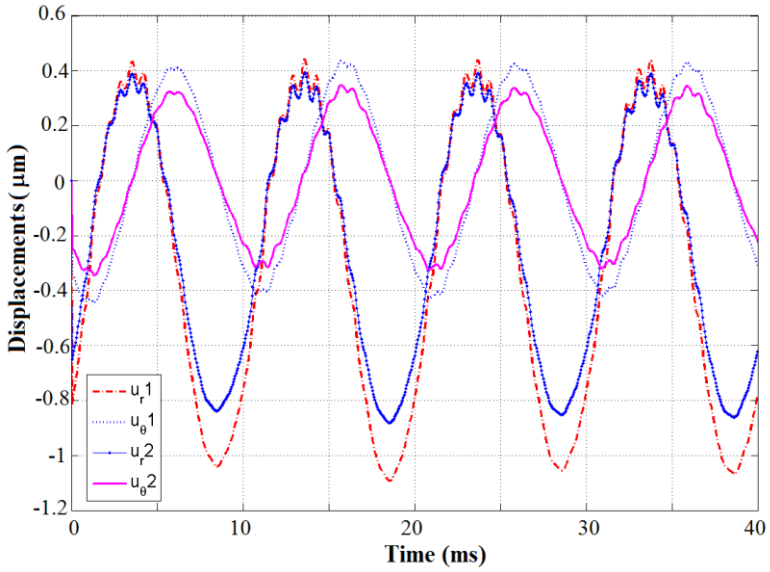

Figure 5.23: Machine I: Displacements in radial and tangential directions as function of time of a node on the tooth of the stator of Machine I. Subscripts r and θ stand for the radial and tangential directions, respectively. Number 1 refers to the case when only magnetostriction is considered. Number 2 is the case when both magnetostriction and the electromagnetic stress tensor are used in the simulations.

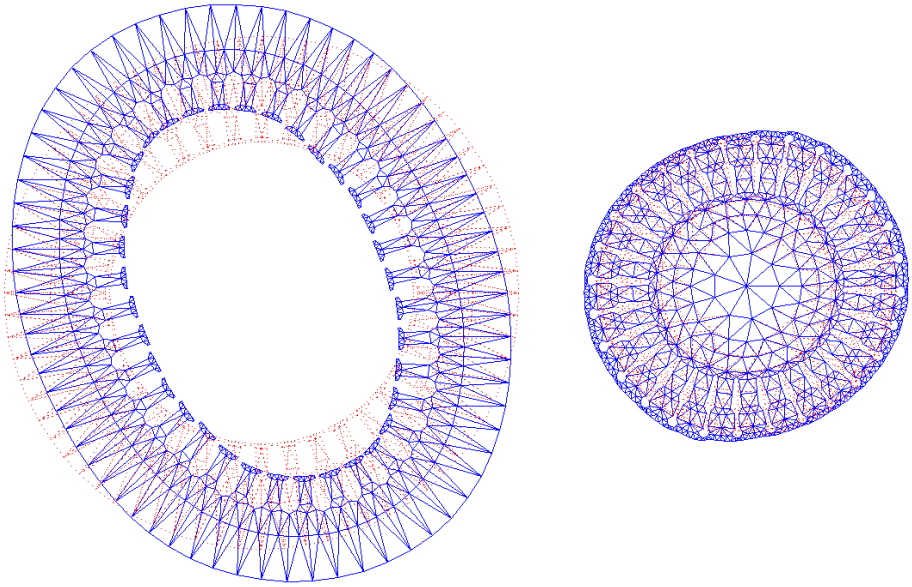

Figure 5.24: Machine I: Deformation of stator (left) and rotor (right); the electromagnetic stress tensor in the air gap is taken into account.

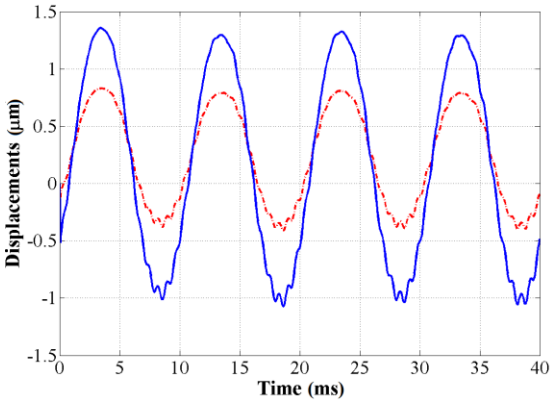

(a) Tooth of the stator, radial direction.

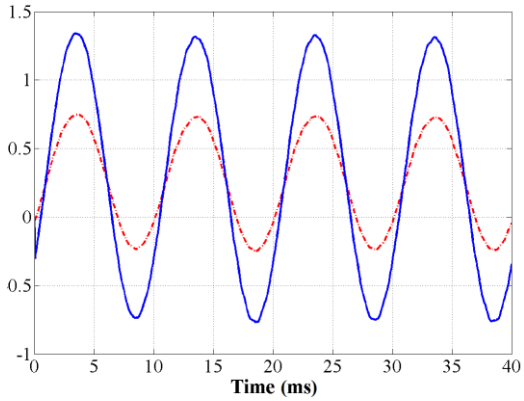

(b) Outer boundary of the stator, radial direction.

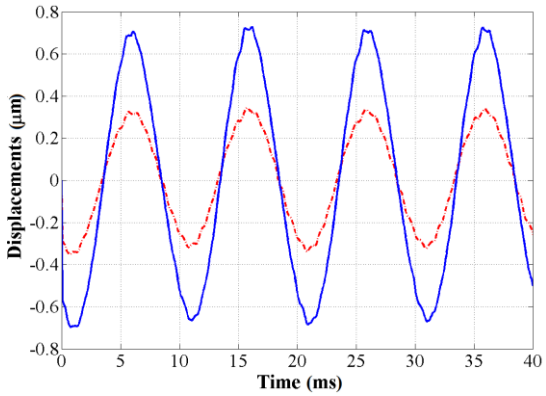

(c) Tooth of the stator, tangential direction.

Figure 5.25: Machine I: Comparison of the radial and tangential displacements of a single node when the stress tensor is *not* taken into account in air (*dotted red*) and when the stress tensor is taken into account (*plain blue*).

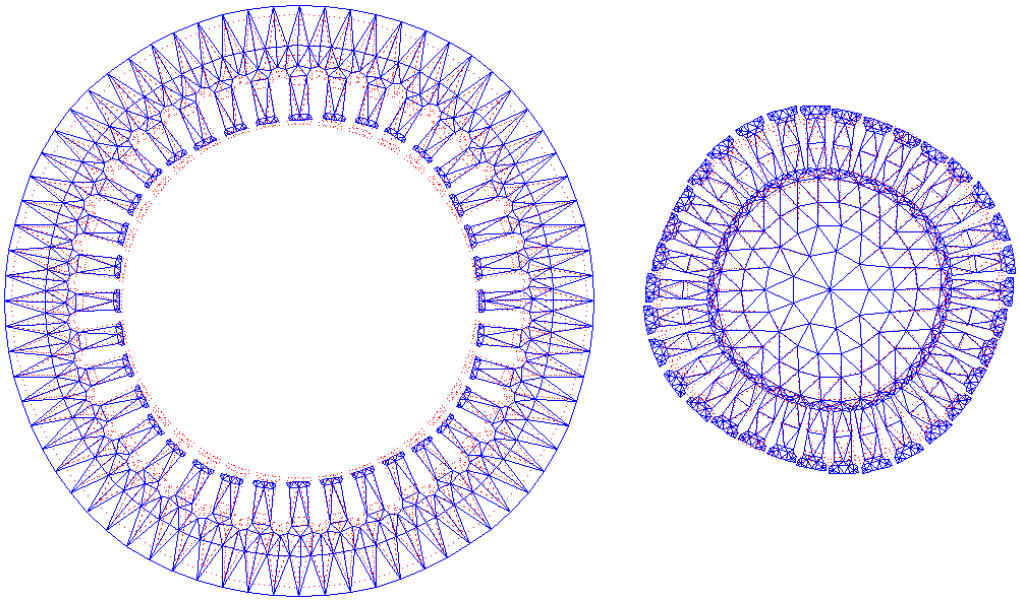

Figure 5.26: Machine II: Deformation of the stator (left) and of the rotor (right) when the electromagnetic stress tensor in the air gap is ***not*** taken into account.

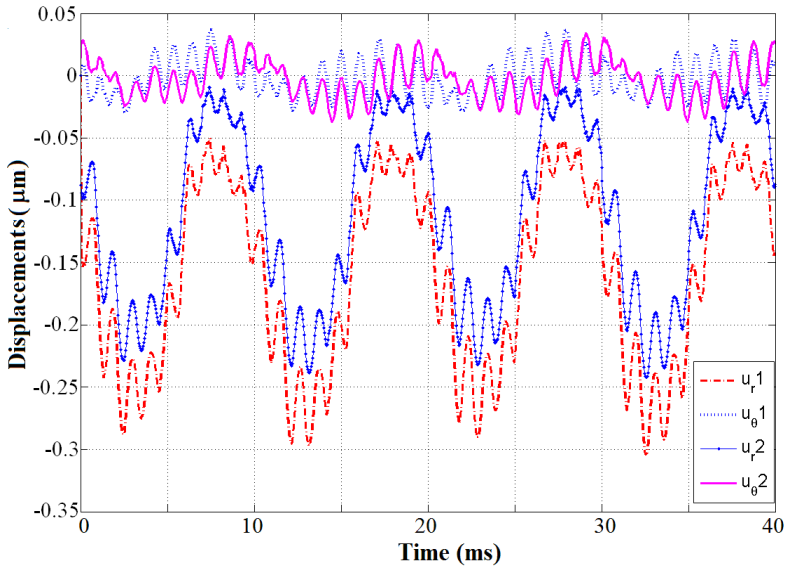

Figure 5.27: Machine II: Displacements in radial and tangential directions as function of time of a node on the tooth of the stator of Machine II. Subscripts r and θ stand for the radial and tangential directions respectively. Number 1 refers to the case when only magnetostriction is considered. Number 2 is the case when both magnetostriction and electromagnetic stress in iron are considered.

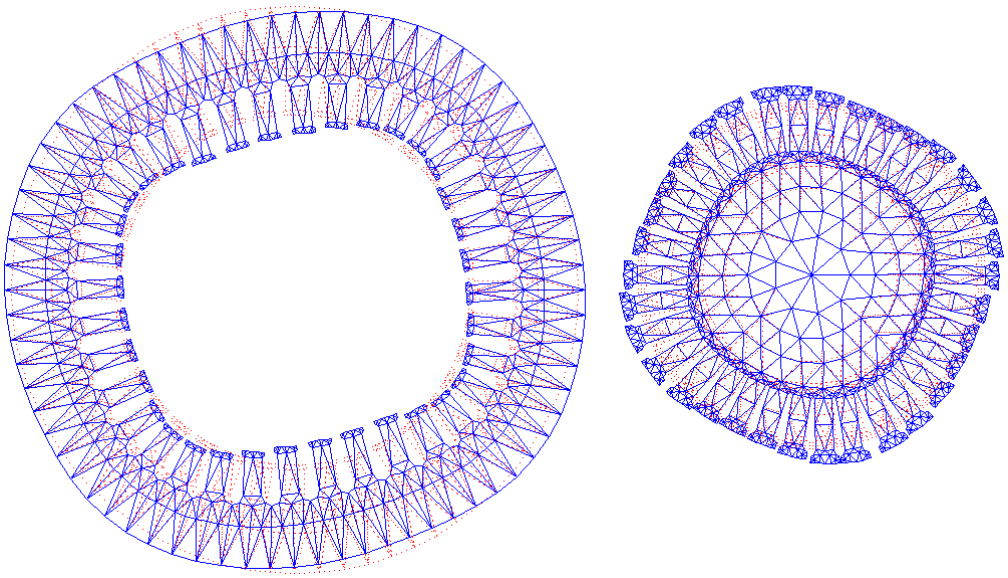

Figure 5.28: Machine II: Deformation of the stator (left) and of the rotor (right) when the electromagnetic stress tensor in the air gap is taken into account.

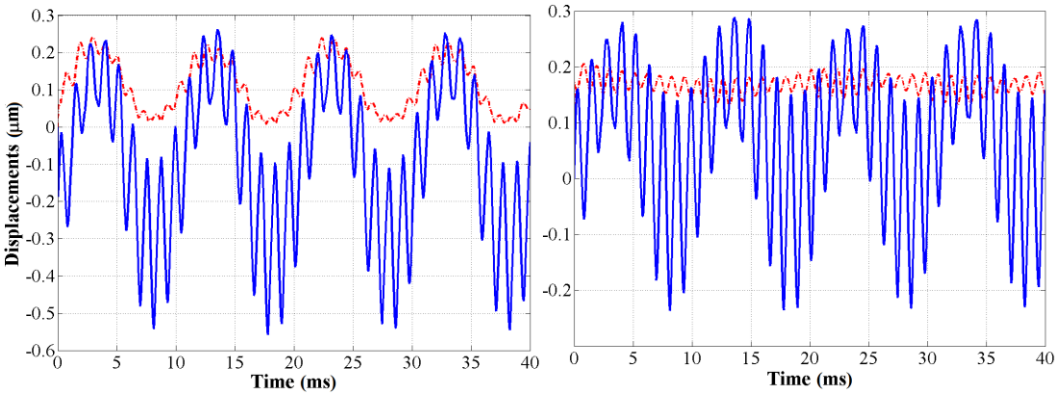

(a) Tooth of the stator, radial direction.

(b) Outer boundary of the stator, radial direction

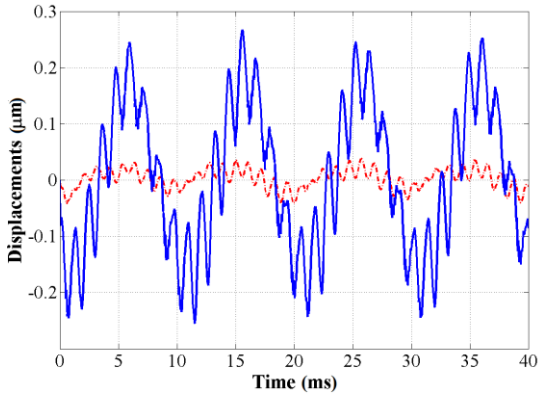

(c) Tooth of the stator, tangential direction.

Figure 5.29: Machine II: Comparison of the radial and tangential displacements of a single node when the stress tensor in air is *not* taken into account in air (*dotted red*) and when the stress tensor is taken into account (*plain blue*).

5.3.3 Simple study for the dynamic case

It was not the main concern of this thesis to study the dynamic case in detail. So the method is presented for a simple embedded beam made of electrical steel, such as that shown in Figure 5.30.

The dynamic case was implemented in the finite element software. For this reason, a beam under magnetic and mechanical loading is presented, so as to assess not only the validity of the implementation but also the influence of the model on the dynamic behaviour.

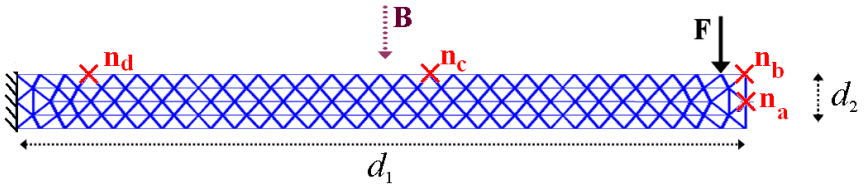

Figure 5.30: Embedded beam structure: general view, d_1=30 cm, d_2 = 2mm.

The recurrence schemes are a subject of interest by themselves and attract a lot of attention. Here, the backward recurrence scheme is chosen, as discussed in Chapter 3, because of its stability, even if it is known to be intrinsically damped numerically. This challenging numerical problem is beyond the scope of this work but has been addressed, for instance, in Zienkiewicz (1967) and Bathe (1996). It is, however, known that to apply the dynamic case a certain time step, which is very small, should be used as an input.

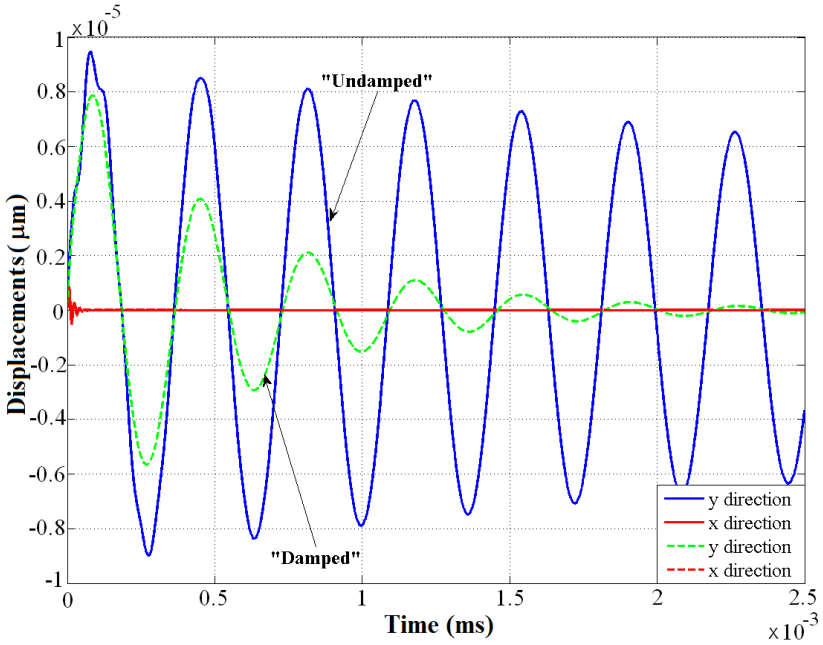

Figure 5.31: Comparison of the damped and “undamped” case, mechanical force only.

The theory predicts that when no magnetic field is applied, and no damping is present, the system should behave as a permanent oscillator. However, there is numerical damping as can be seen in Figure 5.31 in the "Undamped" case. When the damping matrix is included, the system behaves as in the "Damped" case. In this figure, the displacements of node n_b from Figure 5.30 are presented. For a better understanding of the phenomenon, in Figure 5.32 (2), a force impulse is applied at one time step only.

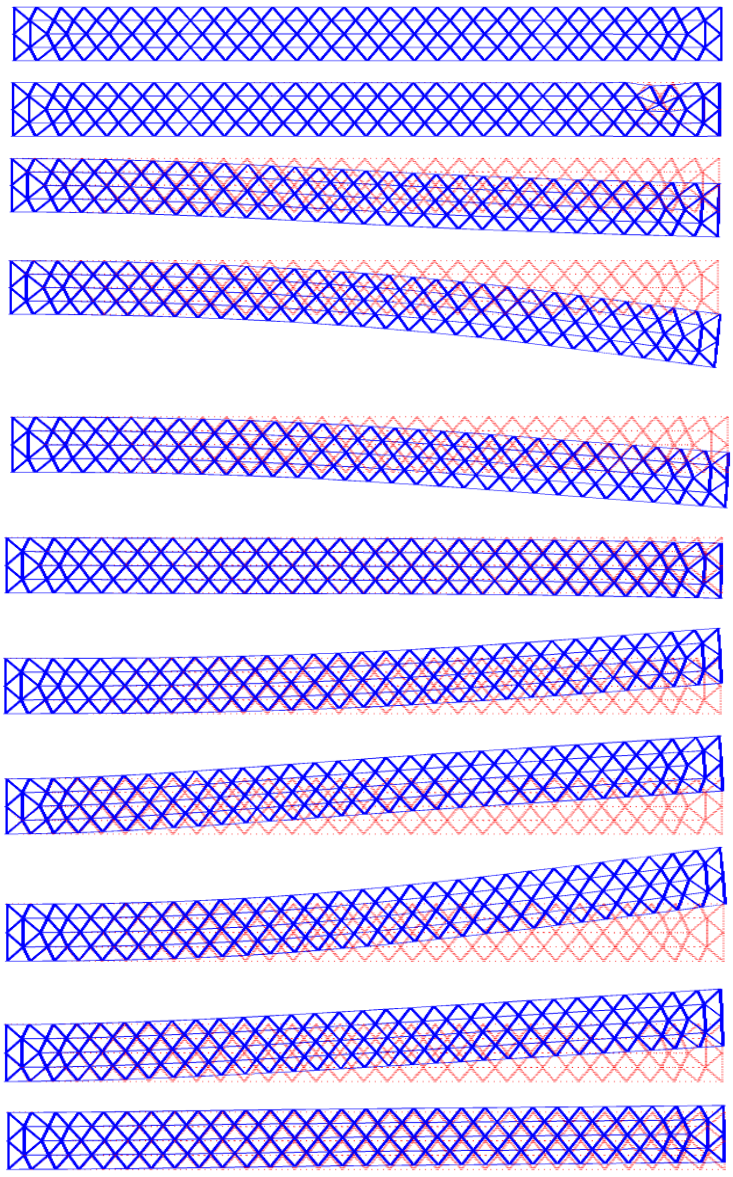

(1) Initial mesh.

(2) Force is applied.

(3) Force has been released, deformation of the beam. Temporary state 1.

(4) Temporary state 2.

(5) Temporary state 3.

(6) Back to original position. Temporary state 4.

(7) Temporary state 5.

(8) Temporary state 6.

(9) Temporary state 7.

(10) Temporary state 8.

(11) Back to original position. Temporary state 9.

Figure 5.32: Embedded beam structure when an external mechanical force is applied.

A constant magnetic flux density of 2 T was applied to the structure, as shown in Figure 5.30, at all time steps. The force was input in the same way as in the previous study. The displacements of four nodes, n_a, n_b, n_c, and n_d, in the *x*- and *y*-directions are illustrated in Figure 5.33. No damping was considered. On one hand, u_1 and v_1 correspond to the displacements when no external field is applied; on the other hand u_2 and v_2 suit the displacements when the external field is applied. From these results, the following can be concluded: the displacements of node n_a are not influenced by the magnetic field; the displacements of node n_b in the direction of the magnetic field, i.e. the *y*-direction, have their average pulled down by 1μm. When approaching the region where the beam is embedded, nodes n_c and, especially, n_d have their DC components shifted in the direction of the field being applied. Except for this observation, the shape of the displacements is similar and seems not to experience more numerical damping.

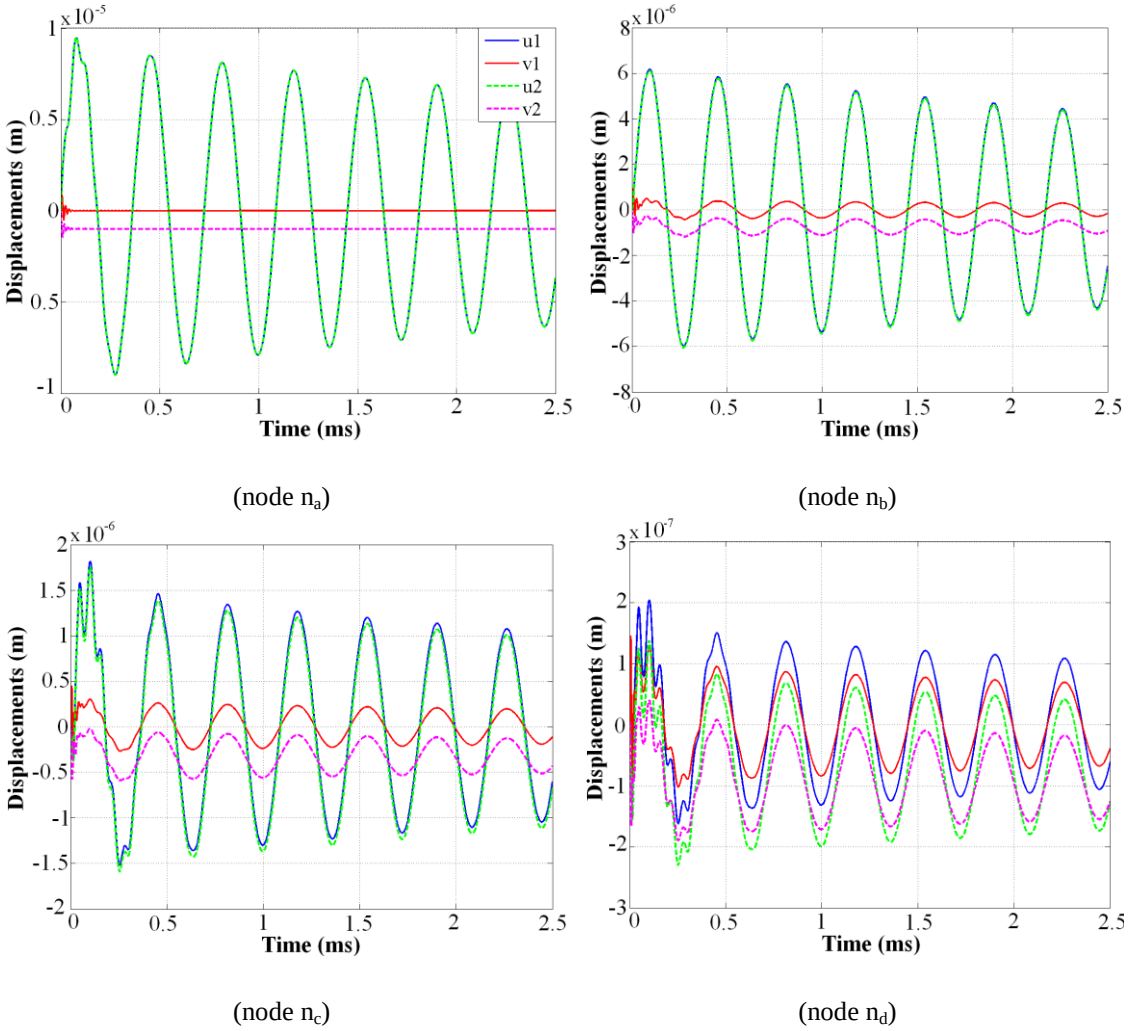

(node n_a) (node n_b)

(node n_c) (node n_d)

Figure 5.33: Displacements of four nodes in the structure as a function of time, B applied.

5.4 Summary

In this chapter, a manifest proof is addressed concerning the fact that the magneto-mechanical coupled model, presented and implemented into a finite element code, is suitable for the computation of displacements in electrical machines.

The test device described in Section 5.1 accounts for the phenomenon of magnetostriction and electromagnetic stress tensor inside the iron. Its design and building have been described and the results from the sensors were analysed. The general output of the measurements to obtain the displacements in the radial direction offers a quantitative value to the stress in iron. The simulated results, however, predict the displacements of the outer stator boundary with negligible error.

In order not to restrict the findings of the study to a device not practically useful in applications, Section 5.2 concentrates on the measurements and simulations of a test induction machine. Measurements by accelerometers were adopted to acquire the acceleration under a given supply frequency and sinusoidal voltage, correspondingly to the previous setup. The overall results indicate that the electromagnetic stress acting at the air-iron boundary pulls the stator and rotor towards each other.

Section 5.3 offers a deeper insight into the model. However exploratory, the research reported discusses the effect of separate terms in the model applied to electrical machines. The results from the dynamic model are an attempt to consider the effect of including damping and mass components into system matrix. Even though the problem was numerically damped, the inclusion of the model did not really affect the outcome of the study.

According to the measured data available and to the simulated results, the model presumably accounts for magnetostriction and the electromagnetic stress tensor with a good approximation. However, further verification is needed in the case of electrical machines for industrial purposes.

Notwithstanding its limitations, this study suggests that with prior knowledge of the properties of the material, displacements can be known as a function of time within a structure such as a rotating electrical machine.

Chapter 6

Discussion

The main thrust of the thesis was established in Chapter 1. Correspondingly, this chapter shows that the research makes a distinct contribution to the previous knowledge in the field of magneto-mechanical coupling. The new methodology is presented as an energy-based magneto-mechanical coupled method and implemented for time-stepping calculations of 2-D geometries of rotating electrical machines. Here, the findings support each research hypothesis according to the present thesis and follow previous work regarding the magneto-mechanical coupling, the measurement and verification methods.

This discussion is organised in such a way that Section 6.1 explains the essential results and also the unexpected ones and Section 6.2 considers practical implications and further research.

6.1 Summary

This work was motivated by the need for an appropriate magneto-mechanically coupled method. The developed new procedure accounts for stresses in electrical steel sheets that originate from magnetic fields and mechanical stresses.

6.1.1 Energy-based coupled model

An energy-based magneto-mechanical model has been derived and solved by the finite element method. It is operational for the computation of electrical machines.

The magneto-mechanical model that has been presented differs from previous research in that the constitutive equations are solved explicitly within a time-stepping scheme for electrical machines. Indeed, the chosen variables, the displacements, and the magnetic vector potential are solved simultaneously, so that none of these needs post-processing.

The model formulated in iron is suitable for evaluating the effect of magnetic forces and magnetostriction in electrical steel sheets. After its justification and verification, the effect of the electromagnetic stress tensor in the air has been accounted for. This approach of considering the latter effect only after the development of the model in ion has been adopted not to minimise the importance of the resulting reluctance forces which are predominant, but to focus on the energy-based magneto-mechanical model.

Chapter 3, together with Chapter 5, showed how to account for magnetostriction and mechanical stress tensor effects in iron, as well as the Maxwell stress tensor in air. These effects cannot be separated directly within the iron. However, it has been clarified that the chosen free energy coupled the magnetic and mechanical fields.

6.1.2 Magneto-mechanical coupled finite element method

In this work, a solid computational-based and measurement-based tool for further investigation in magneto-mechanical problems in electrical machines has been produced. Simulated results on the two- and four-pole machines have been presented, with the electromagnetic stress tensor in air being taken (or not) into account. The electromagnetic stress in air and iron has an opposite direction at the boundaries, which makes the problem difficult to study. Although this assumption was considered by previous researches such as stated in Chapter 2, these investigations have revealed objectively that the contribution of the electromagnetic stress tensor in iron is negligible, as it increases the displacements by only 5%. However, the addition of the same stress tensor to the computation of the displacements on the nodes at the air-iron boundary plays an essential role in the final results. These results have been verified from measurements on an asynchronous machine.

The order of the elements is a drawback in this calculation, as is the meshing, which is not optimal for solving a mechanical problem. At the boundary between the air and the iron, a larger number of elements could lead to a better calculation of the displacements. Besides, mechanical problems commonly require finer meshes and higher-order and/or different types of elements. Despite these facts, the results throughout the thesis have been positively in good accordance with the measurements, as discussed in Chapter 5.

6.1.3 Importance of measurements

Various answers can be advanced to the question of how to compare measurement techniques and verify the validity of the study with appropriate devices.

Within this work, the measurements of the properties of Fe-Si for electrical machinery applications were performed on two different setups. There were striking differences between the magnetostrictive curves measured on the Epstein frame and on the rotational sheet tester. These differences were also observed in a recent publication where the authors compared the laser method and the strain gauge method on a single sheet tester. The differences in the results may have various origins; anyhow, the strain gauges appear to be heavily influenced by an external magnetic field, and their signal is distorted accordingly. The measurements presented in this thesis confirm the work by Enokizono (1990) and Anderson (2004) and support the idea presented by, among others, Yabumoto (2009) of a standardisation of measurements of magnetostriction in electrical steel sheets under stress, as well as at zero stress.

The simulated results were subsequently compared with the measurements on two different verification devices in order to rigorously test the method that was developed. In both cases, the measurements are in good accordance with the simulations. The theoretical model that was developed and its identification and implementation in the finite element software were effective, even under the hypothesis of ideal symmetric 2-D geometry.

On the grounds of this approach, the following points should be considered when taking accuracy problems into account. On one hand, great attention was paid to eliminating sources of errors. For instance, to remove any privileged direction of magnetisation, the sheets were rotated. Additionally, the design of the device allows a more uniform magnetic flux density distribution. Because of the absence of an air gap, it takes only the effect of magnetostriction and the magnetic stress tensor in iron into account. One valuable advantage in the study is that the parameters of the model were identified on exactly the same steel sheet as the ones used for the test device for later numerical simulations. On the other hand, some drawbacks associated with the building of the device should be noticed. One of them, compared to Belahcen (2004), is the roughness of the outer boundary of the device. There are also problems that are specifically associated with the positioning of the accelerometers. Possible but negligible asymmetries in the windings, the preferred direction of magnetisation of the steel sheets, and the damping of the structure as a result of the wooden support presumably affect the measurements.

The measurements from the test asynchronous machine proved to be more complicated. The conclusion from the simulated results was that they complement the measurements. The model was not identified on a similar electrical steel sheet as the ones used in the machine. Finally, the sensors are sensitive to magnetic fields induced by currents in the end-windings.

In conclusion, as discussed in Chapter 5, the peak-to-peak measured displacements matched the computed ones. Overall, the investigation reported in this study contributes to an in-depth knowledge of the stresses acting on a ferromagnetic material with good accuracy.

6.2 Further work

The subject of the thesis covered the study of magnetic forces in electrical machines. This topic is vague and has been studied extensively. Nevertheless, it is the first time that a physically justified energy-based model has been developed for modelling the magneto-mechanical coupling within ferromagnetic materials. It was included in time-stepping finite element software in order to solve the magnetic and mechanical fields in a 2-D cross-section of a rotating electrical machine. Additionally, throughout this work, potential research niches have been raised. These are recalled here and supplemented by suggestions for future work.

6.2.1 Bi-axial stress and rotating magnetic flux density

Relevant research is needed to determine the effect of biaxial stress under a rotating magnetic field. Although the single-valued curves presented in this study give approximately acceptable results, it has been seen that the magnetostrictive phenomenon is a dynamic problem that depends heavily on the frequency. The loops obtained from the measurements in Chapter 4 make it clear that a model that accounts not only for the hysteresis phenomena but also for the dynamic phenomena is needed. Models such as the stress-dependent Preisach or Jiles-Atherton models are already available and could be considered in order to compare the results with those presented in this work.

6.2.2 Other stresses acting on the iron core of the machine

Many other factors affect the magnetic properties of the iron core, such as punching, welding, thermal stresses, and residual stresses.

Further work could envisage an extension of the current magneto-mechanical model to account for the stresses induced by the punching, cutting, and welding processes. Punching causes the magnetic properties of the material to deteriorate, not only in the punched region but also inside the electrical steel sheet. It has long been known that punched regions experience permanent static stresses under plastic

deformation. As indicated in the literature review, this leads to high losses in those regions. This will require, for example, an extreme mesh refinement of the boundaries of electrical steel sheets or other novel approaches, such as better homogenisation methods. The welding process induces thermal stress in the region near it. The computational procedure easily enables extra constraints to be added to a region within the electrical machine that could be both stress- and magnetic field-dependent.

A thermo-magneto-mechanical coupled model is not excluded; its achievement would require better processors, which is conceivable in the future, and also a model that accounts for this phenomenon in an explicit manner. In addition, the stresses in the electrical steel sheets vary with the thermal state of the machine. A magneto-thermo-mechanical coupled method is a challenging option.

Residual stresses are common in almost every electrical machine. Accounting for these static stresses, which originate from the construction of the electrical machine, such as the shrink-fitting of the rotor shaft or of the outer boundary of the stator, is more challenging from a measurement point of view than from a computational point of view. Nevertheless, a comprehensive study of these could bring more insight for industry when building such devices.

Although their influence is supposed to be small, the Lorentz forces acting on the slotting regions have a known influence. Their addition to the computation could be of help in understanding and quantifying the phenomenon.

6.2.3 Study of the vibration modes of electrical machines

The dynamic model in Chapter 3 offers various computational opportunities. The study of the time integration for this problem is complicated, as the time-stepping scheme requires a short time step to account for the natural resonance frequency of such electrical machines, which is usually hundreds of hertz. This high number of time steps makes the procedure slightly inefficient, as it increases the computational time. A suggestion for further investigation is the design and building of a real small electrical machine, with its boundary open and with tiny accelerometers placed on the teeth, as well as on the outer boundary of the stator. The parameters of the electrical steel sheets identified, for example, from the modified Epstein frame, would give approximate parameters for the model. The winding should also be different from the one in the asynchronous test machine; a form wound winding would be more appropriate.

6.2.4 From 2-D problem to 3-D problem

The problem discussed from the very beginning is a 3-D problem treated as a 2-D-magneto- 2-D-mechanical problem. Even if magnetostriction is a 2-D phenomenon, there are some 3-D-related effects in the axial direction of rotating electrical machines that require further attention. Such an example could be the influence of residual stress when the sheets are being punched together.

6.3 Final word

As a conclusion to the work, this energy-based method is suitable for the computation of displacements within electrical machines. Supported by measurements for the identification part and verification devices, the dissertation also offers a tool for further developments in the field of magneto-mechanical coupling.

References

Alkar, K., 2007. *Measuring Power Losses of Electrical Steel Sheets in One- and Two-Dimensional Magnetic Fields*. Master's thesis. Helsinki University of Technology, Espoo, Finland.

Anderson, P.I., Moses, A.J., Stanbury, H.J., 2000, An Automated System for the measurement of Magnetostriction in Electrical Steel Sheet under Applied Stress, *J. Magn. and Magn. Mat.*, Vol. 215-216, pp. 714-716.

Arkkio, A., 1987. *Analysis of Induction Motors Based on the Numerical Solution of the Magnetic Field and Circuit Equations*. Doctoral dissertation. Helsinki University of Technology, Espoo, Finland.

Arkkio, A., 1988, Time-stepping Finite Element Analysis of Induction Motors, *Proceedings of ICEM*, pp. 275-280.

Bathe, K-J., 1996. *Finite Element Procedures*. NewJersey: Prentice-Hall, 1037 pages.

Bastos, J.P.A., Sadowski, N., *Electromagnetic Modeling by Finite Element Methods*. Marcel Dekker Ltd., 510 pages.

Belahcen, A., 2004. *Magnetoelasticity, Magnetic Forces and Magnetostriction in Electrical Machines*. Doctoral dissertation. Helsinki University of Technology, Espoo, Finland.

Belahcen, A., Fonteyn, K., Fortino, S., Kouhia, R., 2006, A coupled magneto-elastic model for ferromagnetic materials, *Proceedings of The IX Finnish Mechanics Days*, Lappeenranta, Finland, von Herzen R. and Halme T. (editors), pp. 673-682.

Belahcen, A., Fonteyn, K., Hannukainen, A., Kouhia, R., 2008, On Numerical Modelling of Coupled Magnetoelastic Problem, *Proceedings of the 21st Nordic Seminar on Computational Mechanics*, Trondheim, Kvamsdal T., Mathisen K.M. and Pettersen B. (editors), pp. 203-206.

Belkasim, M, 2008. *Identification of Loss Models from Measurements of the Magnetic Properties of Electrical Steel Sheets*. Master's thesis. Helsinki University of Technology, Espoo, Finland.

Benbouzid, M., Body, C., Reyne, G., Meunier, G., 1995, Finite Element Modelling of Giant Magnetostriction in Thin Films, *IEEE Trans. Magn.*, Vol.31, No. 6, pp 3563-3565.

Bergqvist, A. and Engdahl, G., 1996, A model for Magnetomechanical Hysteresis and Losses in Magnetostrictive Materials, *J. Appl. Phys.*, Vol. 79, pp. 6476.

Bergqvist, A., 1994. *On magnetic hysteresis modelling*. Doctoral dissertation. Royal Institute of Technology, Stockholm, Sweden.

Besbes, M., Ren, Z., Razek, A., 1996, Finite Element Analysis of Magneto-Mechanical Coupled Phenomena in Magneto-Mechanical Coupled Phenomena in Magnetostrictive Materials, *IEEE Trans. Magn.*, Vol. 32, No. 3, pp. 1058-1061.

Birss, R.R., Faunce, C.A., Isaac, E.D., 1971, Magneto-mechanical Effects in iron and iron-carbon alloys, *J. Phys. D: Appl. Phys.*, Vol. 4, No. 7, pp. 1040-1048.

Bloch, F., 1932, Zur Theorie des Austauschproblems und der Remanenzerscheinung der Ferromagnetika, *Zeitschrift für Physik A Hadrons and Nuclei*, Vol. 74, No. 4-5, pp. 295-335.

Body, C., Reyne, G, Meunier, G., 1997, Nonlinear Finite Element Modelling of Magneto-Mechanical Phenomenon in Giant Magnetostrictive Thin Films, *IEEE Trans. Magn.*, Vol. 33, No. 2, pp 1620-1623.

Bozorth, R.M, Williams, 1945, H.J., Effect of Small Stresses on Magnetic Properties, *Reviews of Modern Physics*, Vol. 17, No, 1.

Bozorth, R.M., Hamming, R.W., 1953 Measurement of Magnetostriction in Single Crystals, *Physical Review*, Vol. 89, No. 4, pp. 865-869.

Brown, W.F., 1949, Irreversible Magnetic Effects of Stress, *Physical Review*, Vol. 75, No. 1, pp. 147-154.

Carman, G.P., 1995, Nonlinear Constitutive Relations for Magnetostrictive Materials with Applications to 1-D problems, *J. Intel. Mat. Sys. A/Struct.*, Vol. 6, No. 5, pp. 675-683.

Cester, P., 2002. *Magnetostriction as Source of Noise and Vibration: Design, Construction and Measurements on an Experimental Electrical Machine*. Tesi di Laurea -Master's thesis-, Università Degli Studi di Padova, Italy, 61 pages.

Chari, M.V.K., 1980, Finite Element Analysis of Electrical Machinery and Device, *IEEE Trans. Magn.*, Vol. MAG-16, No. 5.

Collet B., Maugin, G.A., 1974, Sur l'électrodynamique des milieux continus avec interactions, *C.R. Acad. Sci. Paris*, Vol. B279 pp. 379–382,439–442.

Corner, W.D., Mason, J.J., The Effect of Stress on the Domain Structure of Goss Textured Silicon-Iron, *British J. Appl. Phys.*, Vol. 15, pp. 709-718.

Craik, D.J., Wood, M.J., 1970, Magnetization Changes Induced by Stress in a Constant Applied Field, *J. Phys. D: Appl. Phys.*, Vol. 3, No. 7, pp. 1009-1016.

Dąbrowski, M., Zgodziński, T., 1989, Some Effects of unidirectional stress in Si-Fe sheets, *Physica Scripta*, Vol. 40, pp. 514-517.

Dapino, M.J., Smith, R.C., Faidley, L.E., Flatau, A.B., 1999, A Coupled Structural-Magnetic Strain and Stress Model for Magnetostrictive Transducers, *Proceedings of SPIE, Smart Structures and Materials*.

De Medeiros, L.H., Reyne, G., Meunier, G., 1998, Comparison of Global Force Calculations on Permanent Magnets, *IEEE Trans. Magn.*, Vol. 34, No. 5, pp 3560-3563.

Delaere, K., 2002. *Computational and Experimental Analysis of Electric Machine Vibrations caused by Magnetic Forces and Magnetostriction*. Doctoral dissertation. Katholieke Universiteit Leuven, Leuven, Belgium.

Delaere, K., Heylen, W., Belmans, R., Hameyer, K, 2001a, Finite Element Based Expressions for Lorentz, Reluctance and Magnetostriction Forces, *Int. J. Comp. and A/Math. Electr. A/Electr. Eng.*, No.1, pp. 20-31.

Delaere, K., Heylen, W., Belmans, R., Hameyer, K, 2001b, Strong Magnetomechanical FE Coupling Using Local Magnetostriction Forces, *The Europ. Phys. J. Appl. Phys.*, Vol. 13, No. 2, pp.115-119.

Delaere, K., Heylen, W., Belmans, R., Hameyer, K., 2002, Comparison of Induction Machine Stator Vibration Spectra Induced by Reluctance Forces and Magnetostriction, *IEEE Trans. Magn.*, Vol. 38, No. 2, pp. 969-972.

Delince, F., Genon, A., J.M. Gillard, Hedia, H., Legros, W., Nicolet, A., 1991, Numerical Computation of the Magnetostriction effect in Ferromagnetic Materials, *J. Appl. Phys.*, Vol. 69, No.8, pp.5794-5796.

Dijkstra, L.J., Martius, U.M., 1953, Domain Pattern in Silicon-Iron under Stress, *Reviews of Modern Physics*, Vol. 25, No. 1, pp. 146-150.

Dlala, E., 2008. *Magnetodynamic Vector Hysteresis Models for Steel Laminations of Rotating Electrical Machines*. Doctoral dissertation. Helsinki University of Technology, Espoo, Finland.

Dlala, E., Belahcen, A., Fonteyn, K., Belkasim, M., 2009, Improving Loss Properties of the Mayergoyz Vector Hysteresis Model, *IEEE Trans. Magn*, Vol. 46, No. 3, pp. 918-924.

Dorfmann, A., Ogden R. W., 2003, Magneto-elastic Modelling of Elastomers, *Europ. J. Mech. A/Sol.*, Vol. 22, pp. 497-507.

Dorfmann, A., Ogden R. W., 2005, Nonlinear Electroelasticity, *Acta Mechanica*, Vol. 174, pp 167-183.

Dorfmann, A., Ogden R. W., 2010, Nonlinear Electroelastostatics: Incremental Equations and Stability, *Int. J. of Eng. Sc.*, in press, Vol. 48, No. 1, pp. 1-14.

Dorfmann, A., Ogden R.W., Saccomandi, G., 2004, Universal relations for non-linear magneto-elastic solids, *Int. J. Non-Lin. Mech.*, Vol. 39, pp. 1699-1708.

Du Trémolet de Lacheisserie, E., 1993. *Magnetostriction – Theory and Applications of Magnetoelasticity*. CRC Press Inc. 432 pages.

Duenas, T.A., Hsu, L., Carman, G.P., 1996, Magnetostrictive Composite Material Systems Analytical/Experimental, *Materials Research Society Symposium Proceedings*, Boston, Vol. 459, pp.527-543.

Enokizono, M., Suzuki, T., Sievert, J.D., 1990, Measurement of Dynamic Magnetostriction under Rotating Magnetic Field, *IEEE Trans. Magn.*, Vol. 26, No. 5, pp. 2067-2069.

Enokizono, M., Kanao, S., Shirakawa, G., 1995, Measurement of Arbitrary Dynamic Magnetostriction under Alternating and Rotating Field, *IEEE Trans. Magn.*, Vol. 31, No. 6, pp. 3409-3411.

Enokizono, M., Tanabe, I., 1997, Studies on a new simplified rotational loss tester, *IEEE Trans. Magn.*, Vol. 33, No. 5, pp. 4020-4022.

Espinosa, O., Reisenegger, A., 2003, The Magnetic Stress Tensor in Magnetized Matter, *International Workshop on Strong Magnetic Fields and Neutron Stars*, La Habana, Cuba, pp. 75-81.

Fang, D.N., Feng, X., Hwang, K.C., 2004, Study of Magnetomechanical non-linear Deformation of Ferromagnetic Materials: Theory and Experiment, Proceedings of the Institution of Mechanical Engineers Part C, *J. Mech. Eng. Sc.*, Vol. 218, No. 12, pp. 1405–1410.

Fonteyn, K., Belahcen, A., Arkkio, A., 2006, Properties of electrical steel sheets under strong mechanical stress, *Pollack Periodica, An Int. J. Eng. A/Inf. Sci., Budapest, Hungary: Akademiai*, Vol. 1, No. 1.

Fonteyn, K., Belahcen, A., 2008, Numerical and Experimental Results from a Vertical Yoke System for Measuring Magnetic Properties of Fe-Si Steel Sheets, *IEEE Proc. 8th Int. Conf. Electr. Mach. A/Syst.*, pp. 434 – 438.

Fonteyn, K., Rasilo, P., Belahcen, A., 2009a, Measurement of Magnetic Properties under Alternating Field with a Vertical Rotational Single Sheet Tester, *Przegląd Elektrotechniczny*, Vol. 1, pp. 52-54.

Fonteyn, K., Pyhäranta, E., Belahcen, A., Rasilo, P., Arkkio, A., 2009b, Novel Measurement Device for the Investigation of Magnetostriction in Electrical Machines, *Proc. 10th Finnish Mechanics Days, Jyväskylä, December 3-4, 2009, Finland*.

Fonteyn K., Belahcen, A., Kouhia, R., Rasilo, P., Arkkio, A., 2010, FEM for directly coupled magneto-mechanical phenomena in electrical machines, accepted for publication in IEEE Trans. Magn.

Fortino, S., Kouhia, R., Belahcen, A., Fonteyn, K., 2007, A coupled model for magnetostriction in ferromagnetic materials, *Proc. Int. Conf. on Comp. Meth. Cpl. Prob. Sci. A/Eng., Barcelona, Spain (CIMNE)*, pp. 483-484.

Foster, K., 1984, Stress and Induction Dependence of Hysteresis Losses in Electrical Steels, *J. Appl. Phys.*, Vol. 55, No., 6, pp. 2127-2129.

Ghalamestani, G. S., Hilgert, T., Vandevelde, L. Dirckx, J. and Melkebeek, J., 2010, Magnetostriction Measurement by Using Dual Heterodyne Laser Interferometers, *IEEE Trans. Magn.*, Vol. 46, No. 2, pp. 1351-1354.

Gros, L., Reyne, G., Body, C., Meunier, G., 1998, Strong Coupling Magneto Mechanical Methods Applied to Model Heavy Magnetostrictive Actuators, *IEEE Trans. Magn.*, Vol. 34, No. 5, pp 3150-3153.

Gurtin, E.M., 1981. *An Introduction to Continuum Mechanics*. Academic Press, INC, USA, 264 pages.

Hilgert, T., 2008. *Magnetische krachten en magnetostrictie in elektrisch staal en toepassingen op trillingen van elektrische machines en transformatoren*. Doctoral dissertation. Universiteit Gent, Gent, Belgium.

Hilgert, T., Vandevelde, L., Melkebeek, J., 2005, Application of Magnetostriction Measurements for the Computation of Deformation in Electrical Steel, *J. Appl. Phys.*, Vol. 97, No. 10, pp. 10E101-10E101-3.

Hirvonen, R., 1983. *Epätahtikoneen Rautahäviöt*. Report 16, Helsinki University of Technology, Laboratory of Electromechanics, Espoo, Finland.

Hubert, O., Chaabane, M., Jumel, J., Maurel, V., Alves, F., Bensalah A.D., Besbes, M., Azoum, K., Daniel, L., Bouillaut, F., 2005, A New Experimental Set-up for the Characterization of Magneto-mechanical Behaviour of Materials Submitted to Biaxial Stresses. Application to FeCo Alloys, *Przegląd Elektrotechniczn*y, Vol. 81, No. 5.

IEC 60404-2:1996 Magnetic materials - Part 2: Methods of measurement of the magnetic properties of electrical steel sheet and strip by means of an Epstein frame

IEEE Std 100, 1996. *The IEEE standard dictionary of electrical and electronics terms*. Institute of Electrical and Electronics Engineers, Library MARC record, 6th edition, 1278 pages.

Ivanyi, A., 1997. *Hysteresis models in electromagnetic computation*.Akademiai Kiado, Budapest, 229 pages.

Javadi, H., Lefevre Y., Clenet, S., Lajoie Mazenc, M., 1995, Electro-magneto-mechanical Characterizations of the Vibration of Magnetic Origin of Electrical Machines, *IEEE Trans. Magn.*, Vol. 31, No. 3, pp. 1892-1895.

Joule, J.P., 1847, On the effects of magnetism upon the dimensions of iron and steel bars, *Philosophical Magazine*, Vol. 30, pp. 76.

Kashiwaya, K., 1991, Fundamentals of Nondestructive Measurement of Biaxial Stress in Steel Utilizing Magneto-elastic Effect under Low Magnetic Field, *Jap. J. Appl. Phys.*, Vol. 30, No. 11 A, pp. 2932-2942.

Kikuchi, Y., 1968, Magnetostrictive Materials and Applications, *IEEE Trans. Magn.*, Vol. MAG-4, No. 2, pp. 107 -117.

Kittel, C., 1949, Physical Theory of Ferromagnetic Domains, *Reviews of Modern Physics*, Vol. 21, No. 4, pp 541-583.

Kovetz, A., 2000, Electromagnetic theory. Oxford University Press.

Krah, J., 2005. *Modelling of losses in power transformers from dc to the low kilohertz range*. Doctoral dissertation. Royal Institute of Technology, Stockholm, Sweden.

Krah, J.H, Engdahl, G., 2002, Experimental verification of alternative audio frequency 2-D magnetization set-up for soft magnetic sheets and foils, *Proc. 7th Int. Work. 1&2-D Magn. Meas. A/Test.*, Germany, Technische Bundesanstalt, Braunschweig, pp. 103–108.

Krismanic, G., 2004, Recent developments and trends in measurements of two-dimensional magnetic properties, *J. Electr. Eng.*, Vol. 55, No 10/S, pp. 45-46.

Landau, L., Lifshitz, E., On the theory of the dispersion of magnetic permeability in ferromagnetic bodies, *Physikalische Zeitschrift der Sowjetunion*, Vol. 8, pp. 153-169.

Langman, R., 1990, Magnetic Properties of Mild Steel under Conditions of Biaxial Stress, *IEEE Trans. Magn.*, Vol. 26, No. 4, pp. 1246-1250.

Langman, R., Belle, A., Bulte, D., Christopoulos, T., 2003, Measuring the Permeability of Stressed Steel by the Magnetomotive-Force-Vane Method with

Magnetization Perpendicular to the Surface, *IEEE Trans. Magn.*, Vol. 39, No.5, pp. 2179-2189.

Lee, E.W., 1955, Magnetostriction and Magnetomechanical Effects, *Reports on Progress in Physics*, Vol. 18, pp. 185-229.

Linnemann, K., Klinkel, S., Wagner, W., 2009, A Constitutive Model for Magnetostrictive and Piezo-electric Materials, *Int. J. Sol. A/Struct*., Vol. 46, pp. 1149-1166.

Liu, X., Zheng, X., 2005, A Nonlinear Constitutive Model for Magnetostrictive Materials, *Acta Mechanica Sinica*, Vol. 21, pp.278-285.

LoBue, M., Basso, V., Fiorillo, F., Bertotti., G., 1999, Effect of tensile and compressive stress on dynamic loop shapes and power losses of Fe-Si electrical steels, *J. Magn. Magn. Mater.* Vol. 196–197, pp. 372-374.

LoBue, M., Sasso, C., Basso, V., Fiorillo, F., Bertotti, G., 2000, Power Losses and Magnetization Process in Fe-Si Non-oriented Steels under Tensile and Compressive Stress, *J. Magn. and Magn. Mat.*, Vol. 215-216, pp. 124-126.

Lundgren, A., 1999. *On measurement and modelling of 2-D magnetization and magnetostriction of SiFe sheets*. Doctoral dissertation. Royal Institute of Technology Stockholm, Sweden.

Låftman, L., 1995. *The Contribution to Noise from Magnetostriction and PWM Inverter in an Induction Machine*. Doctoral dissertation. Lund Institute of Technology, Sweden.

Makaveev, D., De Wulf, M., Melkebeek, J., 1999, Field homogeneity in a two-phase rotational single sheet tester with square samples, *J. Magn. and Magn. Mat.*, Vol. 196-197, pp. 937-939.

Maugin, G.A., 1988. *Continuum Mechanics of Electromagnetic Solids*. North-Holland Elsevier, Amsterdam, 598 pages.

Mohammed, O.A., Calvert, T., McConnell, R., 1999, A Model for Magnetostriction in Coupled Nonlinear Finite Element Magneto-elastic Problems in Electrical Machines, *Proc. IEEE Int. Elect. Mach. A/Dri. Conf.*, Seattle, WA, pp. 201-207.

Mohammed, O.A., Calvert, T., McConnell, R., 2001,Coupled Magneto-elastic Finite Element Formulation Including Anisotropic Reluctivity Tensor and Magnetostriction Effects for Machinery Applications, *IEEE Trans. Magn.*, Vol. 37, No. 5, pp. 3388-3391.

Mohammed, O.A., Ganu, S.C., Liu, S., 2003, FEM Analysis and Testing of Magnetostrictive Effects in Electrical Steel Samples for Machinery Applications, *Power Engineering Society General Meeting, IEEE,* pp.1496-1500.

Mohammed, O.A., Ganu, S.C., Liu, S., 2004a, Numerical Analysis of Magnetostrictive Effects in and Electrical Steel Sample Including Experimental Testing, *IEEE Proce. SoutheastCon*, pp. 428-432.

Mohammed, O.A., Liu, S., Abed N., 2004b, Study of the Inverse Magnetostriction Effect on Machine Deformation, *IEEE Procc. SoutheastCon*, pp. 433- 436.

Moses, A.J., Rahmatizadeh, H., 1989, Effects of Stress on Iron Loss and Flux Distribution of an Induction Motor Stator Core, *IEEE Trans. Magn.*, Vol.25, No. 5, pp. 4003-4005.

Nakata, T., Takahashi, N., Fujiwara, K., Nakano, M., 1993, Measurement of Magnetic Characteristics along Arbitrary Directions of Grain-oriented Silicon Steel up to High Flux Densities, *IEEE Trans. Magn.*, Vol. 29, No. 6, pp. 3544-3546.

Nencib, N., Kedous-Lebouc, A., Cornut, B., 1995, 2-D Analysis of Rotational Loss Tester, *IEEE Trans. Magn.*, Vol. 31, No. 6, pp. 3388-3390.

Ossart, F., Hug, E., Hubert, O., Buvat, C., Billardon, R., 2000, Effect of Punching on Electrical Steels: Experimental and Numerical Coupled Analysis, *IEEE Trans. Magn.*, Vol. 36, No. 5, pp. 3137-3140.

Permiakov, V., Dupré, L., Melkebeek, J., Tant, P., Driesen, J., Belmans, R., 2006, Measurement Techniques for Magnetic Characterization of Fe-Si Alloys, *Proc. IEEE Instrum. Meas. Technology Conference*, IMTC 2006, pp. 742-746.

Permiakov, V., Pulnikov, A., De Wulf M., Melkebeek, J., 2003, Measuring Setup for the Investigation of the Influence of Mechanical Stresses on Magnetic Properties of Electrical Steel, *J. Magn. and Magn. Mat.*, Vol. 254-255, pp. 47-49.

Permiakov, V., Pulnikov, A., Dupré, L., Melkebeek, J., 2004, Rotational Magnetization in Nonoriented Fe-Si Steel Under Uni-axial Compressive and Tensile Stresses, *IEEE Trans. Magn.*, Vol. 40, No. 4, pp. 2760-2762.

Pfützner, H., Hasenzagl, A., 1996, Fundamental aspects of rotational magnetostriction", in Moses, A.J., Basak, A. (Eds), *Nonlinear Electromagnetic Systems*, IOS Press, Cardiff, pp. 374-379.

Pitman, K.C., 1990, The Influence of Stress on Ferromagnetic Hysteresis, *IEEE Trans. Magn.*, Vol. 26, No. 5, pp. 1978-1980.

Preston, T.W., Reece, A.B.J., Sangha P.S., 1988, Induction Motor Analysis by Time-Stepping Techniques, *IEEE Trans. Magn.*, Vol. 24, No. 1.

Pulnikov, A., Decocker, R., Permiakov, V., Dupré, L., Vandevelde, L., Petrov, R., Melkebeek, J., Houbaert Y., Gyselinck, J., Wisselinck H., 2004, The Relation between the Magnetostriction and the Hysteresis Losses in the Non-oriented Electrical Steels, *J. Magn. and Magn. Mat., (JEMS' 04),* Vol.290-291, pp. 1454-1456.

Pyhäranta, E., 2009. *Sähkälevyn Magnetostriktio- Testilaite ja Mittaukset*. Bachelor's thesis, Helsinki University of Technology, Espoo, Finland. 28 pages.

Pyrhönen, J., Jokinen, T., Hrabovcová, V., 2008. *Design of Rotating Electrical Machines*. John Wiley & Sons, Ltd, United Kingdom, 512 pages.

Radatz, J., 1997. *The IEEE Standard Dictionary of Electrical and Electronics Terms, 6th edition*. IEEE Standards Office New York, NY, USA, 1278 pages.

Ren, Z., 1994, Comparison of Different Force Calculation Methods in 3-D Finite Element Modelling, *IEEE Trans. Magn.*, Vol. 30, No. 5, pp. 3471-3474.

Ren, Z., Ionescu, B., Razek, A., 1995, Calculation of Mechanical Deformation of Magnetic Materials in Electromagnetic Devices, *IEEE Trans. Magn.*, Vol. 31, No. 3, pp. 1873-1876.

Reyne, G., Sabonnadière, J.C., Imhoff, J.F., 1988a, Finite Element Modelling of Electromagnetic Force Densities in DC Machines, *IEEE Trans. Magn.*, Vol. 24, No. 6, pp. 3171-3173.

Reyne, G., Meunier, G., Imhoff, J.F., Euxibie, E., 1988b, Magnetic Forces and Mechanical Behaviour of Ferromagnetic Materials. Presentation and Results on the Theoretical, Experimental and Numerical Approaches, *IEEE Trans. Magn.*, Vol. 25, No. 1, pp. 234-237.

Reyne, G., Sabonnadière, J.C., Coulomb, J.L., Brissoneau, P., 1987, A Survey of the Main Aspects of Magnetic Forces and Mechanical Behaviour of Ferromagnetic Materials under Magnetization, *IEEE Trans. Magn.*, Vol. MAG-23, No. 5, pp. 3765-3767.

Sadowski, N., Lefèvre, Y., Lajoie-Mazene, M., Bastos, J.P.A., 1992, Sur le Calcul des Forces Magnetiques, *Journal de Physique III France,* Vol. 2, pp 859-870.

Schoppa, A., Schneider, J., Roth, J.-O., 2000a, Influence of the Cutting Process on the Magnetic Properties of Non-oriented Electrical Steels, *J. Magn. and Magn. Mat.*, Vol. 215-216, pp. 100-102.

Schoppa, A., Schneider, J., Wuppermann, 2000b, Influence of the Manufacturing Process on the Magnetic Properties of Non-oriented Electrical Steels, *J. Magn. and Magn. Mat.*, Vol. 215-216, pp. 74-78.

Schoppa, A., Schneider, J., Wuppermann, C.-D., Bakon, T., 2003, Influence of Welding and Sticking of Laminations on the Magnetic Properties of Non-oriented Electrical Steels, *J. Magn. and Magn. Mat.*, Vol. 254-255, pp. 367-369.

Shen, D., Meunier, G. Coulomb, J. Sabonnadiere, J., 1985, Solution of Magnetic Fields and Electrical Circuits Combined Problems, *IEEE Trans. Magn.*, Vol. 21, No. 6, pp. 2288-2291.

Sievert, J., 1996, European Intercomparison of Measurements of Rotational Power Loss in Electrical Sheet Steel, *J. Magn. and Magn. Mat.*, Vol. 160, pp. 115-118.

Silvester, P.P, Ferrari, R., 1983. Finite Elements for Electrical Engineers. Cambridge University Press, 1st edition, 224 pages.

Somkun, S., Moses, A.J., Anderson, Ph.I., Klimczyk, P., Magnetostriction Anisotropy and Rotational Magnetostriction of a Nonoriented Electrical Steel, *IEEE Trans. Magn.*, Vol. 46, No. 2, pp. 302-305.

Spencer, A. J. M., 1971, Theory of Invariants, Continuum Physics, *Eringer A. C. (editor), Academic Press, New York*, Vol. 1, pp. 239-353.

Squire, P.T., 1996, Magnetomechanical Measurements and their Application to Soft Magnetic Materials, *J. Magn. and Magn. Mat.*, Vol. 160, pp. 11-16.

Strangas, E.G., 1985, Coupling the Circuit Equations to the Non-linear Time Dependent Field Solution in Inverter Driven Induction Motors, *IEEE Trans. Magn.*, Vol. 21, No. 6, pp. 2408-2411.

Takezawa, M., Kitajima, K., Morimoto, Y., Yamaski, J., Kaido, C., 2006, Effect of Strain by Mechanical Punching on Non-oriented Si-Fe Electrical Sheets for a Nine-Slot Motor Core, *IEEE Trans. Magn.*, Vol. 42, No. 10, pp. 2790-2792.

Toupin, R.A., 1956, The Elastic Dielectric, *J. Rat. Mech. A/Analy.*, Vol. 5, pp. 849-915.

Tiersten, H.F., 1964, Coupled Magnetomechanical Equations for Magnetically Saturated Insulators, *J. Math. Phys.*, Vol. 5, pp. 1298–1318.

Tumanski, S., Bakon, T., 2001, Measuring System for Two-dimensional Testing of Electrical Steel, *J. Magn. and Magn. Mat.*, Vol. 223, pp. 315-325.

Utsunomiya, T., Nishizawa, H., Kaneta, K., 1991, Biaxial Stress Measurement using a Magnetic Probe Based on the Law of Approach to Saturation Magnetization, *NDT & E International*, Vol. 24, No. 2, pp. 91-94.

Van Wylen, G. J., Sonntag, R. E., Desrochers, P., 1981. *Thermodynamique appliquée*. Editions du Renouveau Pédagogique, Montréal, 736 pages.

Wan, Y, Fang, D., Hwang, K-C., 2003, Non-linear Constitutive Relations for Magnetostrictive Materials, *Int. J. Non-Lin. Mech.*, Vol. 38, pp. 1053-1065.

Vandevelde, L, Hilgert, T.G.D, Melkebeek, J.A.A, 2008, Magnetic Force and Couple Densities and Magnetoelastic Interaction, *IET 7th Int. Conf. Comp. Electromagn*., Brighton, pp. 26-28.

Vandevelde, L, Melkebeek, J.A.A, 2001, Magnetic Forces and Magnetostriction in Ferromagnetic Material, *COMPEL*, Vol. 20, No. 1, pp. 32-51.

Vandevelde, L, Melkebeek, J.A.A, 2002, Computation of Deformation of Ferromagnetic Material, *IEE Proc. on Sci. Meas. Technol*. Vol 149, No. 5, pp. 222-226.

Vassent, E., Meunier, G., Foggia, A., Sabonnadière, J.C., 1990, Simulation of Induction Machine Operation using a Step-by-step Finite element Method, *J. Appl. Phys.*, Vol. 67, No. 9, pp. 5809-5811.

Verma, S.P., Singal, R.K., Williams, K., 1987a. Vibration Behaviour of Stators of Electrical Machines, Part I: Theoretical Study. *Journal of Sound and Vibration*, Vol. 115, No. 1, pp. 1-12.

Verma, S.P., Singal, R.K., Williams, K., 1987b, Vibration Behaviour of Stators of Electrical Machines, Part II: Experimental Study, *Journal of Sound and Vibration*, Vol. 115, No. 1, pp. 13-23.

Vijayraghavan, P., Krishnan, R., 1999, Noise in Electric Machines: A Review, *IEEE Tran. Ind. Appl.*, Vol. 35, No. 5, pp. 1007-1013.

Yabumoto, M., 2009, Review of Techniques for Measurement of Magnetostriction in Electrical Steels and Progress Towards Standardization, *Przegląd Electrotechniczny*, Vol. 1, pp. 1-6.

Yamamoto, T., Taguchi, S., Sakakura, A., Nozawa, T., 1972, Magnetic Properties of Grain-Oriented SiliconSteel with High Permeability Orientcore HI-B, *IEEE Trans. Magn.* Vol. 8, pp. 677-681.

Yastrebov, I.G., Babichev, L.P., 1987, Methods of Measuring the Magnetostriction of Magnetically Soft Alloys, *Izmeritel'naya Tekhnika*, No. 8, pp. 54-56.

Zheng, X., Sun, L., 2006, A Nonlinear Constitutive Model of Magneto-thermo-mechanical Coupling for Giant Magnetostricive Materials, *J. Appl. Phys.*, Vol. 100.

Zhou, H., Zhou, Y., Zheng, X, Ye, Q. Wei, J., 2009, A General 3-D Nonlinear Magnetostrictive Constitutive Model for Soft Ferromagnetic Materials, *J. Magn. and Magn. Mat*., Vol. 321, pp. 281-290.

Zhu, G., Ramsden, V. S., 1993, Two Dimensional Measurements of Magnetic Field and Core Loss Using a Square Specimen Tester, *IEEE Trans. Magn.*, Vol. 29, No. 6.

Zienkiewicz, O. C., 1967 (first published). *The Finite Element Method: Its Basis and Fundamentals.* Butterworth-Heinemann, 6th edition, 2005, 752 pages.

Appendix A

Modified Epstein frame

The main parameters of the modified Epstein frame (Belahcen, 2004) are presented in Table 5. Figure A.1 shows the main dimensions of the setup and sample.

Table 5: Parameters for modified Epstein frame.

Parameter		**Value**
Thickness of the sample		0.5 mm
Length of the sample		300 mm
Width of the sample		30 mm
Cross section area		225 mm^2
Primary winding:	Resistance	0.079 Ω
	Inductance	138 mH
	Number of turns	700
Secondary winding:	Resistance	1.347 Ω
	Inductance	138 mH
	Number of turns	700

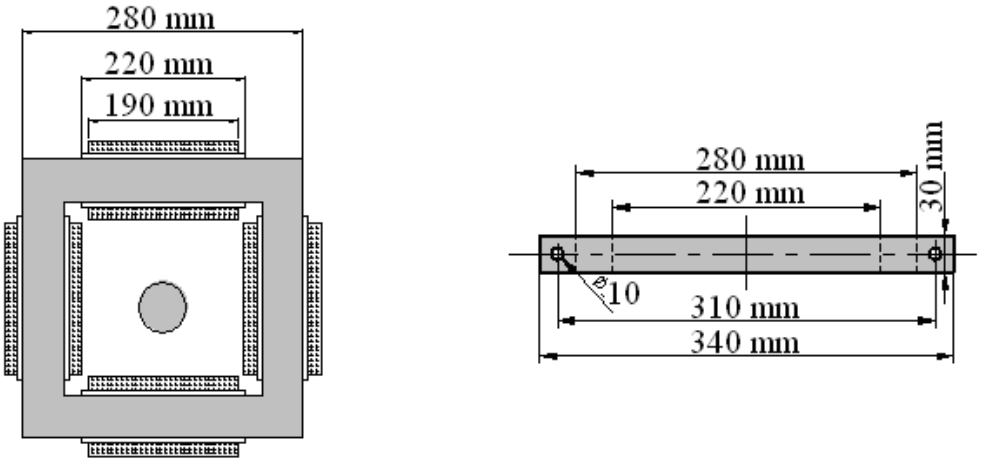

Figure A.1: Schematics of Epstein frame (left) and upper view of sample sheet (right).

Appendix B

Vertical yoke system

The main parameters of the vertical yoke are gathered in Table 6.

Table 6: Parameters for the vertical yoke system.

Parameter	Value
Height of Yoke 1	90 mm
Height of Yoke 2	110 mm
Thickness of Yoke 1	10 mm
Thickness of Yoke 2	10 mm
Thickness of one steel lamination	0.2 mm
Thickness of one polyester sheet	0.19 mm
Resistivity of the lamination	$0.25\ 10^{-3}\ \Omega$m
Number of turns	800
Diameter of copper wires	0.6 mm
Total height of the symmetric yoke system	250 mm

To determine the local flux density in the sample, B-coils are wound through holes drilled in the sheet. For acquiring the magnetic field strength, H-coils were prepared and glued in the centre of the test sheets. The parameters for those sensors are presented in Table 7.

Table 7: Parameters for the sensing coils.

	Parameter	Value
B-coils:	Number of turns	2
	Cross-section area	10 mm^2
	Diameter of the copper wire	0.3 mm
	Diameter of the holes	1 mm
H-coils:	Number of turns	900
	Cross-section area	47 mm^2
	Diameter of the copper wire	0.05 mm

Appendix C

Verification Device

The geometry of the verification device is presented in Figure C.1. Figure C.1 (a) shows the division of the periphery of the three-phase machine into positive and negative phase belts. Parameters in Figure C.1 (b, c and d) are collected in Table 8.

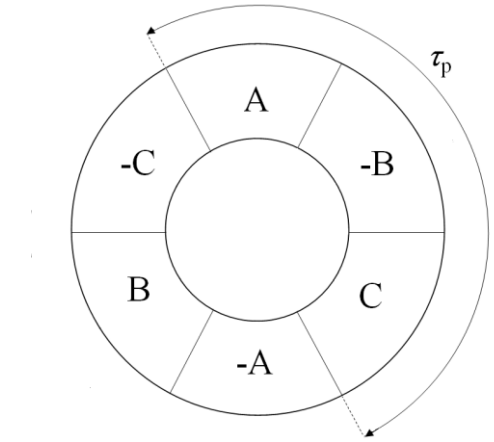

(a)

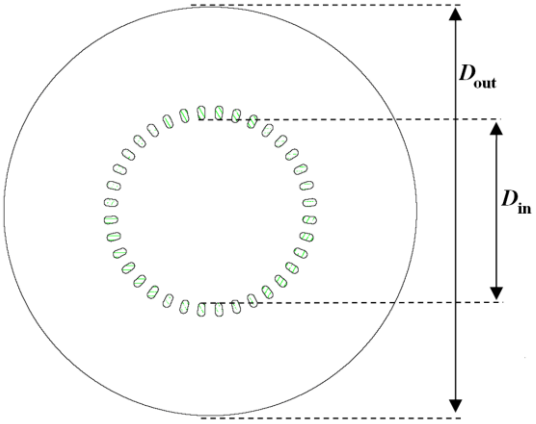

(b) Dimensions and geometry of the test device.

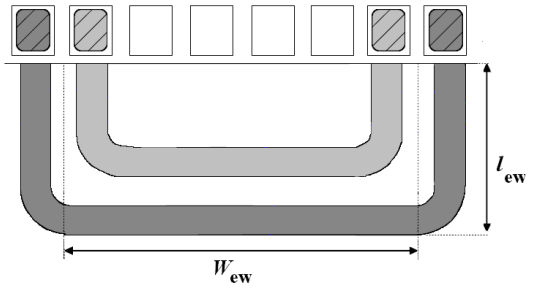

(c) Dimensions for the end-winding.

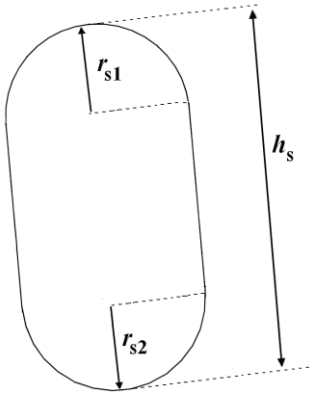

(d) Shape of one slot and its dimensions.

Figure C.1 : Dimensions of the different parts of the test device.

Table 8: Dimensions of the test device and its winding parameters.

Definition	**Parameter**	**Value**
Radius for the shape of the slot	r_{s1}	5.5 mm
Radius for the shape of the slot	r_{s2}	5 mm
Height of one slot	h_s	20 mm
Outer diameter of the device	D_{out}	600 mm
Inner diameter of the slotting	D_{in}	230 mm
Axial length of the device	H_{tot}	100 mm
Number of pole pairs	p	1
Number of phases	m	3
Total number of slots	Q	36
Slots per pole per phase	q	6
Number of parallel wires	g	4
Parallel paths	a	4
Approximated “depth” of end winding	L_{ew}	50 mm
Approximated coil span	W_{ew}	300 mm
Average length of phase winding	l_s	550 mm
Resistivity of copper at 20 C	ρ_{Cu}	1.75 10^{-5} Ωmm
Diameter of copper wire	D_{Cu}	1.5 mm
Minimum effective area of phase winding	A_{ph}	14.14 mm^2
Approximated filling factor for one slot	/	35%
Weight of the assembled device	w	260 kg
Thickness of one single electrical steel sheet	δ	0.5 mm

Table 8 is supplemented by the following definitions

$$\tau_p = \frac{\pi D_{out}}{2p} \quad (130)$$

$$Q = 2mpq \quad (131)$$

$$l_s\lambda_s = 2l_{ew}\lambda_{lew} + W_{ew}\lambda_w, \quad (132)$$

where λ_w and λ_{lew} are the permeance factors of the end-winding, they depend on the cross section of the end winding and the lengths and λ_s = 0.25. Detailed calculations and explanations are found in Pyrhönen (2009), a picture describing the winding is given in Figure C.2.

In the case of a diamond winding, the coil pitches are of equal width. Four turns of four copper wires each are placed in series in the slots. For the construction, 199,

M400-50A- type electrical steel sheets were necessary as in Figure C.3 (a and b). A total of 36 slots were cut out to insert the windings.

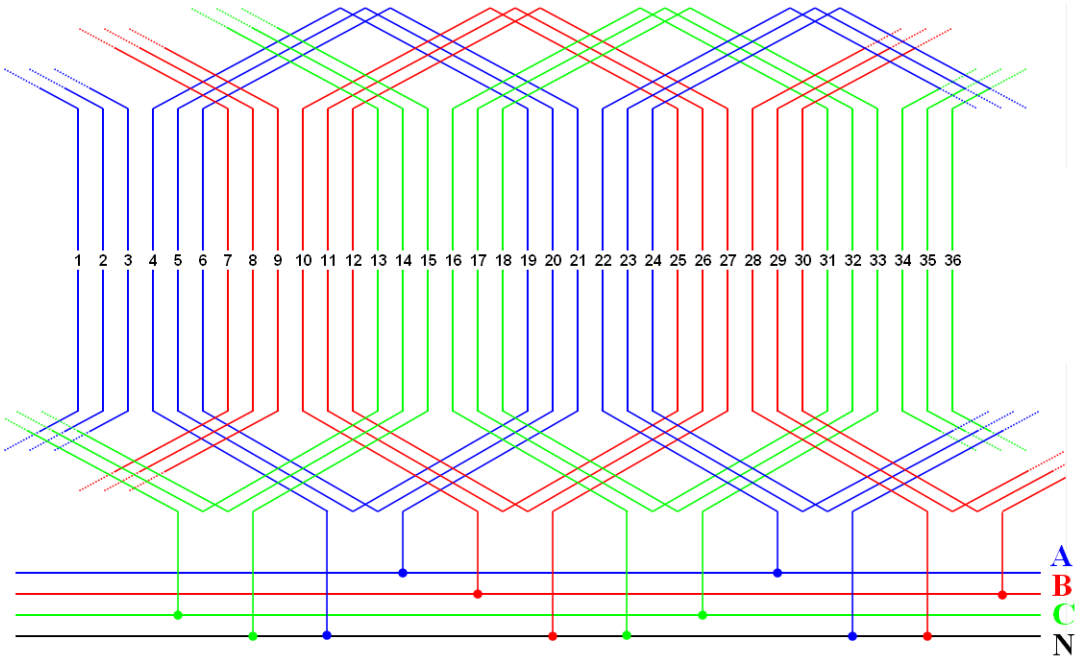

Figure C.2 : Winding layout.

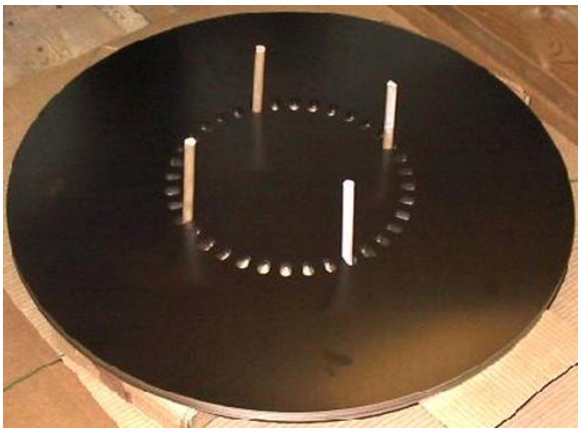

(a) Placing the sheets.

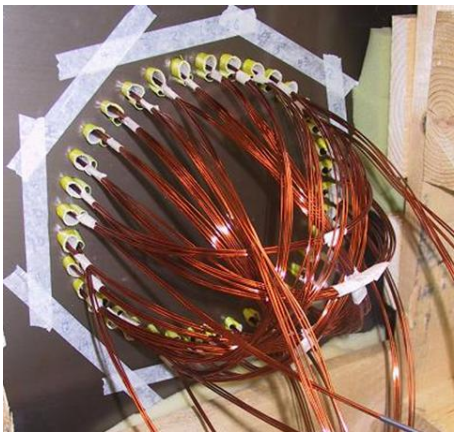

(a) Inserting the copper wires in the slots.

Figure C.3 : Assembling the device.

Appendix D

Test electrical machines

Machines I and II are standard cage induction motors. Machine III is an induction machine built by Hirvonen (1983). First-order elements were used. The magnetic materials of the stator are fully processed non-oriented steel sheets. Data for Machines I and II are presented in Table 9. Their respective meshes and geometries are shown in Figure D.1. The mesh of Machine III was build within this study. Details regarding the mesh are presented in Figure D.2. Specific data is gathered in Table 10.

Table 9: Main parameters used as input for the simulations of Machine I and Machine II.

Data	**Machine I**	**Machine II**
Rated voltage	380 V	380 V
Slip	2 %	3.2 %
Rated current	60 A	27 A
Rated power	30 kW	15 kW
Connection	Delta	Delta
Supply frequency	50 Hz	50 Hz
Temperature of windings	80 ºC	80 ºC
Number of pole pairs	1	2
Number of phases	3	3
Number of parallel paths	2	1
Number of conductors in a stator slot	26	21
Number of layers of the stator winding	1	1
Coil pitch in slot pitches	18	9
Outer diameter of the stator core	323 mm	235 mm
Inner diameter of the stator core	190.2 mm	145 mm
Number of stator slots	36	36
Outer diameter of the rotor core	188.37 mm	144.1 mm
Inner diameter of the rotor core	70 mm	53 mm
Number of rotor slots	28	34

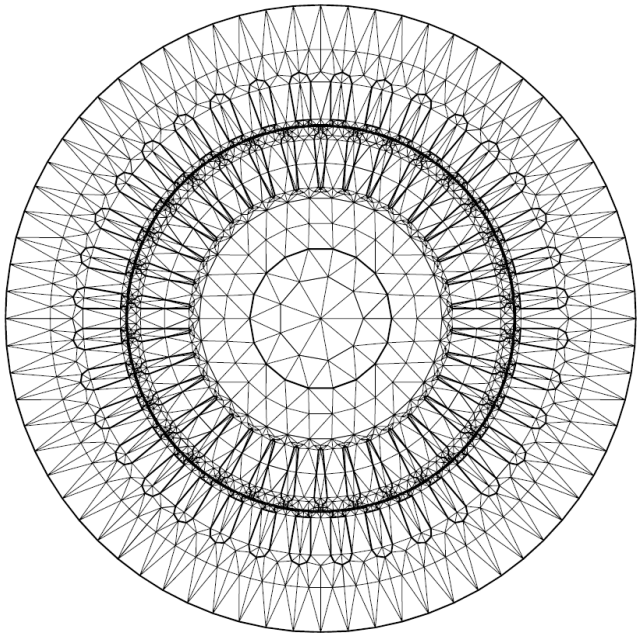

(a) Mesh of Machine I.

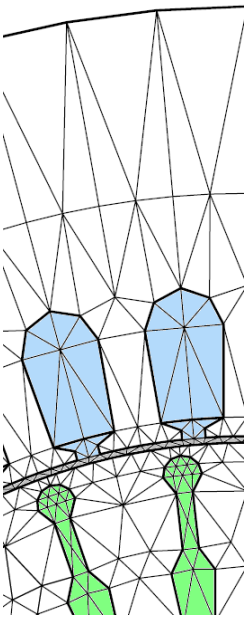

(b) Machine I, zoom on the stator slots, air gap region and rotor slots.

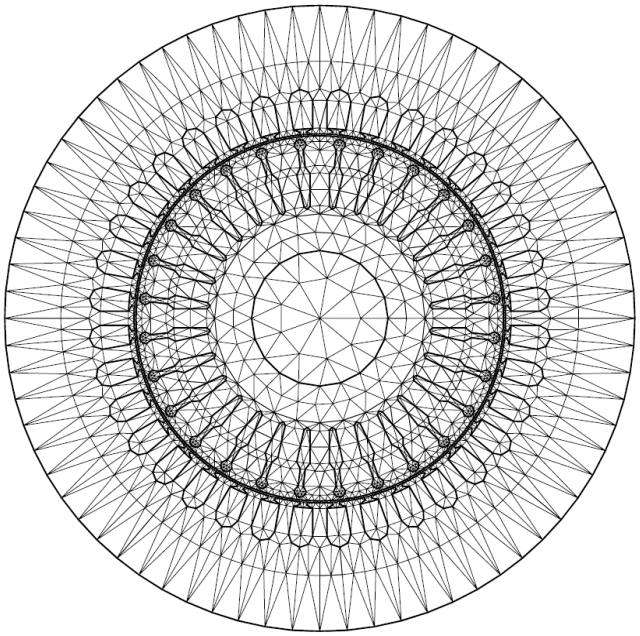

(c) Mesh of Machine II.

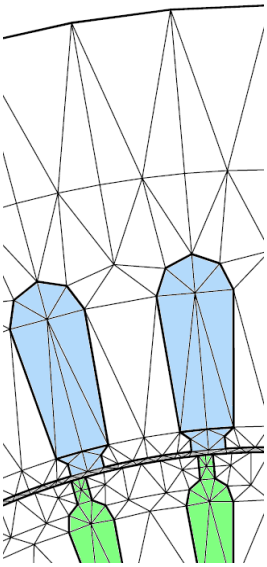

(d) Machine II, zoom on the stator slots, air gap region and rotor slots.

Figure D.1 : The geometry of the cage induction machines.

Table 10: Main parameters for the verification motor.

Data	**Machine III**
Number of pole pairs	2
Number of phases	3
Number of parallel paths	1
Number of conductors in a stator slot	4
Number of layers of the stator winding	1
Effective length of the machine	0.1 m
Outer diameter of the stator core	664 mm
Inner diameter of the stator core	400 mm
Number of stator slots	48
Outer diameter of the rotor core	399 mm
Inner diameter of the rotor core	155 mm
Resistance of a stator phase	0.02 Ω
Stator slot dimensions: H1	63 mm
H2	45 mm
B1	15 mm
B2	1.25 mm
B3	16 mm

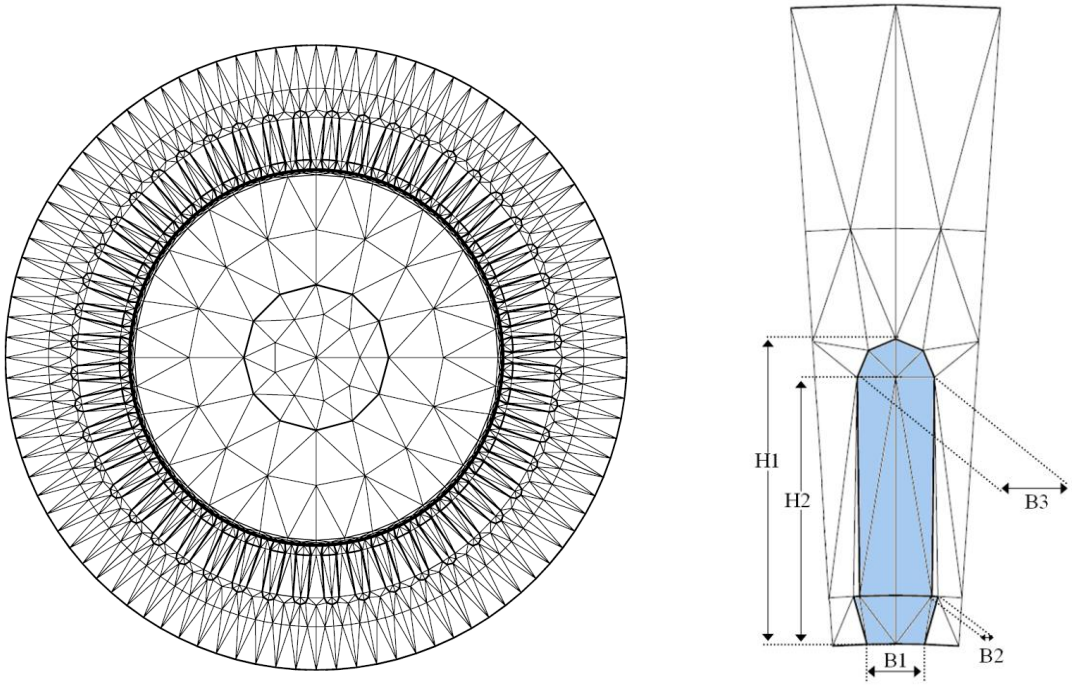

(a) Mesh, elements, nodes. (b) A stator slot.

Figure D.2 : Geometry of Machine III.

ISBN 978-952-60-3287-0
ISBN 978-952-60-3288-7 (PDF)
ISSN 1795-2239
ISSN 1795-4584 (PDF)